Spectroscopy of Two Dimensional Electron Systems Comprising Exotic Quasiparticles

Trevor David Nathaniel Rhone

Submitted in partial fulfillment of the

requirements for the degree

of Doctor of Philosophy

in the Graduate School of Arts and Sciences

COLUMBIA UNIVERSITY

2012

©2012

Trevor David Nathaniel Rhone

All Rights Reserved

Abstract

Spectroscopy of Two Dimensional Electron Systems

Comprising Exotic Quasiparticles

Trevor David N. Rhone

In this dissertation I present inelastic and elastic light scattering studies of collective states emerging from interactions in electron systems confined to two dimensions. These studies span the first, second and third *Landau* levels.

I report for the first time, high energy excitations of composite fermions in the quantum fluid at $\nu = 1/3$. The high energies discovered represent excitations across multiple composite fermion energy levels, demonstrating the topological robustness of the fractional quantum Hall state at $\nu = 1/3$. This study sets the ground work for similar measurements of states in the second Landau level, such as those at $\nu = 5/2$.

I present the first light scattering studies of low energy excitations of quantum fluids in the second Landau level. The study of low energy excitations of the quantum fluid at $3 \geq \nu \geq 5/2$ reveals a rapid loss of spin polarization for $\nu \lesssim 3$, as monitored by the intensity of the spin wave excitation at the Zeeman energy. The emergence of a continuum of low-lying excitations for $\nu \lesssim 3$ reveals competing

quantum phases in the second Landau level with intriguing roles of spin degrees of freedom and phase inhomogeneity.

The first light scattering studies of the electron systems in the third *Landau* level are reported here. Measurements of low energy excitations and their spin degrees of freedom reveal contrasting behavior of states in the second and third *Landau* levels. I discuss these measurements in the context of the charge density wave phases, that are believed, by some, to dominate the third *Landau* level, and suggest ways of verifying this belief using light scattering.

Distinct behavior in the dispersion of the spin wave at $\nu = 3$ is measured for the first time. The study may highlight differences in the first and second *Landau* levels that are manifested through the electron wavefunctions. In addition to intra-*Landau* level measurements, inter-*Landau* level studies are also reported. The results of which reveal roles of spin degrees of freedom and many body interactions in odd denominator integer quantum Hall states.

Contents

List of Tables

List of Figures

Acknowledgements

I often say, life is just a long journey, we better enjoy the ride! I've found that the same applies to completing a Ph.D.. It is an exceedingly difficult thing to do, even with a surfeit of drive and determination. A guiding hand is often needed to help a bright eyed first year graduate student navigate through his Ph.D. career. I am forever indebted to a multitude of angelic beings for helping me along my path to success.

My advisor, Professor Aron Pinczuk has been the north star that has helped me navigate this long voyage. He has been a teacher, mentor and colleague through it all. Providing guidance on getting used to being in an optics lab, low temperature physics, conference talks, journal articles, and general tips for success. His insight, intuition, attention to detail and creativity never cease to amaze me. I have been privileged to learn from a remarkably talented scientist, and fortunate to work alongside someone at the very top of his field. I have also benefited from his support for my career and have enjoyed the opportunities I've had to speak at conferences around the world. I've thoroughly enjoyed the interactions and stimulating discussions with my peers and other top notch principal investigators in condensed matter physics. On a personal note, over the years I have gained a deep appreciation for dark chocolate from the greatest chocolate aficionado I know. I have also adopted a fondness for Altoids mints. I always insist, when offering, that the person takes two.

The expert training and guidance received from Dr. Yann Gallais and Dr. Jun Yan, allowed me to been able to perform the delicate measurements needed to succeed in the lab. I am also happy to have had the opportunity to interact with such marvelous, clever people. It was truly a pleasure to have shared some lab time with them, sitting in the dark, the sounds of the pumps in the background, the soft green glow of the laser light dancing across the ceiling, edging closer to the next discovery. Many thanks Dr. Rui He for being an exceedingly supportive post doctoral research scientist and friend; for helpful discussions, and giving up some of her time to help out in the lab. I will always be grateful to her. I look forward to seeing great things from her as she begins her career as a professor. I would also like to thank Xiuyuan Yang for being a great lab partner. Xiuyuan is credited with acquiring some of the data at higher Landau levels. Without her assistance, Chapter 6 of this dissertation would not have been possible. And thanks to Albert Rigosi for being a pleasant officemate. As he begins his career as a graduate student, I look forward to seeing marvelous things coming out of his drive, passion and intensity for science. I have also had the pleasure of interacting with some of our collaborators, Dr. Vittorio Pellegrini and Sarah Goler and have always enjoyed the trips to Italy in which I get to visit them. I extend gratitude to Dr. Annette Plaut for inadvertently guiding me along as a junior graduate student - I learnt much from the articles she wrote. And as a visiting research scientist, for being a lovely individual and an absolute pleasure to be around. I am also happy to have had the pleasure of a few stimulating discussions with Dr. Fiona Burnell. The few hours we spent chatting and exchanging ideas on physics at $\nu = 5/2$ was very useful for me.

I am grateful for the kind support from and discussions with several faculty members in the Physics department. I've enjoyed chatting with Dr. Allan Blaer throughout my time at Columbia. I've not once found him without a smile on his face and an outstretched welcoming hand. I still remember how enjoyable his Classical

Waves class was - Allan is certainly one of the department's great treasures. Dr. Jim Yardley is another one of those marvelous individuals that you're just happy to know. Even since I've known Dr. Yardley, he's been friendly, supportive and a great mentor. I'm glad for our hours of conversation on career and life after grad school. I would also like to thank Professor Philip Kim for serving as my academic advisor during my first few years at Columbia. I will always remember our pleasant conversations and his warm personality. The time spent volunteering with Prof. Jeremy Dodd in the department's outreach program has not only been a lot of fun, but deeply satisfying. I'm glad for that opportunity and the chance to interact with a great Professor. Professor Michael Tuts, in a way my fellow countryman, us both having ties to Trinidad and Tobago, has been a friend during my six years at Columbia. I've always enjoyed stopping by his office to chat and to get the latest scoop on the large hadron collider. It is sometimes these little things in which you find big value. I am indebted to Professor Bill Zajc for being an amazing graduate student advisor and helping me through the tough transition to graduate school life. I still remember our discussion six years ago about a common interest of ours - going to the gym, and how it helps to combat stress. I would like to acknowledge Professor Igor Aleiner for being a stunning professor and all around nice guy. I'll never forget that it "doesn't take a genius" to do well in life, though unlike him, I don't remember much from my preschool calculus class. I've gained a deep appreciation for group theory from Professor Aleiner - an appreciation that will drive my curiosity and interest for years to come. Professor Marcel Agueros has been a true friend, mentor and colleague of mine for several years. I'm truly privileged and happy to have had a chance to know him. Thanks to Prof. Agueros I had the opportunity to attend the annual meeting of the National Society of Black Physicists and had the chance to excel there, taking home a prize from its poster competition. Prof. Agueros is an outstanding mentor of unmatched caliber; he is also a kind, dedicated and inspiring

friend. I look forward to being in touch for years to come.

A great deal of gratitude goes to my comrades in the physics department office. Lalla Grimes is one of the nicest people I've had the pleasure of meeting. Ciao Lalla! E sempre un piacere! My teaching and research assistantship would simply not have been possible without the tireless efforts of Lydia Argote, Giuseppina (Joey) Cambareri, John T Carr III, Yasmin Yabyabin, Randy Torres Myrna Tengco and Kissoon Ramdass. Thanks especially to Joey, Yasmin, John and Randy, with whom I've had the most interaction - it's been a great pleasure chatting with you over the years.

Of course, this surfeit of gratitude is shared with the Applied Physics and Applied Math department as well as the folks at the Energy Frontiers and Research Center. In particular, I would like to acknowledge Sarita Oxley, Julissa Nicasio, Fran Monar and Niva Ranjeet for being there to offer assistance in purchasing equipment, travel reimbursements and other such things often covered thick in bright blue Columbia tape.

Special thanks goes to Dr. Nicholas Fuller and Dr. Jeffrey Kash whose selfless efforts greatly assisted in my search of vocation in the last year of my Ph.D. There are a few folks with whom I've had positive useful discussions - Dr. Erik Henriksen, Dr. Javier Groshaus and Dr. Jun Zhu. A great big thank you and bow of deep respect to the venerable Dr. Cyrus Hirjibehedin - a truly successful and remarkable graduate student of Prof. Pinczuk, turned successful Professor and mentor. His guidance and achievements have served as a great source of inspiration for me over the years; I thank him dearly. Dr. Hirjibehedin is also credited with acquiring the data that formed the basis of Chapter 4.

Thanks also to the folks at Oxford Instruments - Nick Dent in particular. And to the folks at Coherent - Nicki May has been especially helpful. My work would not have been possible without the great efforts of the folks at Horiba Jobin Yvon -

Jude Jean-Charles and William Pagdon in particular have been exceedingly helpful.

There is one experience in particular which I feel has had a profound impact on me as a person and my success - I studied several styles of martial arts for many years. In the early days, I studied at a place which sculpted great minds and forged great conviction in the hearts of those who gave it their all. Thanks to my dear instructors of Seido Karate, Jamaica - Master Errol Lyn, Kyoshi Tony Robinson, Sensei Betty Simmons, Sensei Kay Lyn and Senpai Michael Young. Thanks also to my many classmates, and students for building my *bushido* (samurai spirit). Thanks also to my more recent martial arts friends - the Columbia Taekwondo club and Moy Yee Kung Fu and Tai Chi association. And special thanks to my yoga instructor for reminding me that when things get tough, "don't forget to breathe".

I have had a great relationship with my mentor (through the minority students office), Dr. Leo Douglas. It has been great to find an individual with such a marvelous character. I found a great deal of support and many a good "get together" over the years from my fellow Jamaican.

Last but certainly not least, my family and friends have been there for me through it all. They have shaped, in more ways than I can tell, my experiences and successes during the course of my doctoral studies. My dearest dad has inspired me and encouraged me as long as I can remember. I love him and miss him more than words can tell. I aspire to be more like the great orator, story teller, achiever and superb individual that he was; to reach far beyond mediocrity, and to work towards achieving greatness in one's actions. Thanks to my mom - for being an educator and for teaching me that it was not good luck, but good management that forged achievement. Many thanks to my brother, Jonathan, and my sister, Traci for all their support and encouragement over the years. Thanks to my friends for sharing life's colorful experiences with me. Thanks to Mariko Sadachi for reminding me that hard work pays off in the end. And thanks to Imre Bartos and Dmitri Efetov

for providing moral support over the years and for reminding me that a good physicist must wear many hats. Salomi Savvatia Asaridou is an especially dear friend; in a letter from Greece she writes, "may every day that passes by be full of fun, joy, health, precious moments, true friends, new adventures, sunny skies, starry nights, blissful mornings, exciting travels and of course lots of love!" The bumpy journey of my Ph.D. just got shock absorbers. She's not only credited with moral support but also with helping in the choosing of some greek symbols for the notation in my thesis - truly the finest assistance possible. An infinite indebtedness to Rachel Lewis for being a dear friend and companion in the icy halls of Butler library. The hours spent toiling inside Butler would not have nearly been as pleasant without just the right amount of peer pressure mixed in with the finest company. Thanks for our inspiring conversations and for encouraging the ubernerd in me.

Chapter 1

Introduction

Two-dimensional electron systems give rise to exceedingly remarkable phenomena in condensed matter systems. The studies of confined systems represent some of the most complex and fascinating areas in research. Exotic quasiparticles emerge from interacting electrons in a magnetic field, which can form fluid, solid and other complex phases. Some flavors of these exotic quasiparticles are so remarkable that they have neither Bose nor Fermi statistics. Related phenomena include, topological insulators, topological quantum computation and the fractional quantum Hall effect (FQHE). Efforts to exploit the link between the fractional quantum Hall effect and topological quantum computation have been growing since the realization that fractional quantum Hall (FQH) states could be used to support topological quantum computation. The fractional quantum Hall state at filling factor 5/2 ($\nu = 5/2$) is a strong candidate for a medium to support topological quantum computation. I will examine extensively how this exotic state may be realized in the laboratory. I will address theoretical considerations and discuss how experimental probes may be used to help build up the understanding of this potentially remarkable state of matter.

The fractional quantum Hall effect occurs in a two-dimensional electron fluid

at low temperature and high magnetic field. Two-dimensionality can arise through various means. For instance, electrons can be confined to the surface of liquid helium or to the surface of some insulator. For the purposes of the quantum Hall effect, the most salutary method of producing a two-dimensional electron system (2DES) is to confine electrons within a solid - sandwiching them between two different types of semiconductors. Modulation-doped gallium-arsenide/aluminum-galliumarsenide (GaAs/AlGaAs) heterostructures have provided an immaculate 2DES for research and for high-performance applications. It is these "ideal" 2DES's displaying strong Coulomb interactions, in the presence of high magnetic field, at low temperature, that gives rise to the complex behaviors that manifest in the fractional quantum Hall effect. Much of the novel physics found in these systems is very sensitive to the impact of disorder, and is observed only in the highest quality samples. Sample fabrication methods will be considered briefly in Chapter 2. Here I highlight that current samples have remarkably long electron mean free paths of the order of 0.1mm or more than 10^5 lattice sites. These immaculate samples have greatly reduced impact of disorder that would destroy the more fragile quantum Hall states. Such delicate states include the state at filling factor 5/2, in the second *Landau* level - whose observation is directly due to the dramatic improvement in sample quality gained from molecular beam epitaxy (MBE) growth and sample structure design with a precision that reaches the atomic scale.

The vast majority of Quantum Hall studies have involved transport measurements. These transport measurements involve measuring a current and voltage and have impact of edge states. Alternative probes, such as optical methods, probe the bulk states of quantum fluids. Optical methods are unique probes which complement existing transport studies and provide venues for characterization which other probes lack.

In this dissertation I discuss our recent inelastic light scattering studies of the

emergent states formed by strongly interacting 2D electrons in the presence and absence of a magnetic field. I focus on applying these techniques towards better understanding the behavior of interacting quasiparticles in the second *Landau* level, especially at $\nu = 5/2$. I begin Chapter 2 with a brief introduction to the key properties of 2D electron systems that are relevant to our studies. I discuss the basic physics of 2DESs and the experimental realizations of such systems in MBE-grown semiconductor heterostructures. This is followed by an overview of the relevant energy scales in interacting 2D systems. These are then used to describe the energies of relevant single-particle and collective excitations of the 2D system. The Chapter includes a general discussion of the phases of 2DES's when interactions dominate. For phases found in zero magnetic field, I highlight the two main kinds of single particle transitions that can occur. For non-zero magnetic fields, I provide an overview of the integer and fractional quantum Hall effects and a brief discussion of electron states in these regimes. Moreover, I introduce a class of phases that exist in higher *Landau* levels - electron "crystalline" phases - and briefly mention how quantum phase transitions are relevant for a careful consideration of these novel phases.

There are several experimental venues for studying the quantum Hall effect. Methods employing the use of electron transport, such as Shubnikov de Haas and Hall resistance measurements, have impact of edge states since electron transport occurs around the edges of a 2DES. In this dissertation, the tool of choice to investigate quantum Hall systems is light scattering. Light scattering methods provide a distinct tool that probes the bulk states of the excitations of quantum Hall fluids. Light scattering has been enormously successful in studying the excitations of fractional quantum Hall fluids[28] since the early 1990's. It has developed into an important characterization tool which complements transport studies of electron fluids in the quantum Hall regime. More importantly, light scattering is a unique probe that can provide information on quantum fluids which is inaccessible by other means.

Chapter 3 describes the essentials of inelastic light scattering in 2D systems hosted by semiconductor heterostructures. Resonant inelastic light scattering is a powerful probe of the excitations in these structures. I review the basic mechanisms of light scattering from electron systems in semiconductor heterostructures, and highlight the physics that can be extracted from light scattering spectra. Next, I describe the experimental setup for milli-Kelvin spectroscopy. While discussing the scattering geometry used throughout this work, I highlight the characteristic wavevector of the light scattering technique and link this to the excitations in systems in which weak residual disorder introduces a break-down of wavevector conservation. This allows light scattering to "trace" the dispersion of excitations. I describe the role of resonant enhancement, which dramatically enhances the scattering cross-section of 2DESs to detectable levels.

In Chapter 4, I report the first light scattering studies of high energy composite fermion excitations of fractional quantum Hall states. These high energy excitations comprise excitations across multiple composite Fermion energy levels and show the topological robustness of fractional quantum Hall states. The study performed primarily at $\nu = 1/3$, has implications for the high energy excitations for the states in the second *Landau* level, such as those at $\nu = 5/2$.

I report the first light scattering studies of the states in the second *Landau* Level in Chapter 5. I discuss the unexpected rapid loss of spin wave intensity for filling factors less than three, which could be interpreted as a loss of full spin polarization. It appears that the possible loss of spin polarization could extend to the state at $\nu = 5/2$. The result has implications for widely accepted theory that describes a spin polarized state at 5/2 - the Moore-Read state. I also describe results that show the formation of inhomogeneous domains in the second *Landau* level. Evidence for these domains arises for $\nu \lesssim 3$ and persists to filling factor $\nu \lesssim 5/2$. I surmise the electron fluid at 5/2 could consist of both polarized and unpolarized domains.

The state at $\nu = 5/2$ has been studied by a variety of means - theoretical calculations [29, 30, 31, 32], transport measurements [33, 6, 34, 17], surface acoustic wave studies [23, 35] and more recently Knight shift measurements [36]. Our light scattering results, the first such studies reported, are compared with existing studies whose conclusions of the behavior of the 5/2 state remain controversial [33, 37, 38]. In Chapter 5, I give a more in depth overview of the studies surrounding 5/2 and highlight the contribution light scattering studies can make towards furthering our understanding of this enigmatic state.

The state at $\nu = 5/2$ exists in the center of the second *Landau* level (N=1 LL) and lies at the crossroads of two vastly different regimes - the first *Landau* level (N=0 LL) and the third *Landau* level (N=2 LL). These distinct regimes are dominated either by conventional quantum Hall states (N=0 LL) or by charge density wave phases (electron "crystalline" phases) ($N \geq 2$). To better understand the state at half filling in the N=1 LL, I compare it to the states at half filling in the N=0 and N=2 LLs. In Chapter 6, I report the first light scattering studies of the electron phases in the N=2 LL. I show that although the phase at half filling in the N=2 LL lower spin branch is not spin unpolarized, there is some reduction of spin polarization. In addition, I consider the existence of signatures of vibrational modes of electron charge density wave phases. I compare and contrast these findings with those of the second *Landau* level.

One of the primary motivations for using light scattering to study the state at 5/2 was to probe its spin degrees of freedom. Studies were focused on low energy intra-*Landau* level excitations (with change in spin) in the second *Landau* level. Chapter 5 describes the collapse of the long wavelength spin flip mode (that is, spin wave fixed at the Zeeman energy) for $\nu \lesssim 3$. In Chapter 7, I expand the analysis of the spin flip dispersion to large wavevectors, and in particular, I address a distinctive feature in the dispersion at $\nu = 3$. I compare the distinctive dispersion at $\nu = 3$

with the dispersion at $\nu = 1$ to attempt to elucidate the differences in behavior of the first and second *Landau* levels. In addition, I describe the dispersion of spin-flip excitations across cyclotron gaps. These measurements of inter-*Landau* level excitations may serve as a tool for probing the spin degrees of freedom of fractional quantum Hall states in the second *Landau* level.

Chapter 8 presents some potentially exciting preliminary results and speculates on their interpretation. In addition, some possibly elucidating future experiments are suggested. Intriguing evidence of what could be interpreted as phase separation around $\nu = 5/2$ due to Coulomb interactions is presented. I propose the use of elastic scattering studies to monitor phase inhomogeneity - domain size and domain binding energy - for states in both the second and third *Landau* levels. In addition to more in depth studies of low energy excitations as a function of small changes in filling factor, other tunable parameters, such as temperature and well width could be examined. Also, further studies of high energy excitations could serve as a useful characterization tool. In addition to excitations across multiple composite fermion energy levels, measurements of high energy excitations could reveal evidence for neutral fermion excitations at $\nu = 5/2$ [39].

Chapter 2

2D Electron Systems in GaAs Quantum Structures

2.1 Overview

The purpose of this Chapter is mainly to provide the framework that will assist us in understanding some fascinating phenomena of strongly interacting electrons in a magnetic field. I will try to build context and to provide the vernacular needed for future chapters.

A two dimensional electron gas exhibits remarkable phenomena under the right conditions of residual disorder, temperature and applied magnetic field. These phenomena, the integer and fractional quantum Hall effect are remarkable manifestations of low-dimensional physics. Electron crystalline or Wigner solid-like structures [23, 40] also exist in 2D electron systems.

I begin with a discussion on the design of the samples in which the two dimensional electron system (2DES) "lives" and discuss how one derives reduced dimensionality from a three dimensional semiconductor heterostructure. I then explore the properties of this 2DES in a zero magnetic field and give a simplified discussion

of the associated eigenstates and eigenenergies.

Applying a magnetic field to the 2DES adds to the richness of phenomena exhibited in these systems. I introduce the formation of *Landau* levels (quantized "orbits" of electrons due to magnetic field) and describe how this gives rise to the phenomena seen in the integer quantum Hall effect (IQHE). In addition, I introduce how the formation of *Landau* levels (LL's) coupled with electron-electron interactions and correlations can give rise to an even richer quantum mechanical effect - the fractional quantum Hall effect (FQHE). The remarkable behavior of the emergent particles of the FQHE comprise a major part of this dissertation.

I very briefly discuss the relevance of quantum phase transitions for 2DES in a magnetic field. I also briefly explore the transition from highly correlated quantum to less correlated regimes, via populating an increasing number of *Landau* levels, and outline the transition from dominating electron fluid to dominating charge density wave phases. I highlight that, under the right conditions, these phases can coexist.

2.2 Sample Design

Advances in fractional quantum Hall studies have been made possible by the tremendous improvement of sample quality. Current state-of-the-art samples utilize molecular beam epitaxy (MBE) [41] to produce high quality two-dimensional electron systems (2DES). A schematic of the layer sequence in a GaAs/AlGaAs heterostructure is shown in Fig. 2.1. In the figure shown, the active layer, or the quantum well (QW) consists of 240 Angstroms of GaAs, sandwiched between two AlGaAs layers. GaAs and AlGaAs have very small lattice mismatch and GaAs/AlGaAs heterojunctions can be grown with very little strain. This enables the MBE growth of multilayered GaAs/AlGaAs quantum structures of extremely high quality. These atomically precise systems create the "clean" environment for electrons to behave

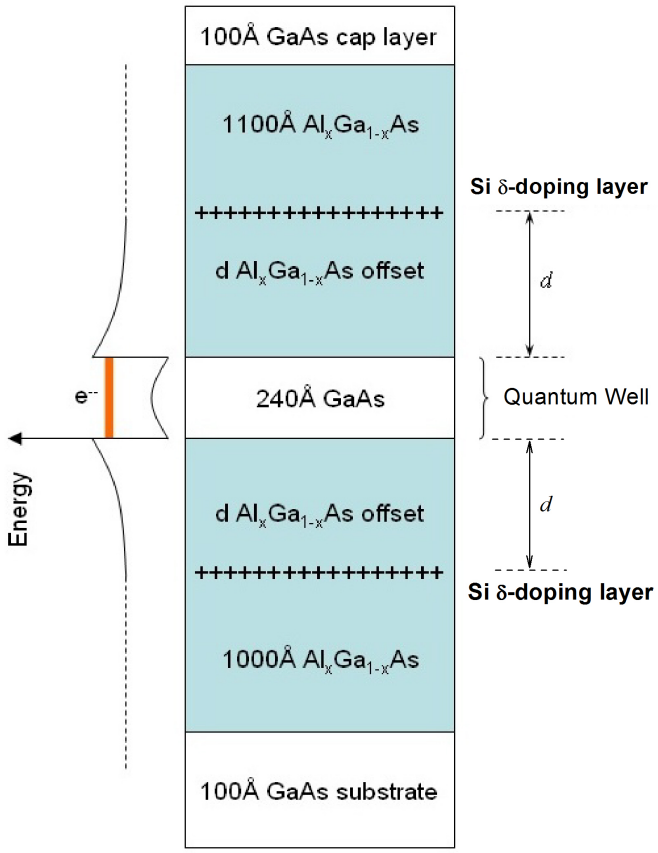

Figure 2.1: Schematic of the design for the AlGaAs/GaAs heterostructure. The active layer or quantum well is located in the 240 $\AA$ region of GaAs, to which electrons have migrated from the doping layers located a distance, d from the quantum well (modulation doping). As shown on the left side, the potential within the heterostructure, $E_c(z)$, depends on the electrostatic potential created by the delta doping layers. $E_c(z)$ is a symmetric function of z because of the presence of doping layers placed symmetrically on both sides of the well.

ideally.

In order to obtain high quality mobile electrons, the GaAs/AlGaAs heterostructure is doped with silicon in an AlGaAs layer. This δ-doping procedure is known as modulation doping (see Fig. 2.1) - a silicon atom when substituted in place of a Ga ion in the AlGaAs lattice frees an electron that migrates to the lower energy states of the GaAs quantum well. A layer of silicon atoms thus gives rise to the mobile 2D electron density that exists in the quantum well. The doping layer can be either on one side of the quantum well (asymmetric doping), or on both sides of the quantum well (symmetric doping). The latter (shown in Fig.2.1) allows for a higher density of electrons. Figures 2.1 and 2.2 illustrate that electrons in a quantum well have a lower potential in the GaAs region than in the AlGaAs layers.

2.2.1 Quantum Wells

To describe the electronic states of the heterostructure, one may use the envelope wavefunction approximation [42]. The wavefunction for electrons is written as,

$$\psi_{q,j}(\vec{r}) = \chi_j(z)e^{iq\cdot\vec{r}}u_j(\vec{r}) \tag{2.1}$$

where q is the wavevector perpendicular to the $\hat{z}$ direction and j indexes the states associated with the reduced dimensionality along the $\hat{z}$ direction. $\chi_j(z)$ is the electron wavefunction for motion in the $\hat{z}$ direction and $u_j(\vec{r})$ is a component of the Bloch function with periodicity such that $u_j(\vec{r}) = u_j(\vec{r}+\vec{R})$ ($\vec{R}$ is the Bravais lattice vector).

We can apply the Hamiltonian

$$H = \frac{-\hbar^2}{2m^*}\frac{\partial^2}{\partial z^2} + V(z) \tag{2.2}$$

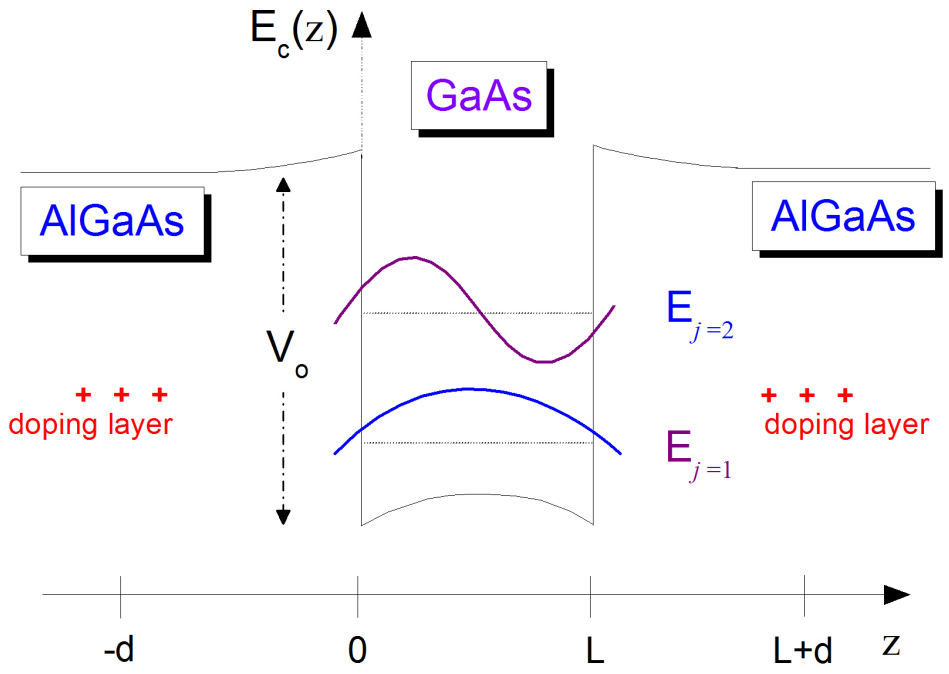

Figure 2.2: Schematic of a quantum well of width L with a sketch of the wavefunctions of the first and second energy levels depicted. The well has energy, $E_c(z) = V_o$ in the region of AlGaAs. In the GaAs region, $E_c(z)$ has a convex shape due to the presence of ionized Si donors. The band bending only depends along z and is symmetric due to the presence of donors placed symmetrically on both sides of the well.

to $\psi_q(\vec{r})$, where the potential $V(z)$ is along the $\hat{z}$ direction.

$$V(z) = 0; (0 < z < L)$$
$$V(z) = V_o; (z < 0, z > L)$$

and m^* is the effective mass of the electrons. As a result, we find that the wave-function in the $\hat{z}$ direction is determined by the following effective mass equation,

$$\left[\frac{-\hbar^2}{2m^*}\frac{\partial^2}{\partial z^2} + V(z)\right]\chi_j(z) = E_j\chi_j(z) \tag{2.3}$$

Using the following boundary condition of continuity in $\chi(z)$ and $\frac{1}{m^*}\frac{\partial}{\partial z}\chi(z)$ across the interfaces, we can find the QW energy levels (discrete energy levels formed due to reduced dimensionality), which is the familiar solution to the finite square well problem in quantum mechanics. Note that the effective mass term in the second condition ensures particle current conservation. In the simplest approximation of large barriers (V(z)$\longrightarrow \infty$) the resulting eigenenergies are the energy levels of the familiar infinite square well:

$$E_j = \frac{j^2\hbar^2\pi^2}{2m^*L^2} \tag{2.4}$$

where j is a positive integer (1,2,3,...) and L is the size of the quantum well. The index j describes the presence of "subbands" or energy levels due to the reduced dimensionality along the z direction. The corresponding eigenstates are

$$\psi_j(z) = Asin(j\pi z/L) \tag{2.5}$$

where A is the normalization constant. More accurate values of the QW energy levels can be obtained by using a finite barrier height, which for $Al_xGa_{1-x}As$ layers

is roughly $x \times 1eV$ in the conduction band for Al concentrations $x < 0.1$ [42]. Combining the simplified QW energy with kinetic energy due to in-plane motion (from the free electron states), the total energy is:

$$E_{j,q} = E_j + \frac{\hbar^2 q^2}{2m^*} \tag{2.6}$$

where q is the wavevector in the plane perpendicular to $\hat{z}$.

The ground state and first excited states are shown in Figs. 2.2 and 2.3. Doping fills the well to a density, n. Since electrons from the delta doping layers migrate from the AlGaAs to fill the QW, as shown Fig. 2.3, the Fermi energy (E_F) may be kept below the second subband ($E_{j=2}$) through the control of the density and QW design (that is, only the lower subband is filled). Figure 2.3 shows energy levels for zero and nonzero perpendicular magnetic field ($B[T]$).

The two dimensional electron system in quantum wells made by MBE can have huge mobilities, ($\mu > 10^7 cm^2 Vs$ in our samples). Mobility is defined as:

$$\vec{v}_d = \mu \vec{E} \tag{2.7}$$

where $\vec{v}_d$ is the drift velocity of electrons, and $\vec{E}$ is the applied electric field. The mobility, μ, varies with electron density, n. In our work, n is changed by selecting samples with different parameters, such as δ-doping layer distance, d. Also, tuning the aluminum concentration, x (in $Al_xGa_{1-x}As$) and changing the density of silicon dopants can modify the 2D electron density. The quantum well samples studied in the thesis were overdoped in the Si layer to provide electrostatic screening of fluctuations in the densities of impurities in the donor layer from affecting the electrons in the quantum well. Overdoping is avoided in transport measurements as it gives rise to parallel conductance which interferes with Hall measurements.

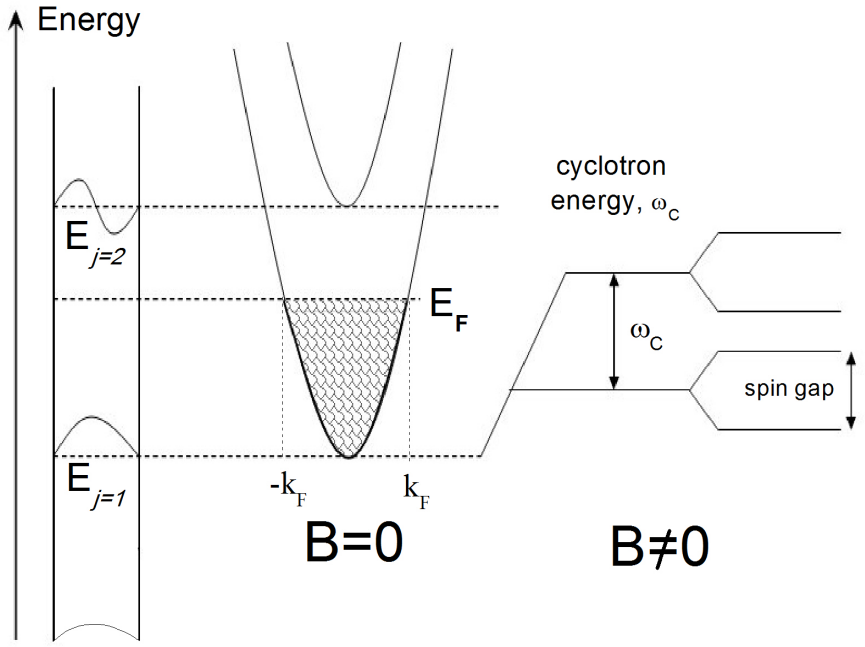

Figure 2.3: Quantum confinement of electrons along the $\hat{z}$ direction gives rise to energy levels or subbands as defined by E_j in Eqn. 2.6. The left panel shows a diagram of the energy levels of the quantum well. The central panel shows the wavevector dispersion of the first and second subband at zero magnetic field. k_F and E_F are the Fermi wavevector and Fermi energy. The right panel shows the quantization of the electron energy due to the presence of a magnetic field. The resulting energy levels are split by the cyclotron energy, $\hbar\omega_c = \hbar eB/m^*c$. The electron spin results in an additional splitting of the "cyclotron energy levels" by the spin gap.

2.3 Basic Properties: zero magnetic field

The reduced dimensionality to two dimensions gives rise to some interesting properties, such as a constant density of states and Fermi energy dependence on density different from that of bulk 3D GaAs. We explore the basic properties of the two dimensional electron system (2DES) by analyzing the density of states, starting with an exploration of the number of states with respect to wavevector that yields $n = g_s k_F^2/4\pi$, where g_s is the factor of 2 from spin degeneracy of electrons. We can derive an expression for the Fermi energy for a 2DES, $E_F = \frac{2\pi\hbar^2 n}{m^*}$ [43].

Coulomb interactions give rise to much of the interesting physics observed in 2D systems. We can measure the relative strength of the Coulomb energy in the system by defining a dimensionless ratio of the Coulomb energy to the characteristic kinetic energy of the electrons. We can examine two regimes - a classical regime, where the temperature is greater than the Fermi temperature, $T_F = E_F/k_B$ and a quantum regime where the temperature is much less than T_F. It is interesting to find that the density dependence of the relative strength of Coulomb interaction in the system changes in different temperature regimes.

For high temperature conditions ($T > T_F$) we compare the Coulomb energy, $E_C = e^2/\epsilon\overline{r}$, (where $\overline{r}$ is the average inter-particle spacing, and ε is the dielectric constant,) with the energy from thermal fluctuations ($k_B T$). To determine how the relative strength of the Coulomb interaction varies with density as it competes with thermal fluctuations, we examine the ratio

$$\zeta = E_C/k_B T = \frac{e^2/\varepsilon\overline{r}}{k_B T} = \frac{e^2\sqrt{\pi n}}{\varepsilon k_B T} \propto n^{1/2} \tag{2.8}$$

For low temperatures ($T < T_F$), E_C now competes with the E_F and we examine,

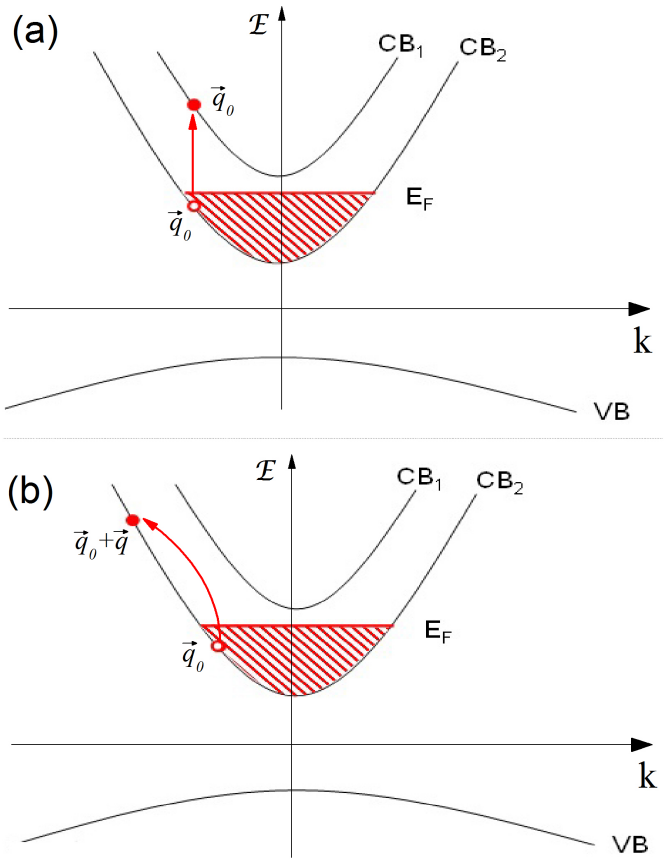

Figure 2.4: Diagram shows (a) intersubband and (b) intrasubband single particle excitations. q is the momentum associated with the intrasubband excitation. Intersubband excitations are excitations that involve more than one subband while intrasubband excitations are excitations that occur on the same subband.

$\xi = E_C/E_F$ to obtain

$$\xi = \frac{1}{\sqrt{n\pi}} \frac{e^2 m^*}{\hbar^2 \epsilon} \propto n^{-1/2} \tag{2.9}$$

The density dependence of ξ is different from that of ζ. That is, for temperatures greater than T_F, the relative strength of the Coulomb interaction increases with increasing density as particles get closer together. The reverse happens in the low temperature limit - as particles move farther apart, the relative strength of the Coulomb interaction increases.

The electrons within the QW can support excitations both within the same subband and across different subbands, as shown in Fig. 2.4. Intrasubband excitations

(excitations with initial and final states within the same subband), have a marked dependence on wavevector.

2.4 2D Systems in Magnetic Fields

The application of a magnetic field to an electron gas has striking consequences. The continuum of energies of the electron gas is quantized into energy levels called Landau levels that are separated by multiples of the cyclotron energy. We can begin to describe this by considering the Hamiltonian:

$$H = \frac{1}{2m^*}\left[\vec{p} + \frac{e}{c}\vec{A}\right]^2 \tag{2.10}$$

where $\vec{p}$ is the in-plane momentum and $\vec{A}$ is the vector potential that satisfies the relation: $\vec{\nabla}\times\vec{A} = B\hat{z}$ for a perpendicular magnetic field B. Depending on the physics we intend to illustrate, the choice of gauge will vary. For the purposes of introducing the energy levels and eigenstates, it is more convenient to use the Landau gauge. Substituting the Landau gauge, $\vec{A} = xB\widehat{y}$, into Eqn. 2.10 yields the following:

$$H = \frac{1}{2m^*}\left[p_x^2 + \left(p_y + \frac{e}{c}Bx\right)^2\right] \tag{2.11}$$

Since there is no y term, H commutes with p_y. That is, $p_y \rightarrow \hbar k_y$ and k_y becomes a cyclic coordinate or a good quantum number for the Landau gauge. Using this translational symmetry in y, we can write the in-plane wavefunction as $\phi_k(\vec{r}) =$

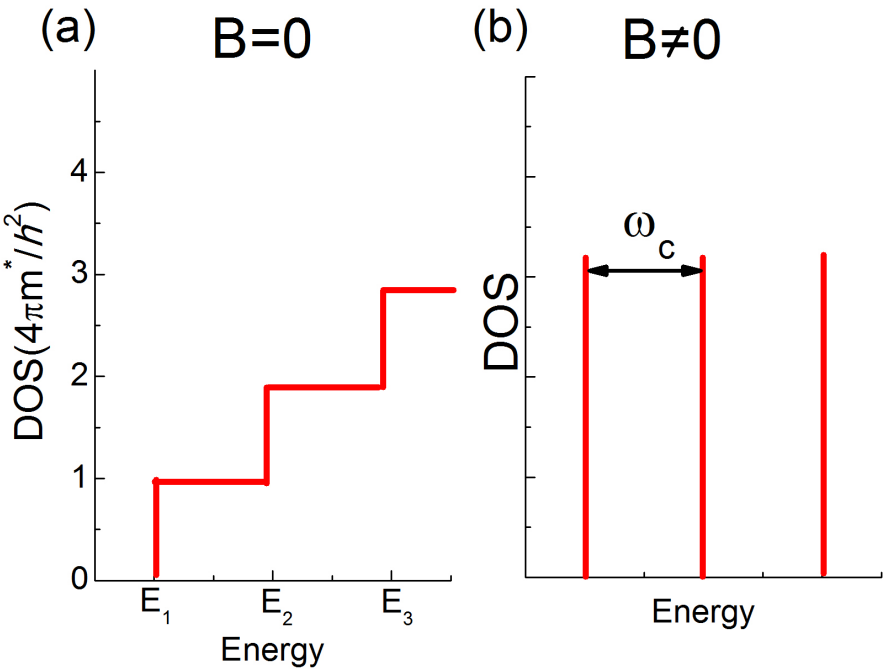

Figure 2.5: (a) The density of states (DOS) of electrons at zero magnetic field is constant within each subband. The DOS is quantized and is a step like function which increases with increasing E_j. (b) The density of states for a finite magnetic field. The energy is quantized into Landau levels which, in the absence of disorder, are δ-functions in the DOS, spaced by the cyclotron energy.

$e^{iky}\xi_k(x)$. Equation 2.11 gives,

$$\begin{aligned} H_k\xi_k(x) =& \frac{1}{2m^*}\left[p_x^2 + \left(\hbar k_y + \frac{e}{c}Bx\right)^2\right]\xi_k(x) \\ =& \left[\frac{p_x^2}{2m^*} + \frac{m^*\omega_c^2}{2}\left(x + k_y l_o^2\right)^2\right]\xi_k(x) \\ =& E_k\xi_k(x) \end{aligned} \tag{2.12}$$

where the cyclotron frequency is $\omega_c = eB/m^*c$, the magnetic length is $l_o = \sqrt{\hbar c/eB}$ and the index k represents the cyclic coordinate k_y. From the second line of Eqn. 2.12 we recognize that this is the familiar one-dimensional harmonic oscillator Hamiltonian centered at $x = -k_y l_o^2$. The energies of the harmonic oscillator are shown in

Eqn. 2.13 and illustrated in Fig. 2.5(b):

$$E_{n,k} = \hbar\omega_c(n + 1/2) \tag{2.13}$$

where n is a positive integer (0,1,2,...). The corresponding eigenstates, known as Landau levels, have single particle wavefunctions represented by,

$$\phi_{n,k}(\vec{r}) = Ae^{iky}H_n((x + kl_o^2)l_o^{-1})e^{-(x+kl_o^2)^2/2l_o^2} \tag{2.14}$$

where H_n are Hermite polynomials. Spin degrees of freedom split the Landau levels by the Zeeman energy, $E_Z = g\mu_B B_T$, where g is the Lande factor, μ_B is the Bohr magneton, and B_T is the total magnetic field. $B_T = B$ for a perpendicular magnetic field. The spin splitting is illustrated in Fig. 2.3.

An important parameter in quantum Hall systems is the filling factor, denoted by ν, which is the number of occupied Landau levels (LL) at a given magnetic field and density. We can write the filling factor as

$$\nu = \frac{n}{G} = 2\pi l^2 n = \frac{n}{B/\phi_o} \tag{2.15}$$

where ϕ_o is the magnetic flux quantum ($\phi_o = hc/e$), n is the electron density and G is the degeneracy per unit area of each LL ($G = 1/2\pi l_o^2 = B/\phi_o$). As B increases, the cyclotron energy increases, the inter-LL spacing increases and consequently fewer *Landau* levels are filled. Note that a non-integer value of ν indicates partial occupation of the highest populated LL.

2.5 Quantum Hall Effects

In 1879 E.H. Hall [44] discovered that electric currents exhibit surprising behavior in a magnetic field. That is, in the presence of a magnetic field (as shown if Fig.2.6) and an applied voltage (longitudinal voltage, V_{xx}), an induced voltage (or transverse voltage V_{xy}) arises that is perpendicular to the applied current, I. The effect was shown to arise from the Lorentz equation,

$$\vec{F} = e(\vec{E} + \frac{1}{c}\vec{v} \times \vec{B}) \tag{2.16}$$

that is, for $E = E\hat{y}$ and $B = B\hat{z}$, a drift velocity arises that is $\vec{v} = e\frac{E}{B}\hat{x}$. If the current is given by $\vec{j} = en\vec{v}$ (e is the charge, n is the 2D density), then we can define a Hall resistivity as follows:

$$\rho_H = \frac{E_y}{J_x} = \frac{B}{nec} \tag{2.17}$$

The Hall resistance, ρ_H in the classical limit is a linear function of the magnetic field

2.5.1 Integer Quantum Hall Effect

A remarkable, unexpected twist to the classical Hall effect was discovered by K. von Klitzing et al. in 1980 [45, 2]. In higher quality 2D electron systems, at lower temperatures and higher magnetic fields the Hall resistance, $R_H = V_H/I$ becomes quantized ($R_H = \rho_H$ in two dimensions). The phenomenon is known as the integer quantum Hall effect (IQHE). Remarkably, the quantization occurs at integer multiples of fundamental constants: $R_H = h/\nu e^2$. Quantum Hall traces (plots showing $R_{xx} = V_{xx}/I$ and $R_{xy} = V_{xy}/I$ versus magnetic field) reveal the existence of plateaus at the special values of $R_H(\nu)$. It was this deviation from the linear behavior in the Hall resistance and its 'exact' quantization that made the IQHE so striking. See Fig.

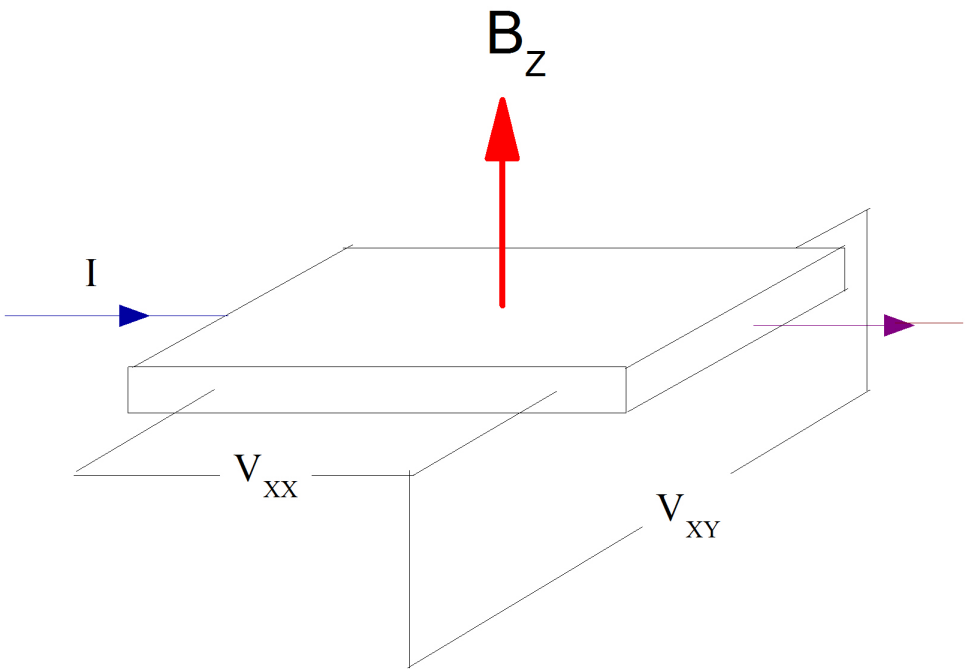

Figure 2.6: Schematic of the Hall resistance measurement set up. The GaAs/AlGaAs heterostructure is placed in a perpendicular magnetic field while current, I flows along the x direction. Longitudinal and transverse voltage is measured as shown by V_{xx} and V_{xy} respectively.

2.7. The origin of plateaus is linked to residual disorder in the 2DES[4]. Residual disorder gives rise to localized states which manifest plateaus in the quantum Hall trace. We can illustrate this nicely if we fix the magnetic field and tune the density - we add electrons so that the Fermi level traverses a region of localized states. The additional electrons will be captured by the localized states and consequently not contribute to transport. The localized states act like a reservoir for the electrons. As a result the Hall resistance remains constant, with small changes in density, as a "magic" filling factor is traversed.

Another important feature of the integer quantum Hall effect is "superflow" current (current flows while resistance goes to zero) in R_{xx} shown as minima in the quantum Hall trace. Also, R_{xx} displays Arrhenius behavior such that, $R_{xx} \sim exp\big(-\Delta/2k_BT\big)$; where $\Delta(\nu)$ is the activation gap for the quantum Hall states and is filling factor dependent. As the temperature approaches zero, $R_{xx} \longrightarrow 0$. That is, there is dissipationless transport.

The seminal work of von Klitzing [2] highlighted the fact that the combination of fundamental constants, h/e^2 has the unit of resistance. Moreover, it provided another means to measure the fine structure constant, $\alpha = e^2/\hbar c$. The Hall quantization in this remarkable phenomenon is universal; it is independent of sample geometry, and material parameters such as the dielectric constant and the electron effective mass.

2.5.2 Fractional Quantum Hall Effect

Two years after von Klitzing's discovery of the integer quantum Hall effect, another unexpected discovery in quantum Hall physics was made by Tsui, Stormer and Gossard. In 1982, the fractional quantum Hall effect [46, 47, 3] was introduced to

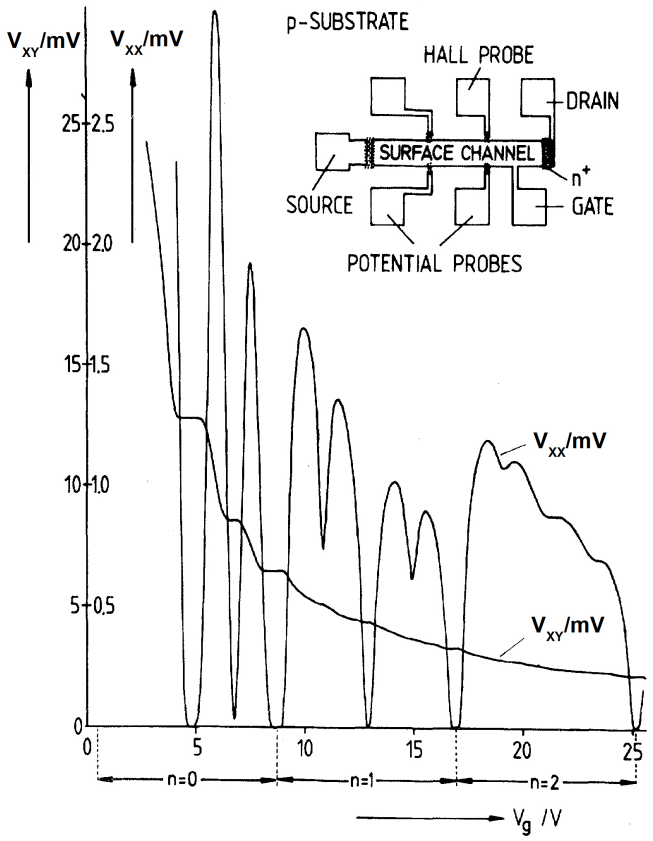

Figure 2.7: Data of a Hallbar measurement which exhibits the integer quantum Hall effect. Both the longitudinal, V_{xx} and transverse, V_{xy} voltage are plotted. V_{xy} forms plateaus and is a monotonically increasing function of the filling factor, ν. ν is tuned by changing n (by applying a gate Voltage, V_g as shown in this figure). V_{xx} has minima which coincide with formation of plateaus in the longitudinal resistance[2].

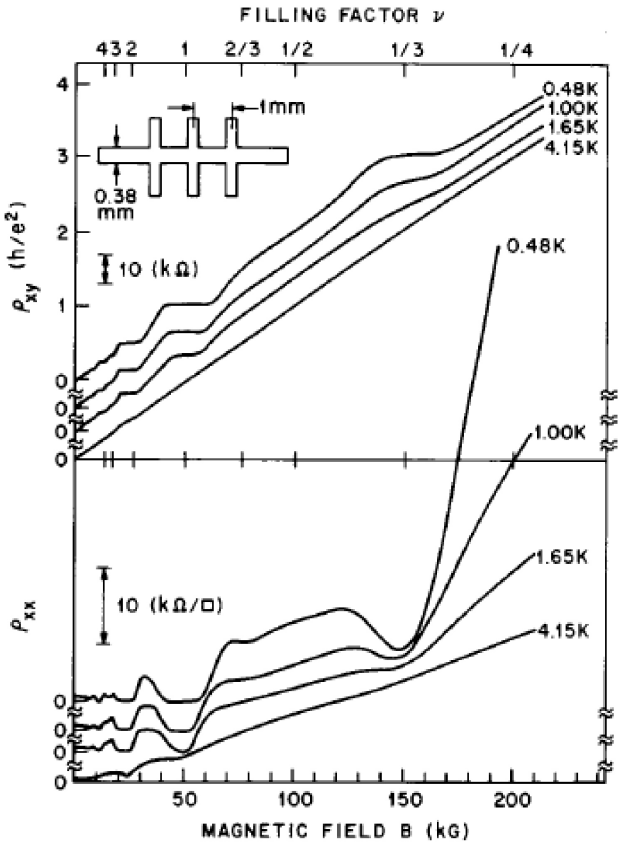

Figure 2.8: Plot of Hallbar measurements which exhibit the fractional quantum Hall effect. The longitudinal resistance, ρ_{xx} and transverse resistance, ρ_{xy} are plotted. ρ_{xy} is a monotonically increasing function of the magnetic field and has plateaus at filling factors which coincide with minima in ρ_{xx}. The fractional filling factor, ν =1/3 was observed for the first time by Stormer, Tsui and Gossard [3]. Extracted from Ref. [3].

the world and described a new class of quantized Hall plateaus defined as

$$R_H = h/e^2\nu \tag{2.18}$$

where ν can be a rational fraction. The state at $\nu = 1/3$ was the first fractional quantum Hall state discovered as shown in Fig. 2.8.

2.5.2.1 Composite Fermions

Prior to the discovery by Tsui, Stormer and Gossard, a theory that predicted the FQHE did not exist. A theory of the fractional quantum Hall effect should explain its behavior both quantitatively and qualitatively. It should explain essential features of the fractional quantum Hall effect such as the sequence of observed fractions, the plethora of states in the lowest *Landau* level (LLL) and the conspicuous absence of states in the higher *Landau* levels ($N \geq 2LL$). In addition, it should include the electron spin as a degree of freedom.

Typically one starts with analyzing the Hamiltonian to try to extract the behavior of the system by tackling the eigenvalue problem, where,

$$\begin{aligned} H\Psi =& E\Psi \\ H =& \sum_j \frac{1}{2m^*}\left[\frac{\hbar}{i}\nabla_j + \frac{e}{c}\vec{A}(\vec{r_j})\right]^2 \\ &+ \frac{e^2}{\varepsilon}\sum_{j<k}\frac{1}{|\vec{r_j}-\vec{r_k}|} \\ &+ \sum_j U(\vec{r_j}) + g\mu_B \vec{B}\cdot\vec{S} \end{aligned} \tag{2.19}$$

The first term in Eqn. 2.19 represents the kinetic energy in a magnetic field with vector potential $\vec{A}$. The second term represents the Coulomb interaction (j and k are indices that label the electrons in the 2D system). The third and fourth terms represent the disorder potential and the Zeeman energy respectively. We will "turn off" these last two terms as simplifying assumptions in our first attempt in tackling the eigenvalue problem. To justify this approach we note that these various terms have different energy scales. In GaAs, with dielectric constant, ε=12.6 and *Lande′* g factor of -0.44, we can consider the following energies to get a feeling for their

relative importance in our GaAs quantum well.

$$\hbar\omega_c = \frac{\hbar eB}{m_b c} \sim 20B[T]K$$
$$V_C = \frac{e^2}{\epsilon l_o} \sim 50\sqrt{B[T]}K$$
$$E_z = 2g\mu_B \vec{B} \cdot \vec{S} = \frac{gm_b}{2m_e}\hbar\omega_c \sim 0.3B[T]K$$
$$l_o = \left(\frac{\hbar c}{eB}\right)^{1/2} \sim \frac{25nm}{\sqrt{B[T]}}$$

The cyclotron energy is always much bigger than the Zeeman energy. The Coulomb term is stronger than the cyclotron energy for small fields but weaker for fields above $\sim 6T$.

Further simplifications can be made in addition to turning off the disorder potential and freezing the spin degrees of freedom. If one considers only behavior in the lowest *Landau* level, one can ignore the energy contribution from the first term in Eqn. 2.19, leaving only the Coulomb term. The reason one can ignore the first term is that it is a constant in the lowest Landau level, and does not play a role in describing the essential physics of the FQHE. The essence of the problem is thus contained in the Coulomb part of the Hamiltonian in Eqn. 2.19:

$$H = \frac{e^2}{\varepsilon} \sum_{j<k} \frac{1}{\vec{r_j} - \vec{r_k}} \tag{2.20}$$

At first glance, the problem is deceptive in its apparent simplicity. In fact, it cannot be solved using a brute force computational approach as this is prohibitive due to the massive incalculable size of the Hilbert space. A solution that involves a perturbative approach is impossible, as there are no small parameters.

Instead, one must use experiment as a guide with which to build a theory that satisfies observations made in the real world. Shortly after the discovery of the

fractional quantum Hall effect, Laughlin was the first to develop a working model that described some states of the FQHE, as we will describe as follows. To find the wavefunction for FQHE states, start with the single particle state of an electron in the lowest Landau level. To do this, it is necessary to consider the first term in Eqn. 2.19. It is convenient for this part of the discussion to write the vector potential, $\vec{A}$ in the symmetric gauge, such that, $\vec{A} = 1/2(\vec{B} \times \vec{r}) = \frac{B}{2}(-y, x, 0)$. In this gauge the eigenvalues of angular momentum, L_z are good quantum numbers [4, 48]. The single particle state in the LLL is the following [4]:

$$\eta_l(z) = (2\pi 2^l l!)^{-1/2} z^l e^{-\frac{1}{4l_o{}^2}|z|^2}$$

with $z = x - iy$ and l being an eigenvalue of L_z. The many electron wavefunction can be written as

$$\Psi = F_A[\{z_j\}] exp\big[-\frac{1}{4}\sum_l |z_l|^2\big] \tag{2.21}$$

where F_A is a polynomial of $z's$ antisymmetric under exchange of two coordinates (the spin part is symmetric and not explicitly shown here). The task is to find $F_A[\{z_j\}]$ as a function of ν.

For the state at ν=1, we note that the wavefunction can be written as follows [4, 49],

$$\Psi_{\nu=1} = \prod_{j<k}(z_j - z_k) exp\big[\frac{-1}{4l_o^2}\sum_l |z_l|^2\big] \tag{2.22}$$

where indices, j,k, and l run from 1 to N, the number of particles.

For $\nu = 1/3$ one can assume that $F_A[\{z_j\}] = \prod_{j<k} f(z_j - z_k)$, where f(z) is $z^{(\phi+1)}$ (where ϕ is an even integer because Ψ has to be antisymmetric under the exchange of two electrons) [49]. This choice of $F_A[\{z_j\}]$ resulted in the Laughlin wavefunction:

$$\Psi_{1/(\phi+1)} = \prod_{j<k}(z_j - z_k)^{\phi+1} exp\big[-\frac{1}{4l_o^2}\sum_l |z_l|^2\big] \tag{2.23}$$

where the choices $\nu = 1/(\phi + 1)$ are defined to be the Laughlin fractions ($\phi = 2$ for $\nu = 1/3$). The caveat of this approach, albeit a brilliant first ansatz, is that it does not describe all the fractions of the FQHE. Further work had to be done to accomplish a more robust theoretical model. Haldane attempted to describe the FQHE states in a hierarchy of "parent" and "daughter" states [50], but was not successful in earnestly predicting experimental results. A more robust theory was needed.

The following approach was motivated by the idea of emergent phenomena and led to the development of "Composite Fermions". Emergent phenomena arise out of collective behavior or many body effects; that is, new physics can emerge when many individual entities act in unison to give rise to a new entity. For instance, many water molecules act together to give rise to water waves. Water waves cannot be attributed to a single water molecule but instead is a property of many molecules. P.W. Anderson's 1972 article, "More is different" [51], highlights the importance of emergent phenomena in physics. We seek to draw an analogy with emergent particles in other condensed matter systems (such as phonons, magnons, Landau quasiparticles and cooper pairs) to the FQHE in order to uncover the emergent "particle" of the FQHE. If we identify such emergent "particles", we can then identify their weak interactions that can be used in our perturbative machinery. Jain first proposed the idea of composite fermions (CFs) - the emergent "particles" of the FQHE systems - that explain the FQHE [52]. A composite fermion is a bound state of an electron and an even number of quantized vortices [4]. The vortices arise from the phase added to the electron wavefunction due to the presence of the vector potential. The vortex of the FQHE is different from the vortex of superconductivity. Instead the vortex of FQHE is a property of the many-body wavefunction of the quantum fluid in Eqn. 2.23. Recall that the complex function, $z = re^{-i\theta}$ has a vortex at the origin since a complete loop around the origin changes θ by -2π. It follows that $(z - z_0)$

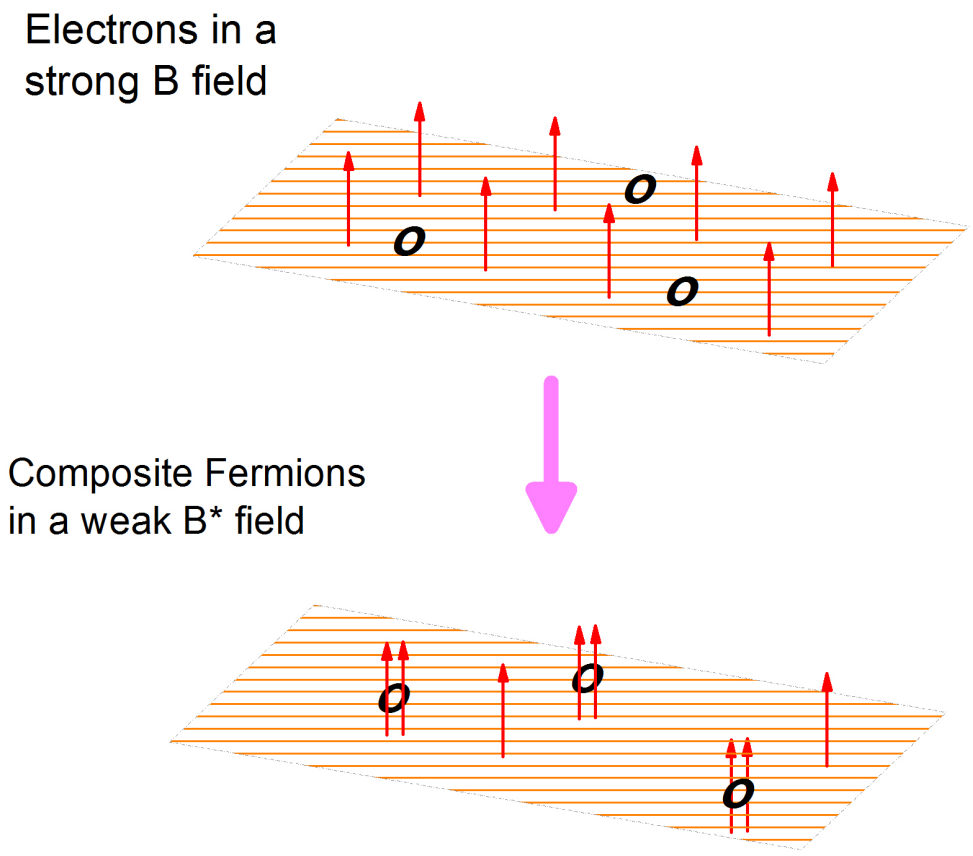

Figure 2.9: Schematic of the formation of composite fermions from interacting electrons in a magnetic field. In the top panel there are three electrons. In the bottom panel these three electrons bind two flux quanta each to form composite fermions in a reduced effective field, B^*. Extracted from Ref.[4, 5].

has a vortex at z_0 and in the case of $(z_1 - z_2)^\phi$, z_1 has ϕ vortices at z_2 and vice verse for z_2. An alternative, qualitative definition for a CF is that it is a bound state of an electron and an even number of magnetic flux quanta, where one quantum, $\phi_o = hc/e = 2\pi l_o^2 B$. Though fluxes do not actually bind electrons in reality and B is uniform throughout the sample (there is no bunching of the field), the "bound flux model" still describes the results quite well. The "binding of flux quanta" to electrons is illustrated in Fig. 2.9.

The next step of explaining the FQHE is to consider the FQHE as an IQHE of composite fermions [4]. The composite fermions live in an effective field, B^* [4].

The total perpendicular field is such that, $B = B^* + \phi n \phi_o$, giving rise to an effective filling factor, $\nu^* = n\phi_o/|B^*|$. Consequently, the resulting fractions may be written as follows: $\nu = \frac{\nu^*}{\phi\nu^* \pm 1}$. The $\pm$ sign in the denominator corresponds to positive and negative values for B^*. Composite fermions form "Landau-like" energy levels called Λ levels that are spaced by an effective cyclotron energy. The notion of Λ levels and fractional filling factor is depicted in Fig. 2.10

Let us examine the wavefunction for composite fermions. We start by rewriting the Laughlin wavefunction in the following convenient form:

$$\Psi_{1/(\phi+1)} = \prod_{j<k} (z_j - z_k)^{\phi} \Psi_{\nu=1} \tag{2.24}$$

Upon examination of Eqn. 2.24, we see that the wavefunction has been constructed by taking the state at $\nu = 1$ and associating ϕ vortices to the wavefunction of each electron. This "binding" of an even number of vortices, ϕ to electrons forms composite fermions that obey fermionic statistics [52]. Based on this observation, Jain suggested the following trial wavefunction for the states $p/\phi p + 1$ [52], where p is an integer, such that $p = \nu^*$:

$$\Psi_{p/(\phi p+1)} = \hat{P}_{LLL} \prod_{j<k} (z_j - z_k)^{\phi} \Psi_{\nu=p} \tag{2.25}$$

where the projection operator, $\hat{P}_{LLL}$, projects the composite fermion wavefunctions into the lowest Landau level [53, 52, 54]. That is, the wavefunctions for fractional states ($\nu = p/(\phi p + 1)$) can be derived from those of IQHE states ($\nu = p$) and the use of the projection operator.

The binding of vortices to electrons reduces the overall energy of the system and makes CFs the favorable ground state [4]. The CF formulation agrees with many features of experiment and makes it a reasonable theory. The FQHE is like an IQHE

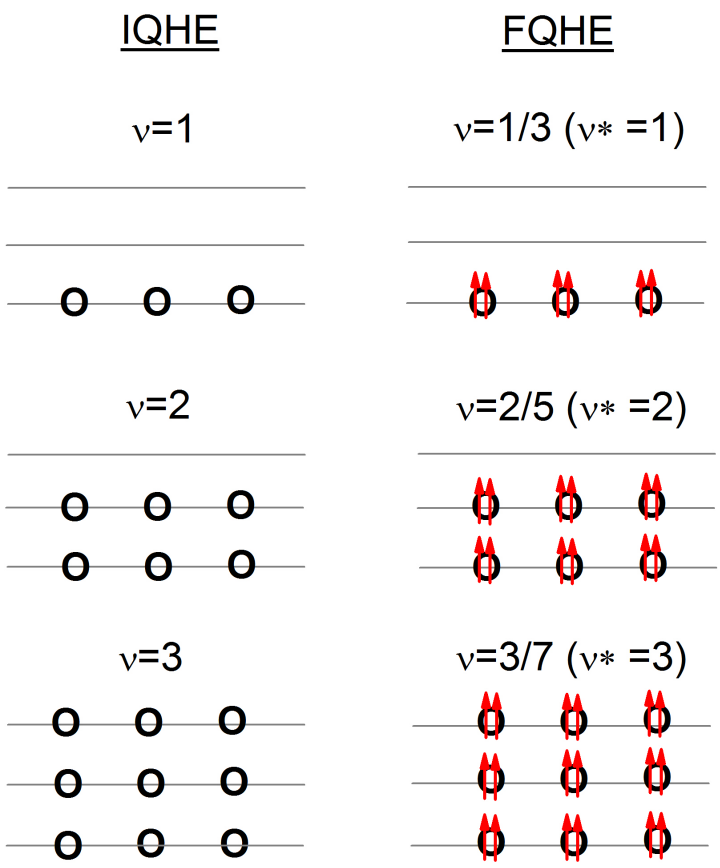

Figure 2.10: The left panel shows electrons occupying a varying number of Landau levels spin split by the spin gap (not shown explicitly). The right panel shows the analogous picture for the fractional quantum Hall effect. Composite fermions fill Landau-like levels called Λ levels, just as electrons fill Landau levels in the IQHE. Whereas the Landau levels are spaced by the cyclotron energy, the Λ levels are split by the effective cyclotron energy. The spin gap is the same for both the IQHE and the FQHE. Extracted from Ref. [4].

of 'new' or emergent particles which we call CFs.

2.5.2.2 Composite Fermions and Spin

In the previous section, we assumed fully spin polarized composite fermions. Experiments have shown that spin degrees of freedom do play a very important role in the understanding of the fractional quantum Hall effect. Understanding the spin degrees of freedom of composite fermion systems will be a major part of this thesis. To articulate how spin may become important, we can compare E_z to the energy of the highest occupied Λ level. If the spin gap is larger than the Fermi energy, then the composite fermions will be spin polarized. That is, only spin up Λ levels are populated, the lowest energy spin down Λ level having greater energy than E_F. Figure 2.10 illustrates the case for $\nu^* = 4$ (4 Λ levels of CFs filled), where CFs can be polarized, partially polarized or unpolarized depending on the magnitude of the Zeeman energy relative to the Fermi energy.

A more formal description of spin can be gained from extending the Hamiltonian described in Eqn. 2.20 by turning on the spin interaction [4]:

$$H = \frac{e^2}{\varepsilon} \sum_{j<k} \frac{1}{|\vec{r_j} - \vec{r_k}|} + g\mu_B B S_z \tag{2.26}$$

We can write down the spin part of wavefunction after we define the density of spin up and spin down CFs such that, $n = n_\uparrow + n_\downarrow$. The spin part of the wavefunction can then be written as, $\Phi_{n_\uparrow, n_\downarrow} = \Phi_{n_\uparrow} \Phi_{n_\downarrow}$. We can also define spin polarization, γ_p, as

$$\gamma_p = \frac{n_\uparrow - n_\downarrow}{n_\uparrow + n_\downarrow} \tag{2.27}$$

The total wavefunction for composite fermions in terms of spin eigenfunction is

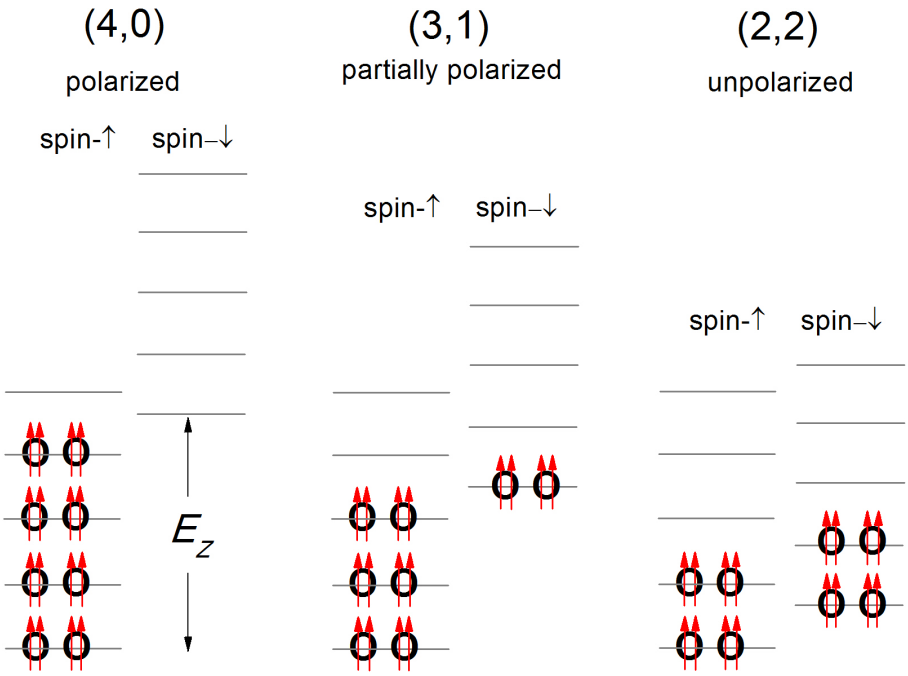

Figure 2.11: Spin polarization in the FQHE manifests itself depending on the relative characteristic energies of the system - the Zeeman energy, effective cyclotron energy and the Fermi energy. This figure considers an example in which four Λ levels are populated. In each panel the energy levels either have spin up (left column) or spin down (right column) CFs. The CFs shown have two flux quanta bound to each electron. The left panel has the Zeeman energy larger than the Fermi energy resulting in fully spin polarized CFs. The CFs have 4 spin up levels populated and 0 spin down levels populated, shown as (4,0). The center panel has slightly lower Zeeman energy such that the Fermi energy is higher than the lowest spin down level. Consequently, one spin down level is populated and the system becomes partially polarized (3,1). The right panel has Zeeman energy much lower than the Fermi energy. This allows for two spin down levels to be populated resulting in a total loss of polarization. Extracted from Ref.[4].

consequently [4]:

$$\Psi_{\frac{p}{\phi p+1}} = \hat{P}_{LLL}\Phi_{n_\uparrow,n_\downarrow}\Phi_l^\phi \tag{2.28}$$

From Eqn. 2.28 we see that the total wave function is coupled to the spin properties of the state. This is an important fact that will be highlighted further in the upcoming chapters.

2.6 Quantum Phase Transitions in 2D electron systems

The concept of phase transitions is pervasive in condensed matter physics and is an important facet of quantum Hall physics. These transitions often involve a change in the symmetry of the system and can be classified in terms of certain characteristics. For instance, first order phase transitions can be loosely described as those transitions which have a discontinuity in the derivative of the free energy[55]. Second order transitions are smooth in the first derivative of the free energy but have a discontinuity in the second derivative. The water to ice transition is an example of a first order phase transition. First order phase transitions typically involve a latent heat at the transition. An example of second order phase transitions is the ferromagnetic to antiferromagnetic transition in magnets where the transition occurs at the Curie temperature. Quantum phase transitions, instead, occur at zero temperature and typically have tunable parameters like pressure or magnetic field which induce the transition.

Phase transitions play key roles in low-dimensional electron systems. A well known example, first proposed by Wigner [56] involves a transition from an electron fluid to an electron solid at zero temperature due to a decrease in electron density. Dominating Coulomb interactions cause classical and quantum phase transitions

to highly correlated states. These transitions typically accompany a change in the symmetry of the state, which may be engendered by a modification in the charge distribution dictated by the electron interaction.

For 2DES's, we have already shown (section 2.3 on Basic Properties) that the parameter ξ is a measure of the relative strength of the Coulomb interaction to the kinetic energy. It has a critical value where a quantum transition can occur. That is, at this critical value, the energy due to Coulomb interactions dominates kinetic energy and the electrons crystallize.

We will come across more examples of quantum phase transitions in later chapters. Identifying phase transitions will be an important undertaking for understanding quantum Hall systems.

2.7 Quantum Regimes in N=0,1,2 *Landau* Levels

The general features of magnetoresistance measurements vary depending of the *Landau* level. Figure 2.12 shows some of these features for small and large values of filling factor. Upon careful examination one finds the following: The first LL is speckled with a myriad of fractional quantum Hall states (that is, R_{xx} goes to zero for fractional values of ν). The second LL comprises precious few FQHE states, while in higher *Landau* levels, these states are entirely absent. More compelling is the unusual behavior of quantum Hall traces in the $N \geq 1$ LL that is described by reentrant integer quantum Hall states (RIQHE). These states are characterized by having integer quantum Hall resistance values while having non-integer filling factors. These RIQHE states are entirely absent in the LLL. Remarkably, they are a common feature of the excited LLs. Another interesting feature of the excited LLs is the presence of phases with anisotropic transport [40], commonly referred to as "stripe phases". Anisotropic transport is clearly seen in Fig. 2.12 for $\nu > 4$.

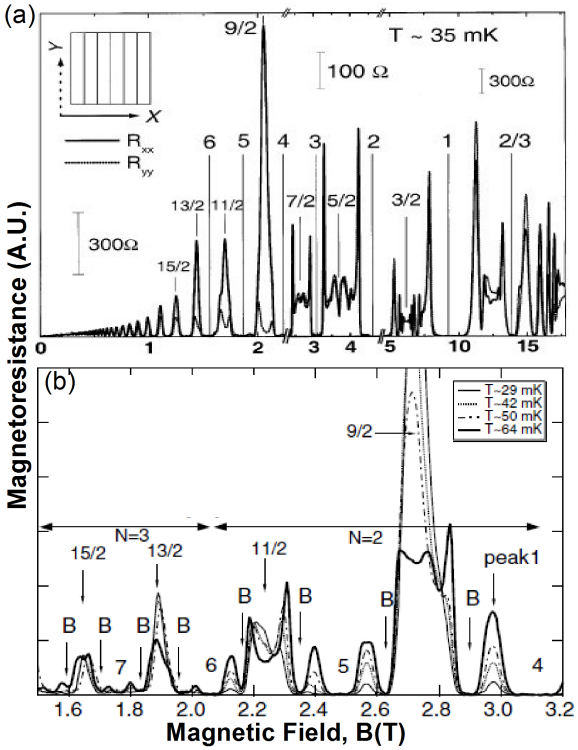

Figure 2.12: (a) Overview of magnetoresistance values across a wide range of magnetic fields. Hall resistance values, $R_{xx} = V_{xx}/I$ and $R_{yy} = V_{yy}/I$ are shown for the x and y directions. The difference in conductivity depending on direction illustrates anisotropic transport. The inset delimits the x and y directions[6]. (b) The R_{xx} plot highlights the presence of bubble phases (RIQHE phases), delimited by "B"[7].

2.7.1 Wigner Crystals, Bubble phases, Stripe phases, Nematic phases and more

Hartree-Fock calculations predicted the formation of a charge density wave (CDW) of electrons in the LLL [57, 58, 59]. These CDW states were expected to be in the form of a Wigner crystal, or a triangular lattice of electrons in two dimensions [56]. This prediction holds for filling factors $\nu < 1/5$, however, for the most part, the LLL is dominated by fractional quantum Hall fluids (FQHL). Nevertheless, the predictions from Hartree-Fock theory become pervasive in the higher LL's [60, 61, 62]. This is a consequence of the different nature of the electron wavefunction in the LLL and the excited LL's. The FQHL is favored in the LLL because the electron wavefunction lacks a node [40], whereas, in the excited LLs, the wavefunction has a node. The nodes reduce the short-range Coulomb repulsion between electrons and blocks the electron-electron correlations that are needed for the formation of the fractional quantum Hall liquid. This key difference in the wavefunction allows for the strikingly different behavior of the phases and plays a substantial role in the relative energetics of the various phases. A detailed discussion can be found in Ref. [21, 22]. In the excited LL's, Hartree-Fock theory predicts, as mentioned in the previous section, the formation of electron solid phases or CDWs of which there are two main categories: bubble phases and stripe phases. Bubble phases comprise a triangular lattice of electron clusters with M electrons per site. Where M=1, we recover the Wigner crystal. Stripe phases are described as being parallel lines of charge, oriented due to some unknown source of rotational symmetry breaking. Moreover, it has been found that thermal and quantum fluctuations could give rise to liquid crystal like phases such as nematic and smectic phases [63]. This adds to the richness of CDW phenomena in the excited LLs.

There is a great deal of evidence from transport [40, 7, 6, 64] and microwave

resonance measurements [23, 35, 65] for the existence of CDW states in the excited LL's. For instance, the anisotropic transport seen in the excited LL's can be explained by the presence of stripe phases - charge transport is only allowed along the direction parallel to the lines of charge and is insulating in the perpendicular direction. RIQHE states arising from bubble phases have isotropic transport and are insulating because of the localization of charge to binding sites in the disorder potential. Work done with microwave resonance claims to be able to detect the vibrational modes of these pinned electron solids.

2.7.2 Competing phases

As I have discussed, there are a great many different phases in two dimensional electron systems in a magnetic field. Revealing interplays between these different phases constitutes a major goal of this dissertation. There is evidence (from transport and microwave resonance studies) for the existence of competing electron fluid and charge density wave phases in the excited LL's. We will use ILS to further probe competition between phases in higher *Landau* levels. This competition is marked in the $N = 1$ and $N = 2$ LL's [7, 66]. The presence of competing phases is not surprising as the ground state energies of these phases are often closely spaced [67], allowing for small changes in some tunable parameter to favor one phase or the other.

Chapter 3

Optical Spectroscopy

3.1 Light Scattering

3.1.1 Overview

Light scattering is pervasive in many aspects of condensed matter science. Since the discovery of Raman scattering by Sir Chandrasekhara Venkata Raman in 1928[68], it has become an invaluable characterization tool for a large variety of condensed matter systems. I will give a brief outline of light scattering focusing on its relevance in two dimensional electron systems (2DES). An account of the history and theory can be found in the book by Hayes and Loudon [69]. I will address how light scattering can be used to characterize 2DES, in AlGaAs/GaAs heterostructures, in both zero and nonzero magnetic field. In particular, I will provide a framework for understanding the heart of this dissertation - remarkable behavior of composite fermions excitations, exotic quasiparticles in the second *Landau* level and striking differences among the excitations in the N=0,1 and 2 LL's.

Of particular interest here is inelastic light scattering (ILS) and Rayleigh scattering (elastic light scattering, RS)[69]. The term "Raman scattering" tradition-

ally refers to scattering of light by optical phonons in solids and by molecular vibrations[70]. In this thesis, I will use Raman scattering to refer to a broad class of inelastic light scattering phenomena, including scattering from elementary excitations associated with degrees of freedom of ions and electrons in crystalline solids. A few exceptions are long wavelength acoustic phonons (sound waves) and acoustic magnons, which belong to a class of inelastic scattering called Brillouin scattering (the energy shifts that are studied here overlap with those of Brillouin scattering). In its simplest form, ILS can be described as a two photon process - the simultaneous annihilation and creation of incident (ω_L) and scattered (ω_S) photons in the scattering medium. Single photon processes also occur and involve optical absorption or optical emission of photons by a medium. Optical emission can be important for exploiting resonance enhancement in ILS measurements. That is, it is useful in identifying the appropriate energies for resonance enhancement. I will describe this in more detail at the end of this chapter.

The two-step light scattering process as a whole satisfies energy conservation rules. However, each step is a virtual process that does not satisfy energy conservation. Incoming photons with energy ω_L, wavevector $\vec{k}_L$ and polarization $\hat{e}_L$ interact with the medium in a manner that results in the creation of a scattered photon of energy ω_S, wavevector $\vec{k}_S$ and polarization $\hat{e}_S$. Energy conservation implies that $\omega_L = \omega_S \pm \omega$. In translationally invariant systems, the wavevector must be conserved in every step of the process. Consequently, the wavevector of the excitation, $\vec{q}$ is equal to the in-plane momentum transferred to the 2DES, $\vec{k} = \vec{k}_L - \vec{k}_S$. Nevertheless, the presence of disorder breaks translational symmetry and gives rise to the break-down of wavevector conservation, some of the momentum being transferred to defects in the sample.

When $\omega_S < \omega_L$, energy is transferred to the 2DES and an excitation at energy ω is created. The process is known as Stokes scattering. If $\omega_S > \omega_L$ then an excitation

is annihilated in the 2DES and the process is known as anti-Stokes scattering. The ratio of intensities of anti-Stokes and Stokes scattering is given by

$$\frac{I_{AS}}{I_S} = \frac{R_{AS}(\omega_L, \omega_{AS})}{R_S(\omega_L, \omega_S)} \frac{n(\omega)}{n(\omega)+1} \tag{3.1}$$

where $R_{AS(S)}$ depends on ω_L, the Stokes scattering photon energy ω_S, and the anti-Stokes scattering photon energy ω_{AS}. $n(\omega) = [exp(\hbar\omega/k_BT) - 1]^{-1}$ is the Bose-Einstein thermal factor[69]. When $R_{AS} \sim R_S$, $I_{AS}/I_S = exp(-\hbar\omega/k_BT)$. At low temperature, such that $\hbar\omega \gg k_BT$, the anti-Stokes intensity is negligible when the electrons are in thermal equilibrium with the sample. In this thesis, I will consider only Stokes scattering.

Spectra in Fig. 3.1 show the energy of the laser, Stokes peak and anti-Stokes peak on two scales: an absolute energy scale and an energy shift scale. One advantage of displaying Raman scattering on both energy shift and absolute energy scales is being able to distinguish between optical emission (single photon processes) and inelastic light scattering (two photon processes), as will be detailed below.

In addition to ILS by collective and single-particle modes of the system, it is also possible for incident photons to excite photoluminescence (optical emission) transitions. The 2DES system absorbs the incident photons by creation of electron-hole pairs across the semiconductor band gap. Photon emission occurs after relaxation of the pair into a state with an allowed optical transition. Because the energy of the emitted photon via luminescence is related only to the energy of the relaxed state, there is little, if any, dependence of the emitted photon frequency on ω_L. Figure 3.2 illustrates that as ω_L is tuned, both Raman peaks and the laser peak shift, while optical emission peaks have fixed energy. To the contrary, on an energy shift scale, optical emission peaks move while Raman peaks are fixed.

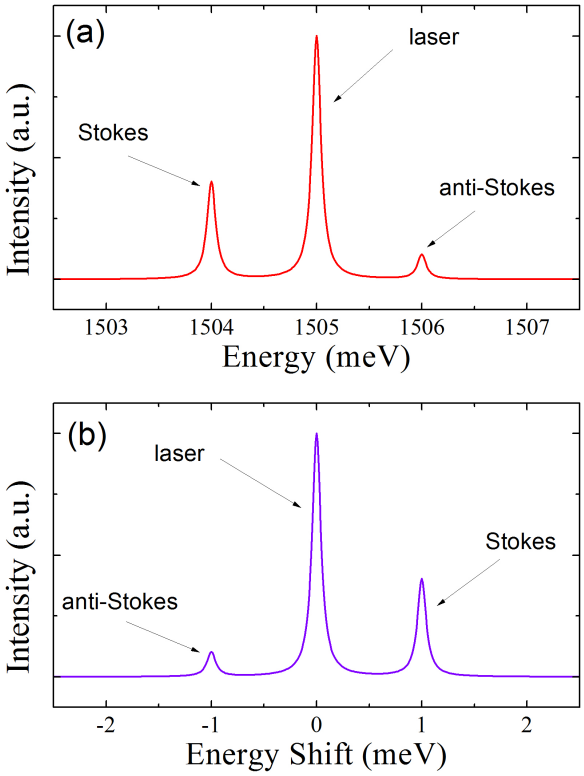

Figure 3.1: Sketch of a light scattering spectrum. Elastic scattering from the laser at ω_L, Stokes scattering from an electronic excitation at $\omega_S = \omega_L - \omega$ and anti-Stokes scattering at $\omega_{AS} = \omega_L + \omega$ are all clearly visible. The spectrum is plotted on different scales: (a) an absolute energy scale; showing the laser peak at ω_L, the Stokes shifted Raman peak and the anti-Stokes shifted peak and (b) an energy shift scale; with positive shift corresponding to lower energy. That is, the laser peak and Raman scattered peaks are on a scale where ω_L is defined to be at zero energy shift, such that Stokes peaks are shifted to the right of ω_L.

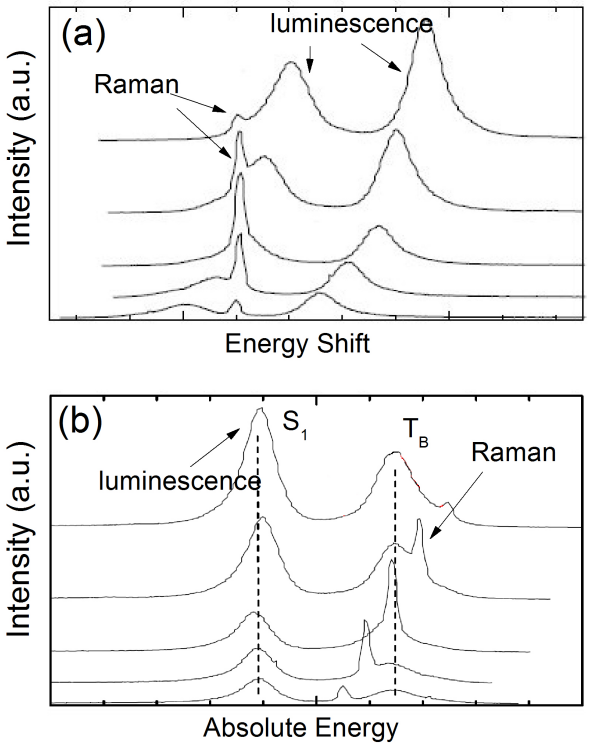

Figure 3.2: Spectra measured at various ω_L translated vertically for clarity (extracted from Refs. [8, 9]) show Raman peaks alongside photoluminescence peaks. The spectra are plotted (a) on an energy shift scale. The mode at a constant shift is inelastic light scattering from the Kohn mode at the cyclotron energy, ω_c of the 2DES. (b) Spectra are plotted on an absolute energy scale. Optical emission (luminescence) peaks are fixed on an absolute energy scale. The peaks labeled S_1 and T_B are identified as photoluminescence.

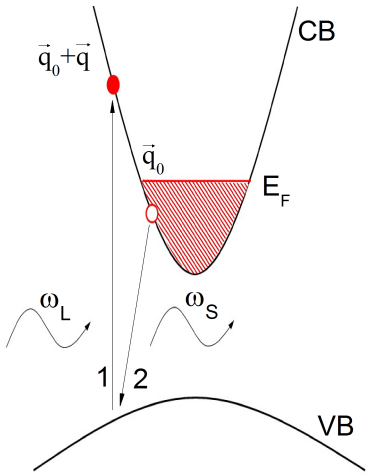

Figure 3.3: Transition diagram that describes single particle excitations from two-step light scattering processes in 3D bulk GaAs. The numbers show the time-ordering of the transitions. ω_L and ω_S are the incident and scattered photons respectively. q is the momentum associated with the intraband excitation, where $q+q_o$ is the wavevector of the excited electron.

3.1.2 Light Scattering in 3D systems: Mechanism and Selection Rules

An overview of light scattering is first given for 3D systems so that we can segue into studying the system of interest - two dimensional electron systems. Though I will try to provide a fairly in-depth framework of the light scattering process, only the main results of the discussion will be pertinent for the following chapters.

The mechanism of inelastic light scattering involves the coupling of the electric moments of the scattering medium to incoming and outgoing photons. For visible or infrared light, the dominant contributions to these electric moments come from the excitations of electrons across energy band gaps, as illustrated in Fig. 3.3. Coupling of ω_L and ω_S to the medium is understood as the modulation of the electric susceptibility by elementary excitations.

The coupling of light to optical transitions of the scattering medium is enhanced when ω_L and ω_S are close to the interband gaps. This leads to a large resonance

enhancement in the intensity of scattered light. These enhancements are referred to as resonant Raman processes and will be described in further detail later in this chapter.

Calculating the differential scattering cross-section (quantifies the number of photons scattered through a small change in angle over a small change in energy) involves parameters describing the modulation of the dielectric susceptibility. With the help of group theory, macroscopic considerations provide symmetry-based selection rules for the polarization of the incident and scattered light. Quantum mechanics is used to describe the resonance enhancement of the Raman scattering process that occurs when photon energies are close to optical transition energies. This approach takes into account the explicit interaction between photons and electronic states of the medium. Resonance enhancement is an important facet of ILS as it enables the observation of processes that would be otherwise too weak to observe.

3.1.2.1 Light Scattering Susceptibilities and Group Theoretical Arguments

Not all excitations can be observed via light scattering. A mode can be Raman "active" or Raman "silent" depending on its symmetry properties. We can predict which modes can observed by understanding the symmetry properties of the light scattering matrix elements. Light scattering radiation is linked to a fluctuating electric-dipole which is set up in the scattering medium by the simultaneous action of the incoming photon radiation and the excitation of the medium[69]. We define a modulated Raman susceptibility, $\delta\chi_{ij}$, a second rank tensor, the form of which is determined by symmetry of the scattering medium and of the elementary excitations.

Now, the polarization is related to the susceptibility as follows:

$$P_i(\omega_S) = \sum_j \delta\chi_{ij} E_j(\omega_L)$$

where, **P** is the polarization and **E**, the electric field. The intensity of light, I is proportional to the square of the polarization[70].

$$|P(\omega_L)|^2 \propto I(\omega_L, \omega_S, \vec{k}) \propto |\hat{e_S} \cdot \delta\chi_{ij} \cdot \hat{e_L}|^2 \tag{3.2}$$

where $\hat{e_L}$ and $\hat{e_S}$ are the unit polarization vectors for incident and scattered photons respectively. Making a series expansion of $\delta\chi_{ij}$ in powers of coordinates that represent the elementary excitations of the scattering medium allows us to tackle the problem of calculating $I(\omega_L, \omega_S, \vec{k})$. The expansion can also be used to determine the selection rules for the polarization of incident and scattered photons, as will be outlined later in this chapter. Though the symmetry properties hold for all kinds of excitations, we will focus on optical phonons for concreteness. The expansion, for the case of vibrational modes in a lattice, is

$$\delta\chi_{ij} = \sum_m R_{ij}^m Q_m(0) + \sum_{mn,qp} R_{ij}^{mn} Q_m(\vec{q}) Q_n(\vec{p}) + \ldots \tag{3.3}$$

where the second rank tensors R_{ij}^m and R_{ij}^{mn} are the first and second order Raman tensors respectively. The first term describes the single phonon coordinate at $\vec{q} = 0$ for first order scattering. The second term has the two phonon coordinates, $\vec{p}+\vec{q} \approx 0$, that describes second order scattering.

Equations 3.2 and 3.3 can be used to calculate inelastic light scattering intensities. The first term of Eqn. 3.3 vanishes for modes that are not Raman allowed modes. Equation 3.2 is used to determine the selection rules for the polarization

of ω_L and ω_S. Modes that are Raman allowed transform according to one of the symmetries of 2nd rank scattering tensors. That is, for allowed scattering, the conditions under which $\delta\chi_{ij}$ is satisfied will be determined only by the transformation properties of the initial and final states under the symmetry properties of the crystal point group [71]. Though an in depth discussion of group theory applied to ILS is beyond the scope of this dissertation, I will highlight a few pertinent results, as well as provide a brief background for these results below.

3.1.2.2 A Quantum Mechanical Approach

ILS by electron systems is best described within a quantum mechanics framework. Consider the Hamiltonian for a system of electrons in a radiation field[69]:

$$H = \frac{1}{2m^*}\sum_j \left[\vec{p}_j + \frac{e}{c}\vec{A}(\vec{r}_j)\right]^2 + \frac{1}{2}\sum_{i\neq j} V_C(\vec{r}_i - \vec{r}_j) \tag{3.4}$$

where V_C represents the electron-electron interaction and $\vec{A}(\vec{r})$ is the vector potential for the photons. We ignore here the presence of a magnetic field. Treating the system perturbatively, we can rewrite the Hamiltonian as

$$H = H_o + H_{int} \tag{3.5}$$

$$= H_o + H_{ee} + H'_{int} + H''_{int} \tag{3.6}$$

$$H_o + H_{ee} = \sum_j \frac{\vec{p}_j^2}{2m^*} + \frac{1}{2}\sum_{i\neq j} V_C(\vec{r}_i - \vec{r}_j) \tag{3.7}$$

$$H'_{int} = \frac{e}{2m^*c}\sum_j [\vec{p}_j \cdot \vec{A}(\vec{r}_j) + \vec{A}(\vec{r}_j)\cdot\vec{p}_j] \tag{3.8}$$

$$H''_{int} = \frac{e^2}{2m^*c^2}\sum_j |\vec{A}(\vec{r}_j)|^2 \tag{3.9}$$

The H''_{int} term is second order in fields and therefore contributes to the light scattering processes described by first order perturbation theory. The H'_{int} term on the other hand, being first order in fields it thus appears in the second order terms of perturbation theory for calculating the light scattering intensity [72].

The scattering rate from an initial state $|I\rangle$ to a final state $|F\rangle$ is determined via time-dependent perturbation theory. The transition rate is given by Fermi's golden rule [69]

$$\frac{1}{\tau_{FI}} = \frac{2\pi}{\hbar}|H_{FI}|^2\delta(E_F - E_I - \hbar\omega) \tag{3.10}$$

where

$$\begin{aligned} H_{FI} =& \langle F|H_{int}|I\rangle \\ &+ \sum_{j>1}\sum_{l_1\ldots l_{j-1}} \frac{\langle F|H_{int}|l_{j-1}\rangle\langle l_{j-1}|H_{int}|l_{j-2}\rangle\ldots\langle l_1|H_{int}|I\rangle}{(E_I - E_{l_{j-1}})(E_I - E_{l_{j-2}})\ldots(E_I - E_{l_1})} \end{aligned} \tag{3.11}$$

for an arbitrary number of j steps of the scattering process, where $E_{F(I)}$ is the final (initial) state and E_{l_j} is the energy of the intermediate state $|l_j\rangle$. The total scattering rate is obtained by summing $1/\tau_{FI}$ over all final states and initial states. Each j-step process involves j corresponding matrix elements of H_{int} acting on combinations of initial, intermediate or final states. The denominator clearly shows how the jth step may result in a maximum in the scattering intensity when one of the terms in the denominator goes to zero. Only two-step and three-step processes are relevant to this dissertation, and will be considered below.

The scattering rate allows us to quantify the differential cross section, discussed previously in terms of dielectric susceptibilities, as follows [73, 74]:

$$\frac{d\sigma}{d\Omega d\omega} = \hbar\frac{\omega_S}{\omega_L}\left\langle \sum_F |M_{FI}|^2\delta(E_F - E_I - \hbar\omega)\right\rangle \tag{3.12}$$

where M_{FI} is the relevant matrix element, and the angle brackets indicate an average over the initial states.

We consider only scattering via single electron states in a semiconductor. Since light scattering is second order in the vector potential, the lowest order perturbation theory expansion of M_{FI} is first order in H''_{int} and second order in H'_{int} [75, 74, 72]. M_{FI} can be rewritten as

$$M_{FI} = r_0 \sum_{\alpha,\beta} \gamma_{\alpha,\beta} \langle F | C^\dagger_\alpha C_\beta | I \rangle \tag{3.13}$$

where $r_o = e^2/m^*c^2$ is the "classical" electron radius. α and β are indices for the electron states, which are characterized by wavevector and spin s_α. $C^\dagger_\alpha$ and C_α are the creation and annihilation operators for the single particle states $|\alpha\rangle$. The quantity $\gamma_{\alpha\beta}$ is

$$\gamma_{\alpha\beta} = \langle \alpha | e^{i\vec{q}\cdot\vec{r}} | \beta \rangle \hat{e}_L \cdot \hat{e}_S \tag{3.14}$$

$$+ \sum_l \left[\frac{\langle \alpha | j_S | l \rangle \langle l | j_L | \beta \rangle}{(E^*_\beta - E^*_l + \hbar\omega_L)} + \frac{\langle \alpha | j_L | l \rangle \langle l | j_S | \beta \rangle}{(E^*_\alpha - E^*_l - \hbar\omega_L)} \right] \tag{3.15}$$

where $j_{L(S)} = \frac{1}{m^*} \hat{e}_{L(S)} \cdot \vec{p} e^{\pm i \vec{k}_{L(S)} \cdot \vec{r}}$, E^*_α (E^*_β) is the energy of the single particle state $|\alpha\rangle$ ($|\beta\rangle$), and E^*_l is the energy of the intermediate state $|l\rangle$. The first term in the expression is due to the $|A|^2$ term of the electron-photon interaction (linked to H''_{int}). The other two terms are due to the second order contributions of the $\vec{p} \cdot \vec{A}$ term (linked to H'_{int}). For intraband scattering the second set of terms in $\gamma_{\alpha\beta}$ almost vanishes (the two terms in the brackets cancel) [76]. Consequently, the term due to H''_{int} dominates. However, for interband transitions, the cancellation of the second and third term does not occur; and as a result H'_{int} is allowed to play a role in scattering. This is an especially significant one since it is responsible for the resonant enhancement of the light scattering cross-section (the denominator vanishes when

the incident photon energy approaches the energy of a gap). The first term in $\gamma_{\alpha\beta}$ is non-resonant. H_{ee} plays no role in the two-step light scattering process described above; but will come into play for three-step light scattering processes discussed below.

band	$\lvert J, J_z\rangle$	wavefunction
cb	$\lvert\frac{1}{2}, +\frac{1}{2}\rangle$	$S\uparrow$
	$\lvert\frac{1}{2}, -\frac{1}{2}\rangle$	$S\downarrow$
hh	$\lvert\frac{3}{2}, +\frac{3}{2}\rangle$	$\sqrt{\frac{1}{2}(X+iY)}\uparrow$
	$\lvert\frac{3}{2}, -\frac{3}{2}\rangle$	$\sqrt{\frac{1}{2}(X-iY)}\downarrow$
lh	$\lvert\frac{3}{2}, +\frac{1}{2}\rangle$	$\sqrt{\frac{1}{6}(X+iY)}\downarrow -\sqrt{\frac{2}{3}Z}\uparrow$
	$\lvert\frac{3}{2}, -\frac{1}{2}\rangle$	$\sqrt{\frac{1}{6}(X-iY)}\uparrow +\sqrt{\frac{2}{3}Z}\downarrow$
so	$\lvert\frac{1}{2}, +\frac{1}{2}\rangle$	$\sqrt{\frac{1}{3}(X+iY)}\downarrow -\sqrt{\frac{1}{3}Z}\uparrow$
	$\lvert\frac{1}{2}, -\frac{1}{2}\rangle$	$\sqrt{\frac{1}{3}(X-iY)}\uparrow +\sqrt{\frac{1}{3}Z}\downarrow$

Table 3.1: Kane model wavefunctions [1] along k_z for the electron states in a GaAs QW near the Γ-point for the conduction band (cb), heavy hole (hh), light hole (lh) and split-off (so) valence bands. Fig. 3.4 shows the bands structure for GaAs and the corresponding valence band states.

We can simplify the expression for the scattering cross-section by considering a particular form for the single electron states in the expression for $\gamma_{\alpha\beta}$. To do this, we will use the Kane model [1] to represent the electronic states for the GaAs band structure. The Kane model is valid for III-V semiconductors in which the relevant states are near the Brillouin zone center or Γ-point. In the Kane model, the conduction band states are s-like (denoted by $S\uparrow$ and $S\downarrow$, where the arrow indicates the orientation of spin). The valence band basis functions have p-like symmetry and are denoted by $X\uparrow, X\downarrow, Y\uparrow, Y\downarrow, Z\uparrow$, and $Z\downarrow$, whose combinations are required to have states of total angular momentum, as shown in Table 3.1.

Hamilton and McWhorter [73] use the wavefunctions of the Kane model along

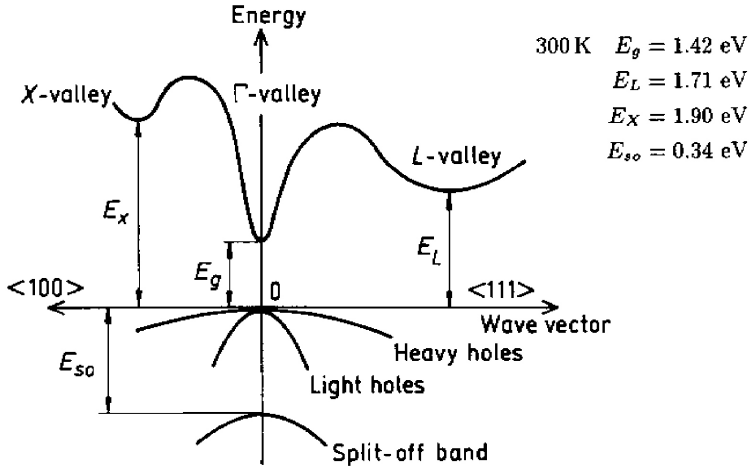

Figure 3.4: Band structure of GaAs [10, 11].

with the approximation: $\omega_L \sim \omega_S$, to yield

$$\gamma_{\alpha\beta} = \langle\alpha|e^{i\vec{q}\cdot\vec{r}}|\beta\rangle\left[\hat{e}_L \cdot \mathbb{A} \cdot \hat{e}_S + i(\hat{e}_L \times \hat{e}_S) \cdot \mathbb{B} \cdot \langle s_\alpha|\vec{\sigma}|s_\beta\rangle\right] \tag{3.16}$$

where $\vec{\sigma}$ represents the Pauli matrices, $|s_\alpha\rangle$ is the spin state of $|\alpha\rangle$, and $\mathbb{A}$ and $\mathbb{B}$ are tensors that are linked to excitations that are spin conserving, and to those that involve a change in the spin state respectively. I will elaborate on this in the upcoming section. There we will find that light scattering from a 2DES in GaAs consists of two distinct components: one that is symmetric in the polarizations and another that is antisymmetric in the polarizations. That is, one is maximized when the polarizations are parallel (polarized) while the other is maximized when the polarizations are perpendicular (depolarized). Off-resonance, we find that $\mathbb{A} \propto \mathbf{m}^{*-1}$, where $\mathbf{m}^*$ is the effective mass tensor, so that the first term is linked to charge density excitations. The matrix elements of the Pauli matrices of the second term indicate that this term is linked to excitations in which the spin quantum number changes. This ability to discern between charge density and spin density excitations

by using polarization selection rules is a powerful feature of inelastic light scattering.

3.1.2.3 Parallel Polarization

This is the case for $\hat{e}_L//\hat{e}_S$. Assuming a parabolic valence band, we can rewrite $\mathbb{A}$ as follows[73]:

$$\mathbb{A} = \mathbb{I}\left[1 + \frac{2P^2}{3m}\left(\frac{E_1^*}{E_1^{*2} - (\hbar\omega_L)^2} + \frac{E_2^*}{E_2^{*2} - (\hbar\omega_L)^2} + \frac{E_3^*}{E_3^{*2} - (\hbar\omega_L)^2}\right)\right] \tag{3.17}$$

where $\mathbb{I}$ is the unit dyadic, $P = |\langle S|p_z|Z\rangle|$ is the interband matrix element of the momentum and E_1^*, E_2^* and E_3^* are the gaps of the Kane model[1] which are associated with the heavy, light and split-off valence bands respectively. The light and heavy hole bands are degenerate, while the split-off valence band has an energy difference of E_{so} (shown if Fig. 3.4).

3.1.2.4 Cross Polarization

Here $\hat{e}_L \perp \hat{e}_S$. The second part of $\gamma_{\alpha\beta}$ in Eqn.3.16, which is antisymmetric in the incident and scattered polarizations can be rewritten as

$$\mathbb{B} = \mathbb{I}\frac{2P^2}{3m}(\hbar\omega_L)\left[\frac{1}{E_0^{*2} - (\hbar\omega_L)^2} - \frac{1}{(E_0 + E_{so})^2 - (\hbar\omega_L)^2}\right] \tag{3.18}$$

The $\langle s_\alpha|\vec{\sigma}|s_\beta\rangle$ term vanishes for states that do not involve a change in spin. That is, the antisymmetric term is proportional to electron-density fluctuations in spin[75]. Consequently, light scattering for depolarized spectra is strongest for spin-density excitations. Recall that H_{ee} plays no role in the two-step light scattering process shown above.

3.1.3 Light Scattering in 2D systems

Our discussion has focused thus far on three-dimensional systems. However, the systems of interest here are two dimensional. Fortunately, much of the results of the discussion pertaining to light scattering in 3D systems is also applicable in 2D systems. To see this, we examine the Hamiltonian describing the in-plane behavior of the electrons in the 3D system and find that, within the effective mass approximation [77], it is equivalent to that of the 2D system. In particular, the polarization selection rules of the confined electrons to photons is the same in both 2D and 3D. That is, the light scattering mechanisms in 2D and 3D systems are similar [77].

Inelastic light scattering is a unique and effective tool for probing 2DES's. This is in part due to resonance enhancement which makes "weak" signals observable by experiment. Moreover, ILS can discern between collective and single particle excitations. In addition, it can differentiate between charge and spin excitations. Consequently, light scattering can be used to "map out" energy level structures with spin degrees of freedom and to estimate electron-electron interaction energies.

ILS in 2D systems, in the simplest form, can be described as a two-step process, similar to that in Fig. 3.3 for 3D systems. Figure 3.5 shows the transition diagram for intersubband and intrasubband transitions in 2D systems, introduced in the previous chapter. Recall that intersubband excitations are excitations that involve more than one subband while intrasubband excitations are excitations that occur on the same subband. From our analysis of ILS in 3D systems, we can write the scattering intensity in 2D systems,

$$I(\omega) \propto \left| \sum_{l_1} \frac{\langle F|H'_{int}|l_1\rangle\langle l_1|H'_{int}|I\rangle}{\omega_I - \omega_{l_1}} \right|^2 \tag{3.19}$$

where $|F\rangle$, $|I\rangle$, are final and initial states respectively. H'_{int} is the interaction Hamil-

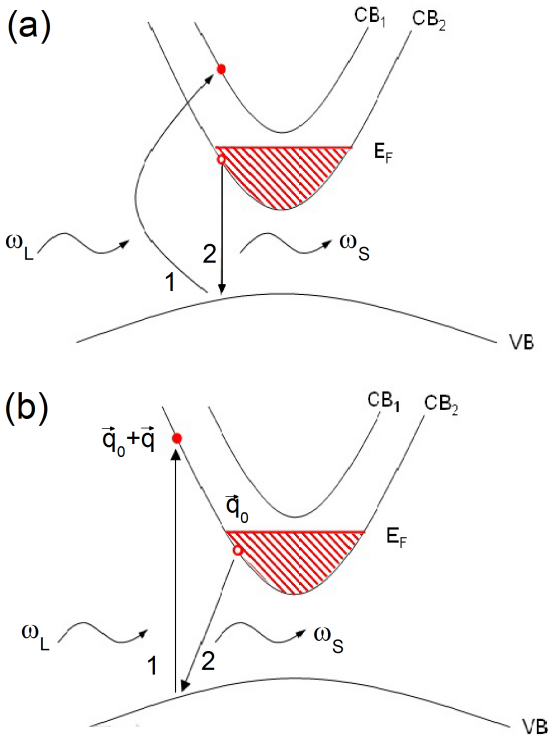

Figure 3.5: Transition diagrams show (a) intersubband and (b) intrasubband single particle excitations from two-step light scattering processes in 2DES in a semiconductor quantum well. The numbers show the time-ordering of the transitions. ω_L and ω_S are the incident and scattered photons respectively. q is the momentum associated with the intersubband excitation, where $q + q_o$ is the wavevector of the excited electron.

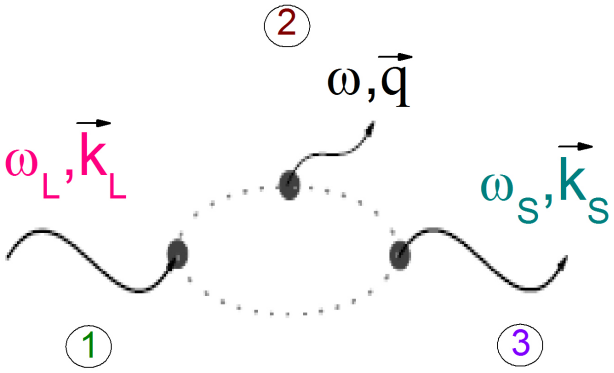

Figure 3.6: A Feynman diagram showing a three step light scattering process. Step 1: the incident photon (ω_L) is annihilated in a process that creates an electron-hole pair. Step 2: the pair interacts with the 2DES to emit a collective excitation of energy ω and wavevector $\vec{q} = \vec{k}$. Step 3: the electron-hole pair is annihilated, creating the scattered photon (ω_S). Alternative time orderings are possible.

tonian, $|l_1\rangle$ are intermediate states and ω_{l_1} represents the corresponding energies for those states. Examining the denominator of Eqn. 3.19 elucidates the existence of a single resonance enhancement condition for two-step ILS. That is, when $\omega_I \to \omega_{l_1}$ the intensity, $I(\omega)$ grows large. This condition can be rewritten as follows: $\omega_I - \omega_{l_1} = \omega_L - (E_o + \Delta_{10}) = \omega_s - E_o \to 0$, where E_o is the band gap between the valence band and the conduction band and Δ_{10} is the intersubband spacing of the conduction band. The expression shows that a resonance arises when either the incoming photon energy, ω_L matches $E_o + \Delta_{10}$ (defined as an incoming resonance) or when the scattered photon energy, ω_S matches E_o (an outgoing resonance).

There exists more complicated higher order Raman processes. Fig. 3.6 shows a Feynman diagram that describes a three-step Raman scattering process. The first and last steps of this three-step process comprise the same steps as the two-step process described previously. The second step however involves an electron-electron

interaction which causes a transition from the first intermediate state to the second intermediate state, resulting in an emission of a collective mode as described by the following:

$$I(\omega) \propto \left| \sum_{l_1,l_2} \frac{\langle F|H'_{int}|l_2\rangle\langle l_2|H_{ee}|l_1\rangle\langle l_1|H'_{int}|I\rangle}{(\omega_I - \omega_{l_2})(\omega_I - \omega_{l_1})} \right|^2 \tag{3.20}$$

Eqn. 3.20 reveals that there is an incoming resonance associated with the l_1 transition, as seen with two-step process. In addition, there is a second resonance, associated with the second term in the denominator, such that

$$\begin{aligned} \omega_I - \omega_{l2} =& \omega_L - (\omega + E_{l2}) \\ =& \omega_S - E_{l2} = 0 \end{aligned}$$

where E_{l2} is the energy of the transition between the states $|l_2\rangle$ and $|I\rangle$. The second resonance condition is described by the overlap of ω_S with an optical gap (outgoing resonance).

3.2 Experimental Considerations

The majority of measurements were performed on a high-quality, symmetrically doped, 240 $\mathring{A}$ wide GaAs single quantum well (sample #3-6-07.3) of electron density, n=3.7x10^{11} cm^{-2} and mobility, μ=17.5x10^6 cm^2/Vs (at T=300 mK). Additional samples were studied in section 3.3. To access temperatures above 1.8K, at zero magnetic field, samples were mounted in a cryostat with windows for optical access. They were attached with rubber cement to a copper holder and were in direct contact with helium gas or liquid. Only portion of the sample was attached to the copper holder, the other portion allowed to contract when cooling to minimize impact of strain.

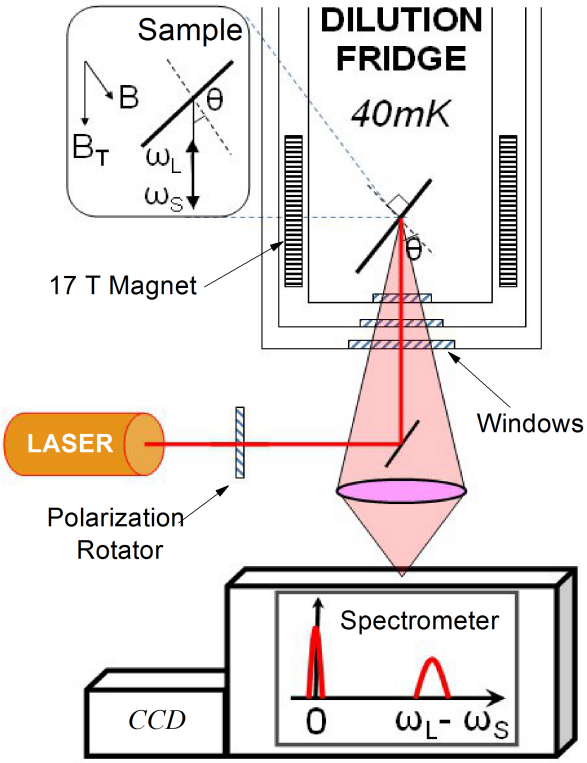

Figure 3.7: Schematic of the experimental setup for optical measurements at millikelvin temperatures. The top left panel shows a blow up of the sample in back scattering geometry.

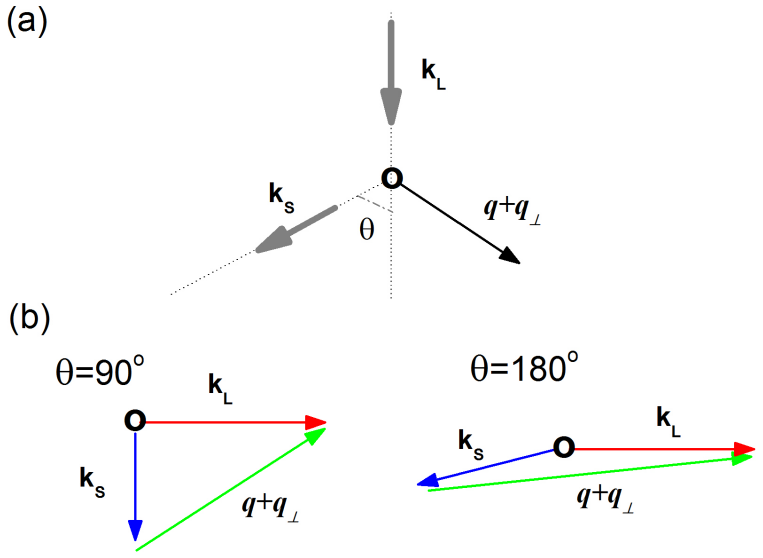

Figure 3.8: Schematic showing different scattering geometries and associated conserved wavevectors. k_L and k_S are the wavevectors of the incident and scattered photons respectively. $q + q_\perp$ represents the wavevector transferred - the in-plane excitation wavevector, q, and the orthogonal component, $q_\perp$. The black circle represents the location of the sample. Both back-scattering ($\theta = 180$) and side scattering ($\theta = 90$) geometries were used for zero magnetic field measurements. The back-scattering geometry was used exclusively for quantum Hall studies.

In order to access temperatures below 1.8K, in finite magnetic field, samples were mounted on the cold finger of a dilution refrigerator with a base temperature of below 40 mK and inserted into the cold bore of a 16 T superconducting magnet as shown in Fig. 3.7. The magnetic field perpendicular to the sample is $B = B_T cos\theta$ as shown in the inset of Fig. 3.7 (B_T is the total applied magnetic field). The samples are attached to the copper rod using copper-loaded grease to improve thermal contact. In addition, thin gold wires were attached to both the GaAs sample via diffused indium dots and to the copper rod to improve thermal contact with the electron gas. The dilution refrigerator used was an Oxford Instruments Kelvinox with a cooling power of $400\mu W$ at 100 mK.

The dilution refrigerator has four parallel windows for optical access. The inner vacuum can of the dilution refrigerator has a bottom window which is mated to a 4 K window mounted on a raised flange on the bottom of the cryostat. Both windows are enclosed in a small area that uses the relatively low heat of vaporization of liquid He to trap He gas in a small pocket, or "vapor lock" to keep boiling He from obscuring the optics path. The third window, the "77 K window", is thermally anchored to the nitrogen jacket. This window at 77 K minimizes blackbody radiation from the room temperature portions of the system. The fourth window is attached directly to the cryostat. All of the windows are made of Spectrosil B, which transmits light in the range of interest, $\sim 800nm$, while blocking black body radiation (peaked at $10\mu m$ at room temperature) at wavelengths greater than $4\mu m$.

The energy of the linearly polarized photons, ω_L and ω_S, are tuned close to fundamental optical transitions of the GaAs quantum well. Tunability is provided via a Ti:sapphire laser with sharp peaks ($< 30\mu eV$) and of photon energy in the range of the fundamental optical gap of GaAs (800nm - 820nm). The Ti:sapphire laser is optically pumped by a Coherent Verdi Diode laser which outputs light at 532nm. The light from the Ti:sapphire laser is linearly polarized. A polarization

rotator is used to rotate this polarization by 90 degrees so that the incident beam is either parallel (polarized) or perpendicular (depolarized) to the scattered beam. The beam is focused by a cylindrical lens to a spot that is about $2mm \times 200\mu m$. The power density is kept less than $10^{-4}\mathrm{Wcm}^{-2}$ to avoid heating of the electron gas at millikelvin temperatures. At higher temperatures, the power density can be up to two orders of magnitude higher.

Wavevector conservation is illustrated in Fig. 3.8. Panel *a* shows the wavevector relationship between k_L, k_S and q for arbitrary θ as shown in the figure. The two diagrams in panel *b* illustrate the case for side-scattering ($\theta = 90$) and back-scattering ($\theta = 180$). The wave vector transferred from the photons to the 2D system is $q = (2\omega_L/c)\sin\theta$, much smaller than $1/l_o$, where $l_o = \sqrt{\hbar c/eB}$ is the magnetic length. However, the presence of weak short-range disorder induces a breakdown of wave vector conservation [78, 79, 80, 81], which allows light scattering to detect the critical points in the exciton dispersion, such as the rotons, because of van Hove singularities in the density of states at these energies. As we will see later on, this serves as a useful tool in identifying large wavevector modes via light scattering.

The experimental setup is constructed to optimize the collection of light with free space optics and prevent electron heating by the incident laser beam. Light is collected by lenses and focused onto the entrance slit of the spectrometer. The solid angle of light scattering that can be collected depends upon the F# of the cryostat. That is, the distance to the window/diameter of window. The immersion cryostat, employed at $B = 0$, has an F# $\sim$2, while the dilution refrigerator has an F# $\sim$4. The lens diameters and focal lengths are chosen by matching the F#'s of the cryostat, collection optics, and spectrometer; and setting the desired magnification of the collection path. The finite solid angle of the collection introduces an uncertainty in the wavevector transferred to the 2DES.

Scattered light is dispersed and recorded by a T64000 triple grating spectrom-

eter, equipped with holographic gratings to reduce the stray light. Measurements are taken either in additive mode or subtractive mode, with high and low resolution respectively. Photons are detected with a multi-channel photodetector, or charged coupled device (CCD) with $13\mu m$ pixels. The combined resolution of the system with entrance slits on the spectrometer set to 50μm is $30\mu eV$. The response of the spectrometer is linearly polarized, so that spectra can be taken with linear polarization of the incident photons parallel (polarized) or perpendicular (depolarized) to the scattered photons' polarization. As discussed in previous sections, excitation modes with changes in the spin degree of freedom are stronger in depolarized spectra, while those modes with changes in the charge degree of freedom are stronger in polarized spectra.

3.3 Light Scattering from Collective Excitations in 2DES's at B=0

Several electronic excitations are accessible via light scattering using a cryostat in the side-scattering configuration at zero magnetic field (at 2K): the plasmon, a collective intrasubband excitation, and also intersubband collective excitations involving charge density (CDE) and spin density (SDE) fluctuations. CDE and SDE modes are linked to Coulomb and spin exchange energies respectively. The intersubband single particle excitation (SPE) is also readily measureable.

Figure 3.9 shows the plasmon mode from a GaAs QW (sample $\#2-25-05.1$, $300\mathring{A}$ width, $\mu \sim 25 \times 10^6 cm^2/Vs$ and $n \sim 2.6 \times 10^{11} cm^{-2}$). The dispersive nature of the plasmon mode is shown through its shift in energy with changes in in-plane wavevector (equivalent to changes in scattering angle, θ). The dispersion, in the

small wavevector limit, described by

$$\omega_p^2 = 2\pi n e^2 q/\varepsilon m^* \tag{3.21}$$

where q is the in-plane wavevector, and ε is the dielectric constant of GaAs Using the light scattering geometry (shown in the inset of Fig. 3.9) we can derive an expression for the in-plane wavevector,

$$q = 2\left(\frac{2\pi}{\lambda_L}\right) sin\theta \tag{3.22}$$

Measurements of the plasmon's dispersion confirms the known electron density of the 2DES to within uncertainty and experimental error.

Figures 3.10 and 3.11 show the intersubband excitations of a GaAs QW (sample $\#9-16-04.2$ with $300\mathring{A}$ wide QW, $\mu \sim 5\times 10^6 cm^2/Vs$ and $n = 1.39\times 10^{11} cm^{-2}$). The spin density excitation (SDE), charge density excitation (CDE) and single particle excitation (SPE) are shown. These excitations, as already mentioned, can be detected using light scattering. The CDE energy is upshifted from the SPE energy due to Coulomb interactions. To the contrary, the energy of the SDE is downshifted from the SPE energy due to exchange effects [82, 83, 84]. Intersubband excitation peaks can be very sharp, with FWHM as low as $\sim 0.10meV$ (in sample $\#3-12-09.1$). These extremely sharp peaks are narrower than those reported in the literature (0.14meV) [84]. The low FWHM is a measure of the high quality of the quantum well; a "dirty" well yielding broad peaks and pristine samples giving narrow peaks. A "back of the envelope" method for considering this is to examine the uncertainty principle [85]

$$\Delta E \Delta\tau \gtrsim \hbar \tag{3.23}$$

were ΔE symbolizes the FWHM and $\Delta\tau$ represents the lifetime of the excitation

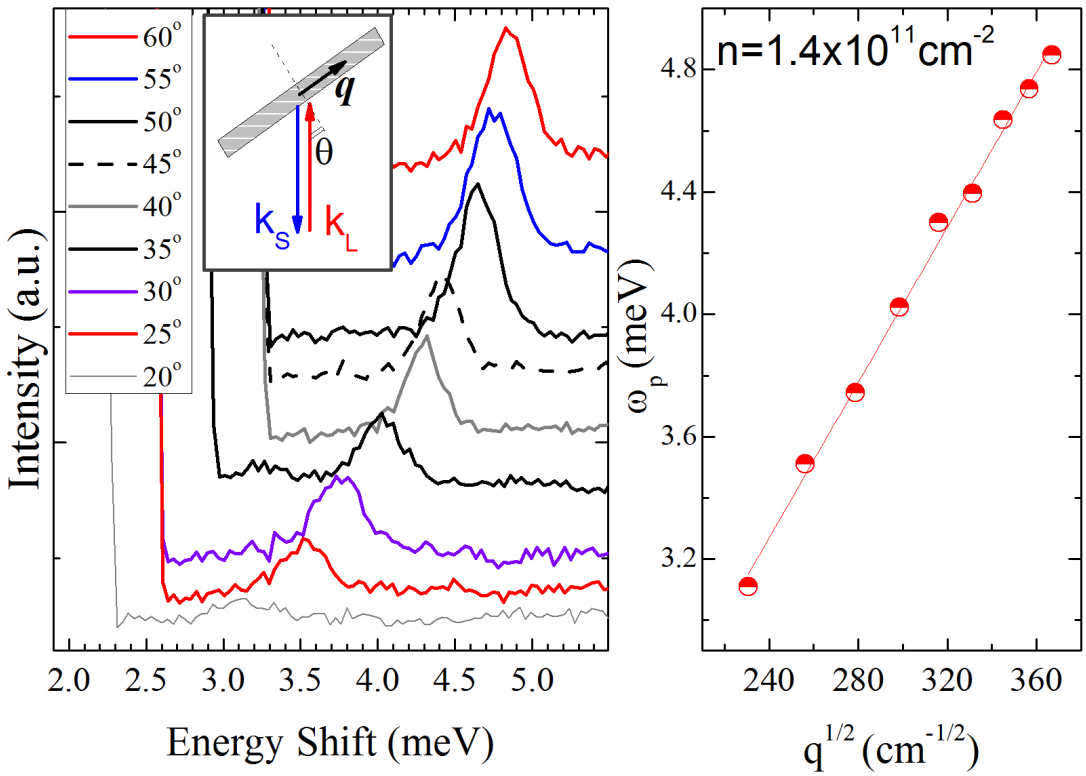

Figure 3.9: Shows the dispersion of the plasmon of a 2DES. (a) The energy of the mode shifts with changes in scattering angle, θ, or in-plane wavevector, q (denoted as $q_{//}$ in the inset). The inset shows the scattering geometry. (b) Momentum resolved scatter plot of the energy with respect to the square-root of the in-plane momentum. The slope of the line gives us a means of experimentally extracting a value for the electron density, n. The value of n found by optical methods is ($\sim 1.4 \times 10^{11} cm^{-2}$). This value is different from that found from transport. This is due to small changes in density seen in "light sensitive" samples (samples whose density changes with varying incident photon power).

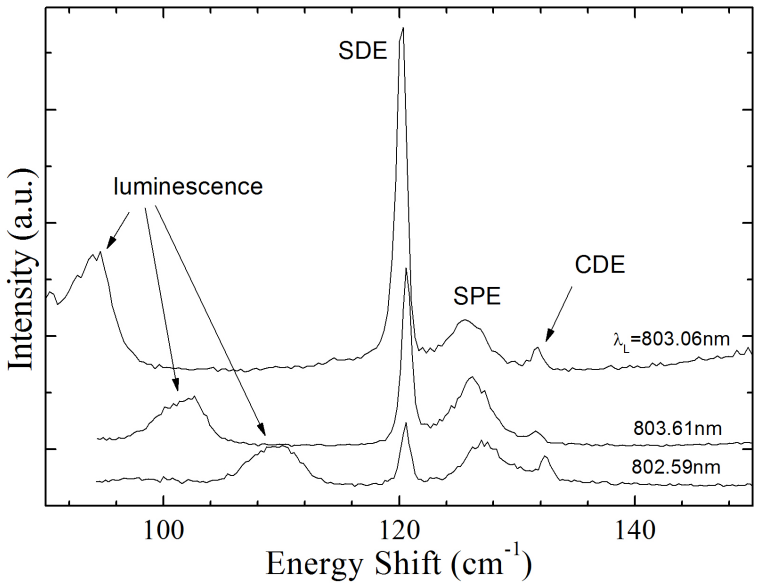

Figure 3.10: Spectra show intersubband transitions in a GaAs QW. Polarization of incident photons is perpendicular to scattered photons (depolarized light scattering). The incident laser wavelengths, λ_L, are indicated. The spin density excitation (SDE) dominates the spectra. The single particle excitation (SPE) is also seen. The charge density excitation (CDE) however is rather weak, as expected from light scattering selection rules.

for homogeneous electron systems. Consequently, the smaller the value of ΔE, the larger the lifetime of the state will be and thus the "cleaner" the 2DES.

The spectra in Fig. 3.11 and Fig. 3.10 clearly show the polarization rules' ability to distinguish between charge and spin density excitations.

We can "finger print" the 2DES by studying its Raman spectra. Thus far we already have a means to measure electron density, Coulomb interaction energy, Exchange energy and the quality of the 2DES. Let us now examine how light scattering might be useful for characterizing quantum Hall systems.

3.4 Light Scattering in the IQH Regime

The Integer Quantum Hall Effect (IQHE) can be accessed at a magnetic field of roughly $1T$ ($1T = 10^4$Gauss). At this field, the magnetic length, l_o is $\sim 250\mathring{A}$,

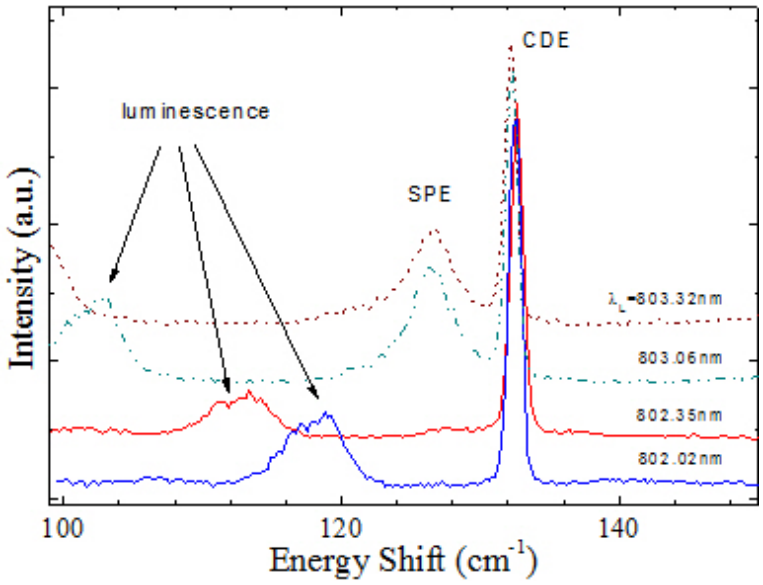

Figure 3.11: Spectra show intersubband transitions in a GaAs QW. Incident photon polarization is parallel to scattered photons (polarized Light scattering). The incident laser wavelengths, λ_L, are indicated. The charge density excitation (CDE) dominates the spectra. The single particle excitation (SPE) is also seen. The spin density excitation (SDE) however is rather weak, as expected from light scattering selection rules

as shown by Eqn. 3.22. In light scattering the maximum wavevector that can be transferred to the 2DES is $k_{max} \approx 1.5 \times 10^5 cm^{-1}$ ($k_{max} l_o \approx 0.4$). Consequently, in the case of wavevector conservation, only long wavelength modes, with $k < 1/l_o$, of dispersive charge or spin density excitations can be accessed by light scattering.

The lowest energy charge density excitation, where *Landau* level index changes by one and spin degrees of freedom are fixed, is described by Kohn's theorem. This Kohn mode is pinned at the cyclotron energy, ω_c [86]. While forbidden by lowest order selection rules, this long wavelength mode has been observed via light scattering at $\nu = 1$ [87]. The dispersion of the Kohn mode or magnetoplasmon mode for $q \ll 1/l_o$ is described as [88]

$$\sqrt{\omega_c^2 + \omega_p(q)^2} \tag{3.24}$$

Light scattering can also access long wavelength inter-Landau level spin flip excitations as well as intra-Landau level excitations. Intra-Landau level spin flip excitations, or spin waves, have long wavelength energy fixed at the Zeeman energy according to Larmor's theorem [12].

The break-down of wavevector conservation allows light scattering to probe shorter wavelength excitations [89, 90, 87]. I will illustrate this in greater detail in later chapters. The strongest light scattering response arises from critical points in the dispersion which results in van Hove singularities in the density of states. Consequently, light scattering modes are not restricted to the long wavelength limit. That is, intermediate wavelengths, such as ql_o, as well as large wavevector modes can also be accessed [89, 90, 87, 91]. That is, light scattering can probe the major features of dispersive IQHE charge and spin excitations. These probes provide information on electron-electron interactions and exchange self-energy of the 2DES in the IQHE regime. Light scattering proves to be a good characterization tool for 2DES in finite magnetic field, as was already shown for zero magnetic field.

3.5 Light Scattering in the FQH Regime

The foundation for light scattering in the fractional quantum Hall (FQHE) regime is in many ways similar to that of the IQHE. For instance, there exists a restriction of wavevector transfer for translationally invariant systems which breaks down in the presence of disorder. In the FQHE regime however, the excitations of quasiparticles of the quantum liquid are probed. Light scattering studies have already reported a great variety of long wavelength, low energy charge and spin density excitations [28]. I will describe in later chapters the plethora of both long wavelength and large wavevector modes that exist in fractional quantum systems. As we will see in Chapter 4, showing that FQHE systems can have large wavevector, high energy

modes, has implications for the topological robustness of composite fermions [92, 5].

Light scattering can probe inter-Λ level (Landau-like levels for composite fermions) excitations. It gives information of energy level structure and the strength of quasi-particle interactions of FQHE systems. Furthermore, as I will describe in later chapters, light scattering provides a unique probe of both the charge and spin degrees of freedom of highly correlated electron systems that can give rise to exotic forms of matter. Fractional quantum Hall states of particular interest include that at $\nu = 5/2$, the best known even-denominator state, theoretically shown to have a spin-polarized ground state [93] and have non-abelian braiding statistics [32]. The latter which could make this state useful for realizing topological quantum computation. The former which light scattering has the capacity to probe [94, 95, 66, 5].

3.6 Monitoring spin polarization with spin waves

The study of spin degrees of freedom will be a central part of this thesis. Light scattering is a delightful tool for this study as it provides a unique, direct probe of the bulk states of quantum fluids. As we have seen in this Chapter, the polarization selection rules of ILS allows one to discern between spin and charge degrees of freedom. Light scattering methods may be applied to study a 2DES in a magnetic field like that shown in Fig. 3.12(a) where a 2DES at $\nu = 1$ is depicted. For instance, light scattering can monitor the changes in spin degrees of freedom during the creation of the "spin exciton" or spin wave (SW) shown in Fig. 3.12(b). The SW dispersion at $\nu = 1$ (extracted from Ref. [12]) is displayed in Fig. 3.12(c) and shows that the energy of the SW in the long wavelength limit is E_Z. Light scattering measurements will reveal spectral weight at an energy shift, E_Z from the laser.

In the previous Chapter, we quantified spin polarization in Eqn. 2.27 by comparing the number of electrons occupying upper and lower spin branches of the *lth*

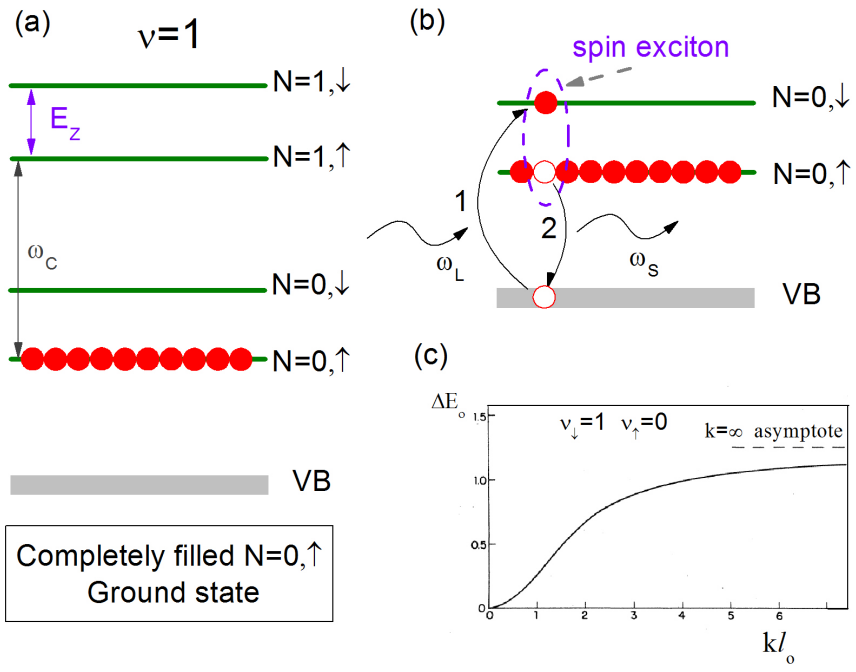

Figure 3.12: (a)*Landau* level diagram showing *Landau* levels spaced by the cyclotron energy and spin split by E_Z. The ground state at $\nu = 1$ is depicted - the lower spin branch of the N=0 LL is completely filled. (b) An excited state of $\nu = 1$ is shown. Incoming photons create a "spin exciton" or spin wave which, in the $q \to 0$ limit, has its energy fixed at E_Z according to Larmor's theorem[12]. The numbers indicate the time ordering of the light scattering process. (c) The dispersion of the spin wave extracted from Ref. [12]. In the long wavelength limit, the spin wave energy is the Zeeman energy.

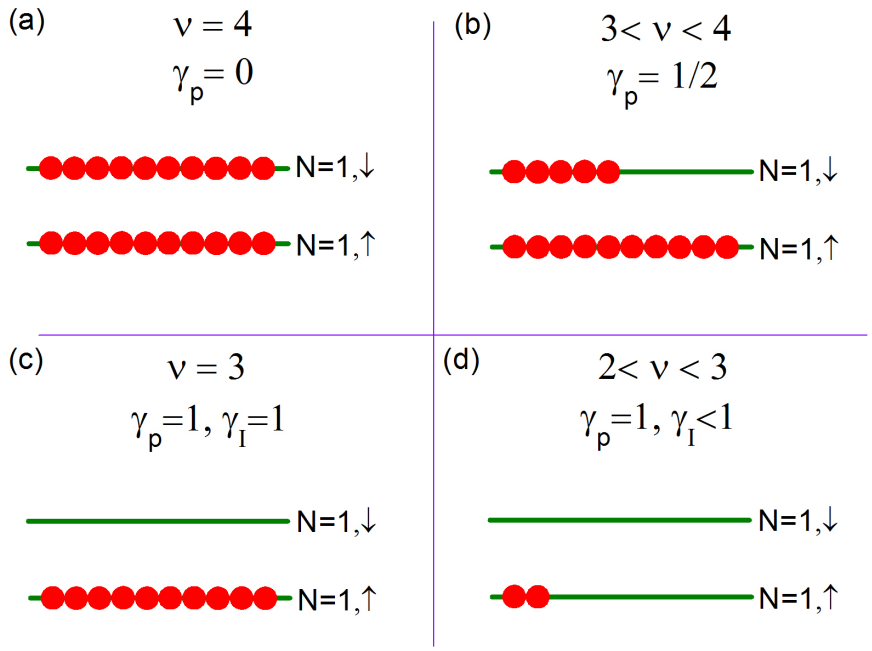

Figure 3.13: Spin wave intensity is determined by γ_p and the number of electrons available for light scattering . Spin polarization depends on the relative number of electrons occupying lower and upper spin branches, as defined in Eqn. 2.27. (a) both the upper and lower spin branches are fully occupied at $\nu = 4$ resulting in zero net polarization. (b) For $3 < \nu < 4$ the upper spin branch is partially occupied allowing for some finite spin polarization. (c) The upper spin branch is completely empty and the lower spin branch is fully occupied yielding maximum spin polarization and spin wave intensity. (d) Though the system remains fully spin polarized, as the lower spin branch empties, there are increasingly fewer electrons available for light scattering. Consequently, in this single particle picture, we expect the SW intensity to decrease with the number of available electrons.

LL: $N = l, \downarrow$ and $N = l, \uparrow$ respectively. The intensity of the SW is expected to depend sensitively on the net polarization of the 2DES. The intensity of the SW also depends on the number of spins available to participate in the light scattering process. I attempt to quantify this by defining an expression for the SW intensity, γ_I (applicable to the N=1 LL),

$$\gamma_I = \frac{n_\uparrow - n_\downarrow}{n_\uparrow + n_\downarrow} \times \frac{n_\nu}{n_{\nu=3}} \tag{3.25}$$

$$\gamma_I = \gamma_p \times \frac{n_\nu}{n_{\nu=3}} \tag{3.26}$$

illustrated by Fig. 3.13. $n_\uparrow$ ($n_\downarrow$) represents the electron density in the lower (upper) spin branch of a *Landau* level and γ_p is the spin polarization as defined in Eqn. 2.27. n_ν is the number of electrons occupying the highest occupied energy level while $n_{\nu=3}$ is the maximum number of electrons that can occupy a filled energy level at $\nu = 3$. We have limited our considerations to the range $2 < \nu < 3$.

Since the SW is a long wavelength excitation, one expects its supporting medium to have a spatial extent greater than the wavelength of the SW. The quantum fluid in the lowest LL, in the presence of disorder, is expected to have a relatively large spatial extent of $\lesssim$ micron dimensions [96]. ILS studies [94, 97, 98] have demonstrated that the FQH fluid in the LLL supports the SW mode. If heterogeneity (i.e. its length scale) were increased further; for instance, if the supporting medium were to break up into submicron domains ($\ll 1\mu m$), then the excitation giving rise to the SW may be suppressed. That is, if translational symmetry is completely broken, the SW excitation may be destroyed. Rotational symmetry is another important symmetry linked to the SW excitation. Having rotational symmetry implies angular momentum is conserved. Larmor's theorem tells us that the long wavelength spin wave excitation is fixed at the Zeeman energy. The spin precession in Larmor's

theorem requires that angular momentum is conserved. Consequently, if there is some mechanism that destroys the rotational symmetry of the system, we might also expect Larmor's theorem to breakdown.

3.7 Optical Emission

3.7.1 Overview of Optical Emission

Optical emission measurements constitute a huge part of research in condensed matter physics and other fields of science. With respect to GaAs quantum wells, optical emission occurs when electrons and holes are excited to some energy above the Fermi energy. Electrons and holes then thermalize to some state $|i\rangle$ where they then relax to a state $|f\rangle$ via the emission of a photon. Though luminescence is much easier to measure than light scattering, optical emission data are exceedingly difficult to interpret. Consequently, only a very qualitative and rudimentary discussion will be given here, largely for the purposes of putting our light scattering machinery into better context. A detailed account of optical emission in GaAs quantum wells is available in Ref. [42].

3.7.2 Optical Emission from 2DES

When incident photons have energy ω_L greater than the sum of the optical band gap and Fermi energy of the QW, the 2DES will luminesce. Figure 3.14 shows optical transitions of conduction band electrons recombining with valence band (VB) holes. The electron-hole recombination results in the emission of light of a range of wavelengths. Panel (a) of Fig. 3.14 shows the 2DES being excited by a photon and subsequently thermalizing. Thermalization is the process by which excited electrons and holes return to a relaxed state via phonon scattering [99]. Panel (b) shows light

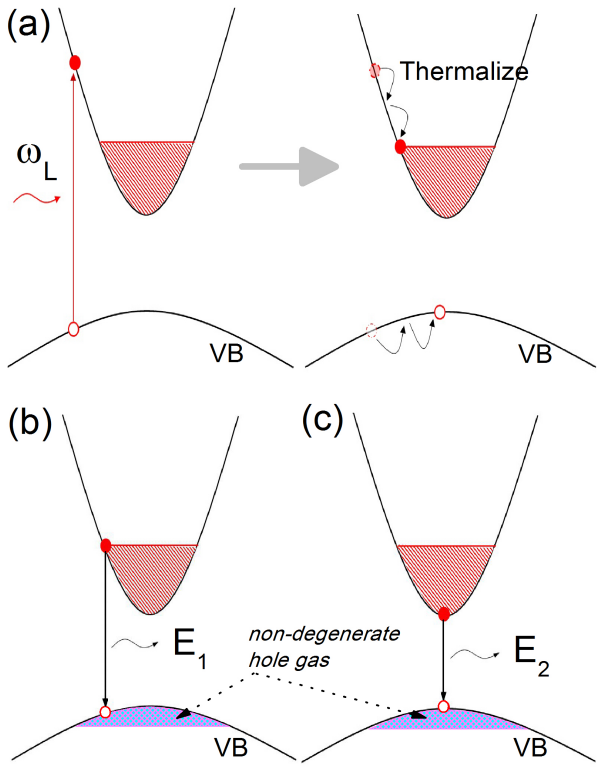

Figure 3.14: The optical emission process is illustrated. (a) An electron hole pair is created by an incident photon of energy ω_L. The photoexcited electron then thermalizes. (b) Optical relaxation takes place resulting in an emission of a photon. The transition can be "high" energy, the maximum energy, E_1 due to recombination of an electron from the top of the Fermi sea with a VB hole. (c) An electron at the bottom of the conduction band may also recombine with a VB hole. This results in a minimum energy transition, E_2. The non-degenerate hole gas is explicitly shown in panels b and c. A marvelous discussion on optical emission in GaAS QWs can be found in Ref. [13].

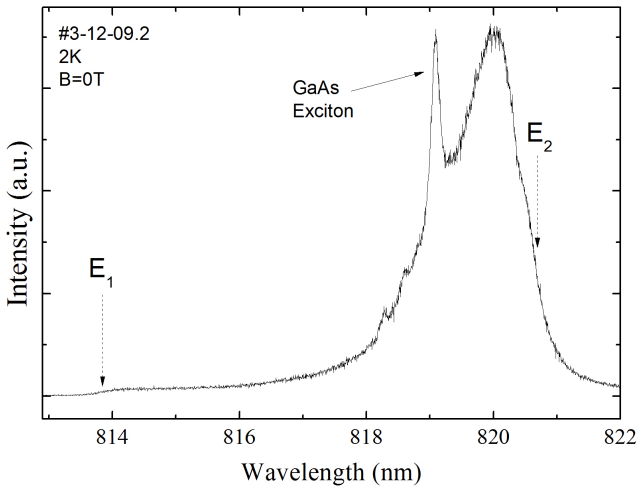

Figure 3.15: An example of a zero magnetic field spectrum due to optical emission from a GaAs QW (width of 300$\mathring{A}$ and $n = 2.9 \times 10^{11} cm^{-2}$). As discussed in Fig. 3.14, the short wavelength (high energy) cut-off is described by E_1, while the long wavelength cut-off is pegged at E_2.

emitted from the top of the Fermi level while panel (c) shows light emitted from the bottom of the conduction band. The emitted photons have maximum and minimum energies, E_1 and E_2 respectively (and a range of intermediate energies not explicitly shown). The difference in energy, $E_1 - E_2$ is equivalent to E_F (not accounting for a correction due to the curvature of the valence band, which is typically $\sim 15\%$). Optical emission measurements at zero field allow us to extract the Fermi energy and consequently the electron density. The density is given by the relation [13]

$$n = \frac{2m^* c}{\hbar}\left[1/\lambda_1 - 1/\lambda_2\right]\left[1 + \frac{m^*}{m_h}\right] \tag{3.27}$$

where λ_1 and λ_2 are the wavelengths for the energies E_1 and E_2 as described by Fig. 3.14 and 3.15. m^* is the effective electron mass and m_h is the hole mass in the valence band. The term, $(1 + \frac{m^*}{m_h})$ represents the correction due to the curvature of the valence band.

An example of zero field luminescence is shown in Fig.3.15 and delimits the energies E_1 and E_2 described in Fig. 3.14. The high energy cut off at E_1 is known

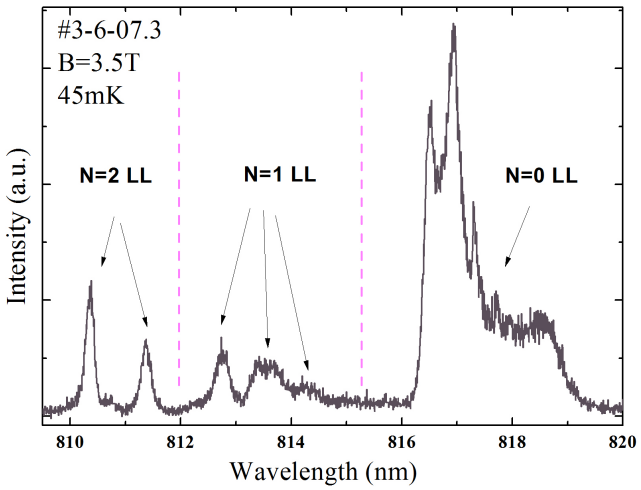

Figure 3.16: Spectrum shows optical emission from a 2DES at $B = 3.5T$ ($\nu = 4.56$). The broad continuum of spectral weight seen in Fig. 3.14 at 0T breaks up into sharp peaks as energy levels become quantized and spaced by the cyclotron energy and Zeeman energy. The optical emission from different Landau levels is delimited.

as the Fermi step, because of the step-like onset of the spectral weight at E_1. The low energy cut-off of the optical emission is ideally sharp. However, because our 2DES lives in real samples, there is broadening due to disorder. The exciton of GaAs is seen at energy within the energy range of the quantum well optical emission ($\lambda \sim 819nm$ in Fig. 3.15).

Fig. 2.3 showed that a finite magnetic field quantizes the continuum of zero magnetic field electron energies. Optical emission can occur from the resulting quantized levels (provided they are populated with electrons), as illustrated in Fig. 3.16. This figure shows optical emission from a 2DES that formed Landau levels, three of which are populated, as indicated by the presence of three sets of peaks at discrete energies. Each set of peaks is spaced by roughly ω_c. The formation of doublets in luminescence spectra could be due to spin splitting of the Landau levels by $B[T]$. There may be additional peak splitting (the formation of triplets for instance), as seen for the N=1 LL and the N=2 LL in Fig. 3.16, that cannot be explained by spin splitting alone. An explanation of this behavior lies in other complicated processes,

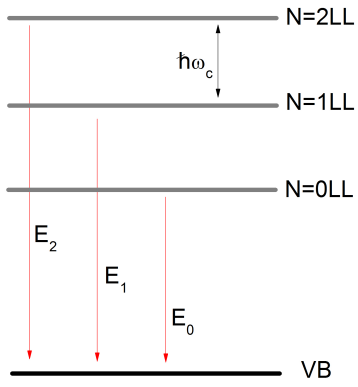

Figure 3.17: A schematic of Landau levels from which optical transitions occur that produce optical emission at discrete energies. Spin splitting by the Zeeman energy is not explicitly shown in the conduction band. In addition, the heavy hole, light hole and split-off valence band levels are not explicitly shown.

like that of the "shake-up" [100, 101, 102], an in depth discussion of which is beyond the scope of this thesis. The shake-up is analogous to the Auger effect; electron-hole recombination will emit a photon and excite an electron to a higher energy level. The energy debt for the electronic excitation results in a reduced photon emission, which shows up as an extra "low" energy peak in optical emission spectra. The optical emission shown in Fig. 3.16 is under magnetic field, B= 3.5T. This magnetic field corresponds to a filling factor of $\nu = 4.56$, this value tells us that the 1st and 2nd LLs are fully occupied, and that the 3rd LL is only partially filled. A schematic of the energy level transitions is shown in Fig. 3.17. The spin splitting of the Landau levels, along with the heavy hole (hh) and light hole (lh) states are not explicitly shown, though they impact the allowed transitions due to restrictions from angular momentum conservation.

Though there is a great deal of information that can be gleaned from optical emission spectra [103, 100, 104, 101, 105, 106, 107], I will primarily use luminescence spectra to assist in resonance Raman scattering measurements. Energies of optical

gaps can be determined from optical emission spectra. I then match the incident photon energy to the energy of the highest partially occupied or unoccupied state to boost the intensity of scattered light to within measurable limits via resonance enhanced Raman scattering.

In the next few chapters I will apply these optical methods to address unanswered questions and areas of interest in quantum Hall research. Optical studies provide a unique probe of 2DES's that will complement the plethora of existing studies in quantum Hall research. In particular, inelastic light scattering provides a measure of the energy of an excitation as well as information about its spin and charge degrees of freedom, that is inaccessible by other means.

Chapter 4

Measurements of High Energy Composite Fermion Excitations

4.1 Overview

Studies of collective states of matter have proved enormously important both because of the fundamental physics they reveal and the role they play in stimulating technological innovation. The electron liquid that manifests in the fractional quantum Hall effect emerges as a result of interactions between electrons when the dimensionality is reduced to two and the Hilbert space is further restricted by application of an intense magnetic field [46]. The liquid represents a cooperative behavior that does not subscribe to concepts such as Bose-Einstein condensation and Landau order parameter. The fractional quantum Hall liquid is the realization of a topological quantum state of matter, the understanding of which has influenced development in a wide variety of fields, such as the recent topological insulators, cold atoms, graphene, generalized particle statistics, quantum cryptography, string theory and more [108, 32, 109, 110, 111, 112].

This overview, an extension of the discussion of quantum Hall physics in Chap-

ter 2, continues the introduction to the intriguing properties of fractional quantum Hall systems. I start by introducing the link between topology and the fractional quantum Hall systems. Topology is the study of the properties of geometric configurations that are invariant under smooth deformations. The FQHE phases are topological phases in that at low temperature and energies, and for long wavelengths, all their observable properties remain invariant under smooth deformations[32, 4]. It is this ability for a topological phase to remain invariant under smooth perturbations that make it useful for potential applications in fault-tolerant quantum computing[32]. In this section we attempt to quantify topological robustness of composite fermions (CFs) in a light scattering experiment. CF quasiparticles in the fractional quantum Hall liquid provide a framework to interpret much of the phenomenology in magneto-transport. It is not yet known up to what energies they remain intact. In addition, the extent to which CFs can form *Landau* like energy levels has not been explored experimentally. This study of CF excitations examines the structure and robustness of CFs. We probe the high-energy spectrum of the ν =1/3 fractional quantum Hall (FQH) liquid directly by resonant inelastic light scattering, and report the observation of a large number of new collective modes[5]. Supported by theoretical calculations[5, 92], we associate these observed excitations with transitions across two or more CF levels. Formation of quasiparticle levels up to high energies is direct evidence for the robustness of topological order in the fractional quantum Hall effect. Topological order is a new kind of organization of particles that is analogous to but goes beyond the Landau symmetry-breaking description. Topological order can be described by a new set of quantum numbers such as quasiparticle fractional statistics[113].

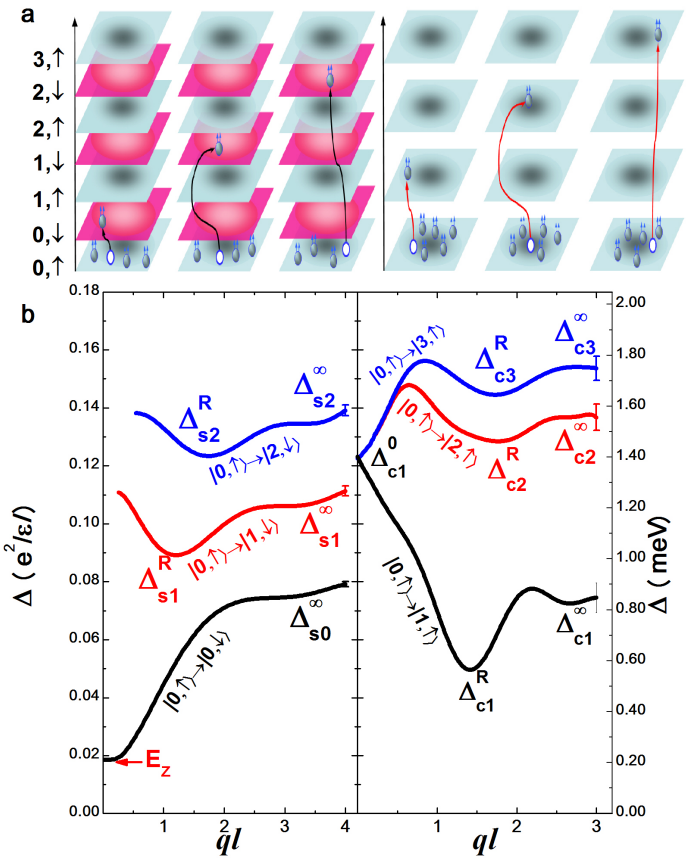

Figure 4.1: Schematic diagram of composite-fermion excitons accompanied by theoretical calculations of their dispersions. (a) The right panel shows pictorially the spin-conserving excitations $|0,\uparrow\rangle \rightarrow |K,\uparrow\rangle$ across K Λ levels. The left panel shows the spin-flip modes $|0,\uparrow\rangle \rightarrow |K,\downarrow\rangle$ (b) Calculated dispersions of CF excitons for a 35 nm wide GaAs quantum well with an electron density of 5.0×10^{10} cm^{-2}. The right (left) panel shows the dispersions for SC (SF) modes. The error bar at the end of each curve represents the typical statistical uncertainty in the energy determined by Monte Carlo method. Critical points in the dispersion are labeled[5].

4.2 Background

Neutral excitations (excitations whose net charge remains zero, such as excitons) provide a unique window into the physics of the FQH liquid. Early theoretical treatments of the lowest neutral collective mode of the FQH state at ν=1/3 employed a single mode approximation [114], as well as exact diagonalization studies on small systems [115], and demonstrated a minimum in the dispersion, which, following the terminology used in superfluid Helium, is called a "magneto-roton." Subsequently, the collective modes at this and other fractions were understood in terms of composite Fermions (CFs) [52] as described in Chapter 2. Recall that, despite their exceedingly complex collective character, CFs act as almost free particles (insofar as the low energy behavior is concerned) [46] and form "Λ levels". The neutral excitations are described as inter-Λ-level exciton collective modes of CFs [116, 14, 117, 118], in close analogy to the electronic collective modes of the integral Hall states. A cartoon depicting Λ level excitons is shown in Fig. 4.1.

Light scattering experiments probe the bulk states of quantum fluids. The experiments we performed that are described here minimize the impact of edge states, which are an integral part of magnetotransport measurements. Byszewski et al. [119] report the detection of neutral excitations of CFs in the FQH regime using optical emission. Optical emission measurements also probe the bulk states of quantum fluids. Using optical emission, Byszewski et al. observed signatures of the existence of CF excitons. More precisely, the optical emission from CF energy levels was detected. We can also detect CF energy levels using light scattering. The light scattering experiment discussed in this Chapter serves to explore in further detail the energy level structure of CFs and to probe the topological robustness therein.

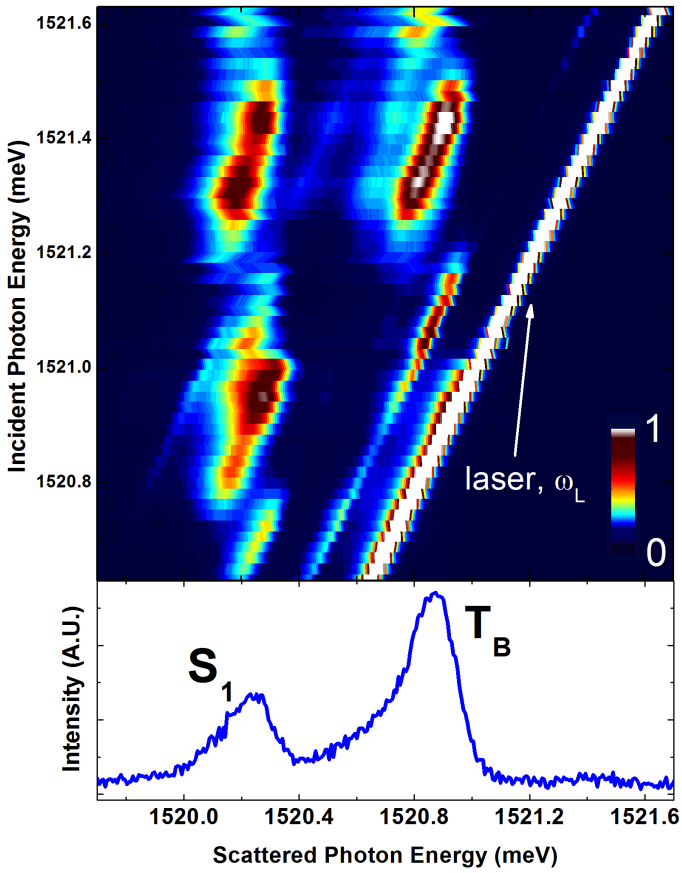

Figure 4.2: Novel high energy excitations at $\nu = 1/3$ plotted in absolute energy units. The main experimental result is plotted on a scattered photon energy scale. We confirm that the spectral response is due to inelastic light scattering from excitations of the quantum fluid at 1/3 filling. The excitations resonate with the singlet (S_1) and triplet (T_B) luminescence peaks. The excitations follow the laser peak, identifying them as inelastic light scattering excitations. The excitations sit on top of a weak luminescence background. The two-dimensional electron gas at $\nu = 1/3$ is tilted at θ=30^o in a magnetic field, B_T= 8.0 T at 70 mK.

4.3 Results and Discussion

We reported the excitation spectrum of the FQH fluid at ν=1/3 in a previously unexplored energy range[5]. Our principal finding is the existence of several well defined collective modes at energies substantially exceeding those of the highest previously reported spin-conserving (SC) and spin-flip (SF) modes [78, 120, 79]. Further, we provide compelling evidence, supported by a detailed comparison between theory[5, 92] and experiment, that these neutral modes represent a new family of excitations involving CF transitions across several Λ levels ($\Lambda L's$). CF $\Lambda L's$ provide a single particle-like interpretation of the complex states of strongly interacting electrons in the FQH regime whose existence can only be confirmed through experiment. The direct experimental observation of the integrity of $\Lambda L's$ at energies far above the Fermi energy demonstrates that CFs are more robust than previously thought, bolstering the expectation that the quasiparticles of other topological states of CFs, such as the proposed nonabelian quasiparticles of the paired Pfaffian state at 5/2 [32, 121], will also have comparably robust character.

The intensity of the scattered light at ν=1/3 is displayed in Fig. 4.2, which has an absolute energy scale. The colorplot illustrates the changes in intensity of light scattering peaks (indicated by changes in color) with respect to scattered photon energy as the incident photon energy is tuned. Panel (a) shows that when the incident photon energy is tuned, different FQH modes are excited. The energy of the modes excited increases with increasing photon energy. The resonance enhancement of the intensity of excitations in inelastic light scattering experiments depends sensitively on both the frequency of the incident laser light and on the energy of the FQH mode. Not all modes are thus visible in a single spectrum and a scan over a range of incident photon energies is necessary to obtain a more complete picture. Fig. 4.2 (b) shows the optical emission peaks that are used to locate the energy of optical

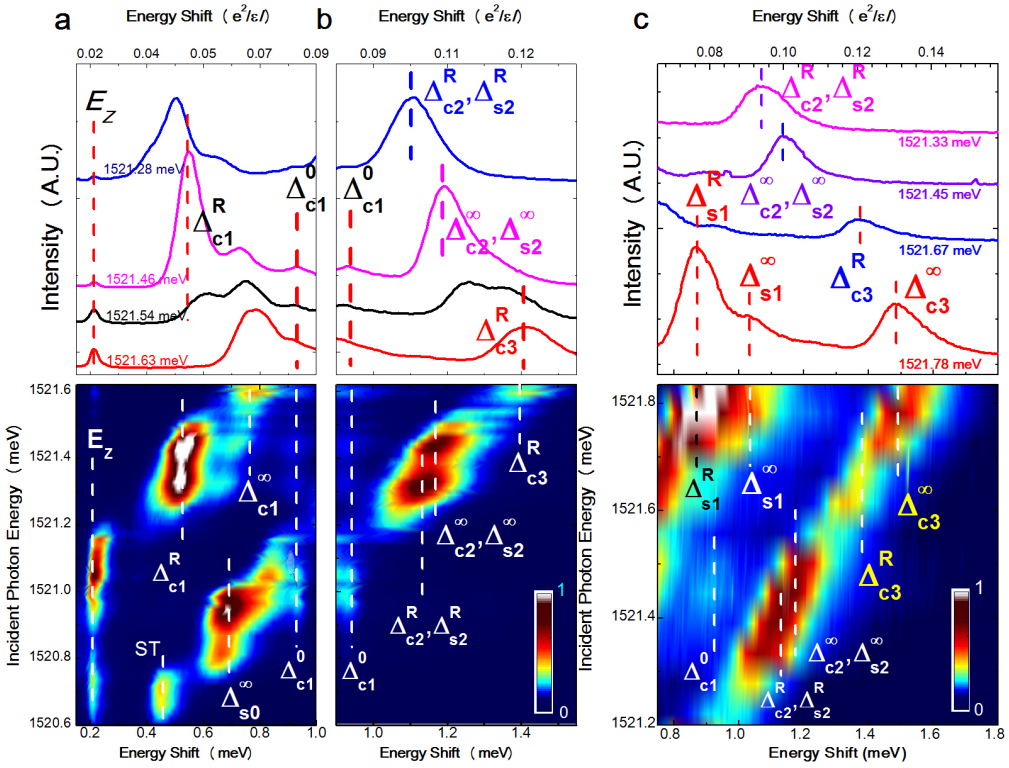

Figure 4.3: Inelastic light scattering spectra of excitations at ν=1/3 as a function of the energy shift (with total magnetic field B_T =8.0 T, 33nm wide QW, $5.6\times10^{10}cm^{-2}$ and a tilt of 30^o). The energy is shown in units of $e^2/\epsilon l_o$ on the top scale, where l_o is the magnetic length and ε is the dielectric constant of GaAs. The upper panels show peaks of several modes for certain selected incident photon energies. The lower panel contains a color plot of the intensities of both (a) "low energy" and (b),(c) the novel high energy modes. The vertical lines mark the positions of the collective modes. The symbols, explained in the text, identify the modes with excitations of CFs across several $\Lambda L's$, both with and without spin reversal.

gaps used in resonant enhancement of light scattering. To better identify modes, I replotted the light scattering data on an energy shift scale, as shown in Fig. 4.3. Data are shown as raw spectra (top panels) and as a colorplot (bottom panels). The data displayed are now a function of the energy transfer $\omega = \omega_L - \omega_S$. Each peak indicates the presence of a collective mode. The collective mode energies are marked by vertical lines and labeled by comparing data with theoretical predictions; I will describe this in more detail below. The previously observed modes lie at energies below ~ 1 meV, as seen in Fig. 4.3a. The most striking feature of the spectra shown in Fig. 4.3b and 4.3c is the existence of a number of new modes all the way up to 1.6 meV, the largest energy exchange accessed in our experiments.

It is natural to interpret these new modes in terms of excitations of CFs across K levels, where K is an integer or zero. These excitations are referred to below as "level-K excitons". Previous experiments at $\nu = 1/3$ had reported only level-1 SC excitons and level-0 SF excitons [78, 79, 28, 122]. Level-2 and level-3 CF excitons were recently investigated theoretically[92] in the context of the splitting of the 1/3 collective mode at small but nonzero wave vectors [122]. Because the modes may also involve spin reversal, we adopt the notation in which we denote the level-K spin-conserving modes by Δ^{α}_{cK} and the level-K spin-flip modes by Δ^{α}_{sK}. The superscript indicates the wave vector position of the mode: we have $\alpha = 0$ for the zero wave vector mode, $\alpha = \infty$ for the large wave vector limit, and $\alpha =$R for a roton mode. Identifications of the various modes shown on Fig. 4.3 are based on the analysis below.

4.3.1 Theoretical Considerations

The dispersions of the SC and SF excitons can be obtained by the method of CF diagonalization (without *Landau* level mixing and disorder) [123, 92]. CF diagonal-

ization is the mathematical process in which IQHE wavefunctions are transformed into FQHE wavefunctions or CF wavefunctions and the eigenenergies of the resulting quasiparticles calculated. For a more accurate comparison, two realistic effects are included: The finite width modification of the interaction is incorporated via a self-consistent local density approximation. Also, Λ level mixing is allowed by considering the *five* lowest energy CF excitons. A combination of these two effects results in a 20 % reduction of the energy of the level-2 and level-3 excitons, and a smaller ($\sim$ 10 %) reduction in the energy of the level-1 exciton[92]. Figure 4.1 shows the full theoretical dispersions of the CF exciton branches for SC and SF modes as taken from Ref. [92]. The calculations were performed for 200 (100) particles for SC (SF) modes and reflect the thermodynamic behavior (that is, it embodies the characteristics of a macroscopic system not limited by finite size effects) [5]. The three dispersion curves indicated in Fig. 4.1b are assigned as level-0, level-1 and level-2 for SF modes and level-1, level-2 and level-3 for SC modes, in order of increasing energy. The residual interaction between CFs in principle mixes the different "unperturbed" level-K excitations; however, the modes do not mix significantly at large ql_o, which allows the continued use of the level-K nomenclature even for mixed modes. In the zeroth order approximation, interacting electrons form non-interacting CFs. Nevertheless, some "left over" interaction is needed to explain the full breadth of phenomenology of the FQHE, though, most fractions can be explained using the non-interacting CF approximation discussed in Chapter 2. Figure 4.4 shows a comparison of the CF excitons with exact diagonalization studies on a finite system and serves to corroborate the effectiveness of CF theory.

Level-1 SC modes and level-0 SF modes have been identified in previous experiments [122, 78, 79]. The mode at 0.46 meV is a spin texture (ST) mode as already shown in Refs. [79, 78]. Of interest here are the higher lying modes. We proceed by sorting the experimental values of the new modes in ascending order and matching

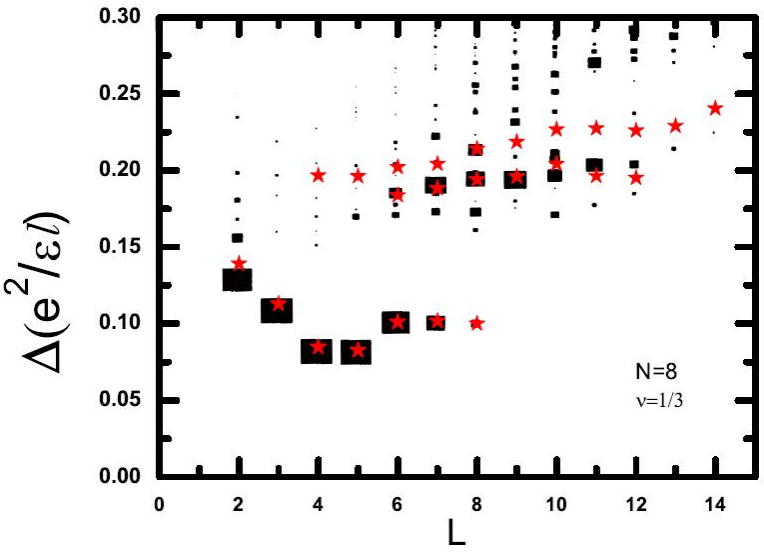

Figure 4.4: Comparison of CF excitons with exact diagonalization results (in spherical geometry) for eight particles at $\nu = 1/3$. The red stars show the CF exciton dispersions for the lowest three SC branches for this system as a function of the total orbital angular momentum L. The exact spectra are taken from Ref.[14]. The area of each black rectangle is proportional to the normalized spectral weight under the state; larger spectral weight implies greater intensity in Raman scattering. The level-1 and level-2 CF excitons closely trace lines of high spectral weight; it is possible that still higher modes will become identifiable in the exact spectra for larger systems. The other states in the exact spectrum are interpreted as made up of multiple excitons, which are expected to couple less strongly to light [15].

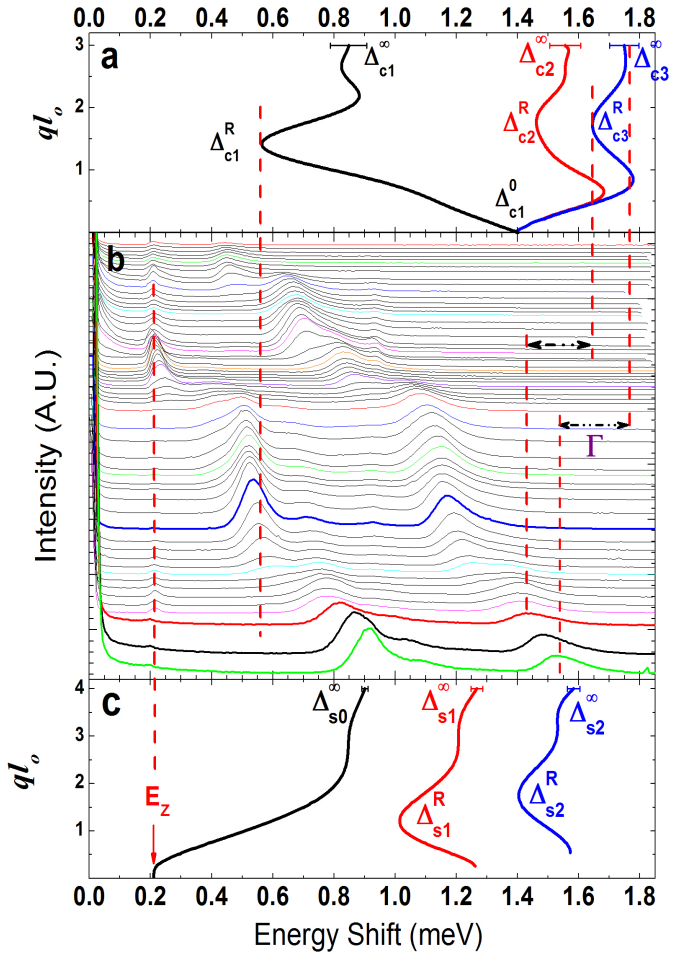

Figure 4.5: Raw spectra are compared with theoretical calculations (from Ref. [5]) of charge and spin modes. (**a**) Shows the theoretical dispersion of charge modes of composite fermion Λ levels at 1/3 filling. (**b**) Waterfall spectra are in order of increasing incident photon energy from top to bottom. These spectra show the original data used to construct the colorplot in Figs. 4.2 and 4.3. Dashed lines are a guide to the eye and show that for the lower energy modes, the discrepancy between experiment and theory is small. Higher energy modes are shifted from experiment due to disorder, Γ (∼0.22 meV). (**c**) Shows the theoretical dispersion of spin modes of composite fermion Λ levels at 1/3 filling [5].

them up with theoretical values. Fig. 4.5 compares experimental and theoretical data. Fig. 4.5(b) shows light scattering spectra of low and high energy modes. Panels (a) and (c) show the calculated dispersions for charge and spin modes respectively [5]. Dashed lines illustrate how critical points in the dispersion (such as Δ_{c1}^{R} in panel (a)) delimit the energies of peaks in ILS. The resulting comparison between theory and experiment is summarized in Fig. 4.6. The theoretical results for the energies of level-1 excitons are in excellent agreement with the experimental results. The only exception is the long wavelength collective mode Δ_{c1}^{0}, for which the discrepancy is closer to 35 %, but a $\sim$ 20 % agreement is achieved when screening of the single exciton by two-roton excitations is taken into account [124]. This correction, not included in the calculation shown in Fig. 4.1, is incorporated in Fig. 4.6.

4.3.2 Experimental considerations and comparison with calculations

It is significant that mode energies predicted by theory agree to within 0.2-0.3 meV with measured energies, which translates into a better than 20 % agreement. It should be stressed that a similar level of deviation between the theoretical and experimental values of the excitation energies has been found in the past for other excitations, and attributed to disorder. We judge the overall comparison between theory and experiment to be quite good, and take it as a strong support of the identification of the high energy collective modes ranging from about 1.0 meV to 1.6 meV in terms of transitions of composite fermions into higher levels.

Before closing this Section, we note that because of the presence of a large number of modes, sometimes two or more modes happen to lie at very nearby energies, and therefore may not be resolved in our experiments. For example, for

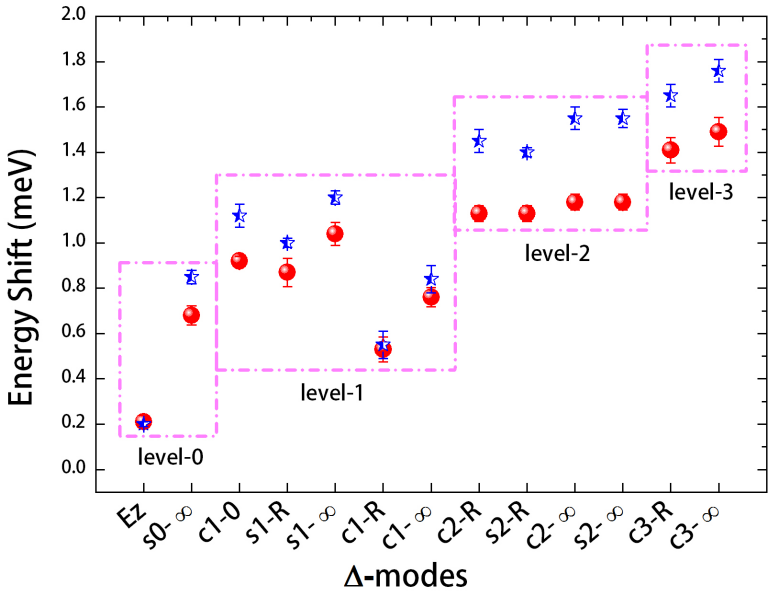

Figure 4.6: Comparison between experimental energies (from Fig. 4.3, red circles) with theoretical CF exciton energies (from Fig. 4.1, blue stars), organized according to the level of the excitation. The identification of experimental modes is explained in the text. The discrepancy between theory and experiment, less than 0.2-0.3 meV, is presumably caused by disorder. Estimated error bars for the experimental values are shown, unless smaller than the symbol size [5].

SC modes, the energy of the level-3 roton overlaps with the small q (q$l \sim 0.6$) critical point of the level-2 exciton (see Fig. 4.1b). As another example, the small q (q$l \sim 0.8$) critical point of the level-3 exciton overlaps in energy with the large wave vector limit of the level-3 exciton. When encountering such a situation, we have, for simplicity, arbitrarily assigned one of the possible labels to the observed mode (Δ_{c3}^{R} and Δ_{c3}^{∞}, respectively, for the above two cases). The assignment remains tentative in such cases, and more sensitive experiments in the future may reveal further finer structure.

4.4 Summary

This study describes the first light scattering studies to show that CFs can be excited across multiple $\Lambda L's$. Moreover, this is the only experimental work that has excellent agreement with theoretical predictions. This work allows a quantitative estimate for the robustness of the topological quantum states of the FQHE. Furthermore, the results reported in this Chapter set the stage for further investigations in other FQH states in GaAs, and also in other two dimensional systems, such as graphene, where the FQH physics is in its infancy [109, 110]. I will present in later chapters examples of other large wavevector, high energy modes in the context of higher *Landau* level excitations.

Chapter 5

Studies of Spin and Inhomogeneous phases in the second *Landau* Level

5.1 Overview

In this chapter, the spin degrees of freedom in quantum phases of the second Landau level are probed by resonant light scattering. In uniform systems, the long wavelength spin wave mode, which monitors states of spin polarization, is fixed at the Zeeman energy in the fully spin polarized state at ν=3. This is a consequence of Larmor's theorem and is illustrated in Fig. 5.1. Fig. 5.1a shows the spectral weight due to the long wavelength spin wave excitation fixed at E_Z. Fig. 5.1c shows an energy level diagram of the spin exciton that gives rise to the spin wave, the long wavelength dispersion of which is shown in panel (b). Monitoring the SW provides insights on spin degrees of freedom that seem to us more reliable than other methods such as the Knight shift [36] or optical emission spectroscopy [125]. Surprisingly, as we will see in this Chapter, at lower filling factors the intensity of the Zeeman

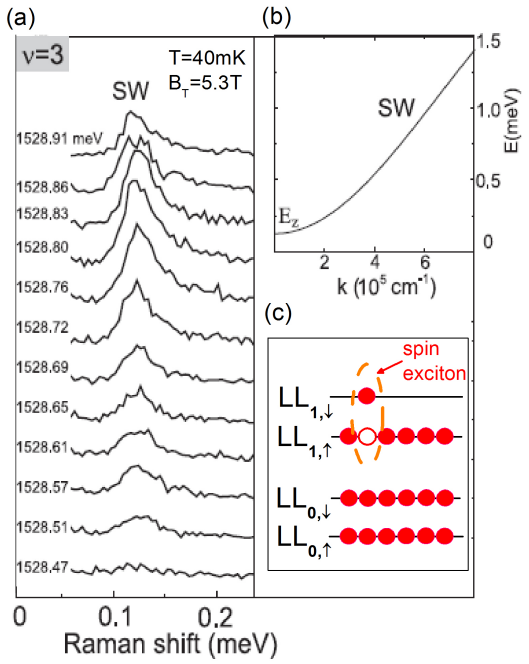

Figure 5.1: (a) Inelastic light scattering spectra of the intra-LL SW mode at $\nu = 3$ and $B_T = 5.3$ T taken at different laser photon energies (shown on the left). (b) Shows the SW dispersion curves calculated within the Hartree-Fock approximation [12, 16] for a 24 nm wide quantum well. The long-wavelength region of the SW dispersion is shown. (c) Energy level diagram shows the excited state at $\nu = 3$ that gives rise to the SW excitation.

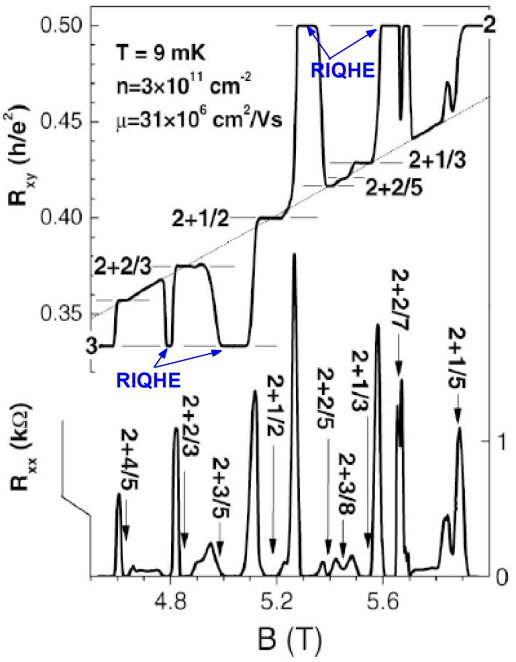

Figure 5.2: Magnetoresistance trace for filling factors $3 > \nu > 2$. The state at $\nu = 5/2$ is delimited along with other magic filling factors in the N=1 LL. Reentrant integer quantum Hall effect phases (RIQHE) are shown with arrows. RIQHE states are states which have non-integer filling factors yet have R_{xy} values of neighboring IQHE states. Taken from Ref. [17]

mode collapses, suggesting the emergence of complex phases and significant loss of spin polarization. A novel broad continuum of low-lying excitations emerges that dominates near ν=8/3 and ν=5/2. Resonant Rayleigh scattering, simultaneous to inelastic light scattering experiments, reveals that the quantum fluids for $\nu < 3$ break up into robust domain structures of distinct phases. Domains for $\nu < 3$ have smaller size than inhomogeneous regions at $\nu = 3$ [66, 96]. These domains may be small enough to disrupt the long wavelength SW. While many theoretical studies consider the state at $\nu = 5/2$ to be fully polarized, our results reveal unprecedented roles for spin degrees of freedom.

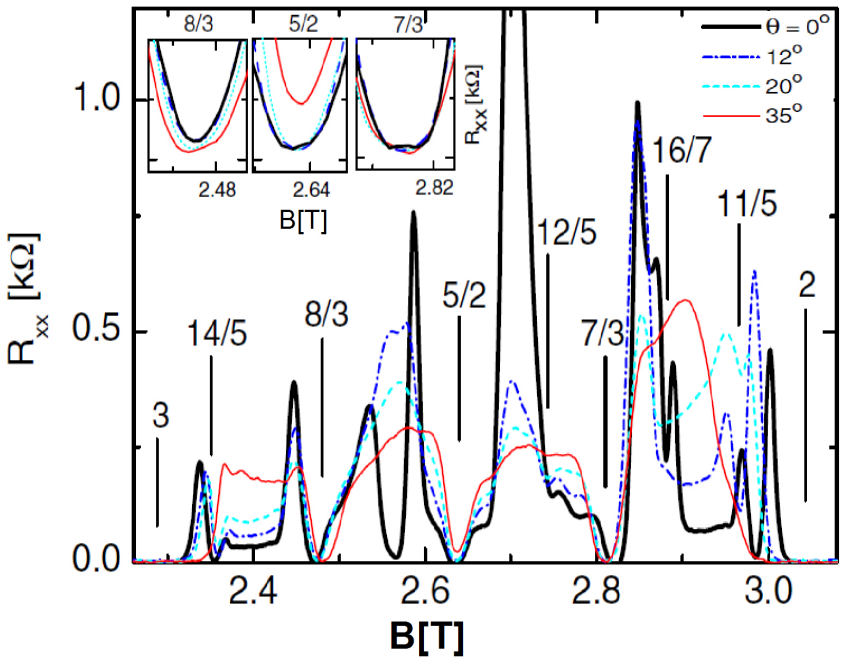

Figure 5.3: Magnetoresistance trace (longitudinal resistance, R_{xx} versus changes in the perpendicular magnetic field, $B[T]$) around $\nu = 5/2$ showing the effect of varying sample tilt, θ (T = 20 mK). The inset is an enlargement showing the trend of the minima at $\nu = 8/3, 5/2$ and $7/3$. These data are taken from Ref. [18].

5.2 Background

The study of the quantum Hall effect in the second (N=1) Landau level (LL) is at the forefront of physics research. In the second LL lies the state at filling factor $\nu = 5/2$ (shown in Fig. 5.2 and 5.3) [126, 127, 17], the best known even denominator quantum Hall state - defying the paradigm of odd-denominator fractional quantum Hall states [49, 52] and leaving a challenge to the understanding of quantum Hall physics. The 5/2 quantum Hall state is predicted to realize a non-abelian phase (discussed later in this section) - the Moore-Read Pfaffian [93], an exotic form of matter, still unconfirmed experimentally. The Moore-Read state may facilitate the implementation of topological quantum computation [32]. Efforts are being made to confirm the remarkable properties of the 5/2 state [121].

The discovery of the first even-denominator fractional quantum Hall state at $\nu = 5/2$ by Willett et al.[126] has engendered a great wealth of scientific interest in the origin of this enigmatic state. After 24 years of investigation, there still remains many open questions on the nature of the state at 5/2. Soon after its discovery, Eisenstein et al. found that the activation gap at 5/2 was reduced with increased tilt or in-plane magnetic field [33]. At first this seemed to suggest that the state at 5/2 was spin unpolarized. Nevertheless, subsequent to that finding, a great many theoretical studies garnered strong evidence for a fully spin polarized 5/2 state. For instance, the work by Morf [30] is accepted as providing numerical evidence for a spin-polarized state. Subsequently, a great deal more work was done at 5/2, much of which has focused on its spin degrees of freedom. To date, the debate on whether or not the state at 5/2 is spin polarized or not continues[128, 36, 66, 38, 37, 125, 30].

As described by Moore and Read, the Pfaffian wave function is a p-wave paired BCS state of composite fermions at 5/2 filling [93, 29]. The "p-wave" term describes the even symmetry of the spin part of the wavefunction - it is a spin triplet which

is even under exchange [72]. Consequently, the state is spin-polarized. The quasiparticles at 5/2 pair to form a gapped or incompressible state; contrasting with the compressible Fermi sea at $\nu = 1/2$, where there is no energy gap between the ground and excited states.

Much of the interest in the state at 5/2 is driven by the prediction that its excitations should obey non-abelian braiding statistics [32, 121, 129]. What does it mean to have non-abelian braiding statistics? How is it different from Fermi or Bose statistics? In mathematics, the term non-abelian refers to the property that the multiplication of two elements in a group does not commute. In physics, for abelian particles like bosons of fermions, winding a particle A around a particle B and vice verse are equivalent processes that will only result in multiplying the wavefunction by a sign. There is another class of abelian particles called "anyons" - the exchange of which will result in multiplying the wavefunction by a phase, $e^{i\theta}$. The special cases, θ=0 and π correspond to bosons and fermions respectively. A marked difference in the behavior of particles under exchange arises in the case of non-abelian particles. Exchanging two non-abelian particles does not just multiply the wavefunction by a phase, instead it takes the system from one ground state to the other. Another remarkable property of non-abelian particles is that the order of the exchange of particles defines the properties of its ground state. It is this remarkable property that lies at the heart of using particles with non-abelian statistics as the starting point for developing topological quantum computation. As already alluded to, particles with non-abelian statistics are predicted to be realized in quantum Hall systems, in particular, in the quantum fluid at $\nu = 5/2$. The excitations from the ground state at $\nu = 5/2$ form the quasiparticles that braid and obey non-abelian statistics. An excellent review article that goes into much more detail that can be allowed here is given by Stern [121]. Even more in depth discussions can be found in Refs. [32, 129].

Despite the numerical evidence that the Moore-Read state at $\nu = 5/2$ should be spin polarized [30]; a definitive experimental verification is still lacking. For instance, transport measurements [17, 130, 38] suggest that the role of spin for the states at ν=5/2, 8/3 and 7/3 disagrees with accepted theoretical models. For example, Fig. 5.3 illustrates that the state at $\nu = 5/2$ grows weaker with tilt, whereas a spin polarized state is expected to grow stronger with tilt [18, 33]. Consequently, these tilt measurements seem to contradict the prediction that the state at $\nu = 5/2$ is spin polarized. Nevertheless, great strides towards understanding the 5/2 quantum Hall state and its spin degrees of freedom have been made with recent experimental and theoretical work [131, 132, 133, 134, 135, 125, 37, 136]; though a complete understanding still evades our grasp.

Resolving the "puzzle" of spin states of the 5/2 quantum Hall state has emerged as an important challenge that would create key insights on the physics of quantum fluids in the second LL. Read [29] had suggested using the Knight shift to study the spin polarization of the 5/2 state. Recent Knight shift results, though controversial, support the idea of spin polarized fluids throughout the second Landau level [36]. Rhone et al. [133] have used inelastic light scattering to study the spin polarization of states in the second LL and at $\nu = 5/2$ in particular. The work suggests that quantum fluids observed at 5/2 may not have full spin polarization. However, this interpretation must be qualified due to the formation of robust domain structures of sub-micron size. These domain structures could suppress the SW excitation - our indicator of spin polarization. Further evidence for the loss of spin polarization at 5/2 has been presented in theoretical work [134] and is reported in an optics experiment [125]. In addition, recent theoretical evidence supports the existence of domains for filling factors close to 5/2 [26].

Unlike transport measurements, which have impact of the edge states of the quantum fluid, light scattering measurements probe the excitations of the bulk states

of the quantum fluid, albeit there are edge states at the boundaries of distinct domains. Consequently, light scattering is a unique tool which serves to provide further insight into the complex behavior of the highly correlated states of quantum fluids.

Furthermore, there is evidence for competing phases in the second LL, first seen from magnetotransport measurements [17]. Fig. 5.2 illustrates that the FQHE state at $\nu = 5/2$ is surrounded by two reentrant integer quantum Hall effect (RIQHE) states. That is, the quantum Hall fluid at 5/2 is surrounded, at slightly higher and lower filling factors, by "electron solid" (charge density wave) phases. The presence of both electron solid phases and fluid phases implies competition between these phases. Parameswaran et al. [26] describe a mechanism for phase separation at filling factors close to 5/2. The effect is linked to the claim that the Moore-Read state is a type-I superconductor in the presence of Coulomb interactions. In analogy with cooper pairs in conventional BCS superconductivity, the coherence length, ξ of these paired quasiparticles is much greater than their screening length, λ. The coherence length, ξ characterizes variations in the superfluid order (i.e. the region over which Pfaffian order decays). The screening length, λ characterizes the decay of density deviations. In the limit $\lambda \ll \xi$, the quasiparticle has a peculiar "vortex structure" - with magnetic flux spanning a region of size λ while the order parameter is suppressed over a much larger region of size ξ. That is, the charge density is confined to a much smaller region, λ, than the region over which the Pfaffian order decays, ξ. According to Parameswaran [26], it is energetically favorable for these particles to agglomerate in the presence of Coulomb interactions. That is, the energy gained by overlapping regions of size ξ is greater than the energy cost due to coulomb interactions from regions of size λ. This agglomeration is linked to frustrated phase separation of quantum phases [137, 138] which form domains and assemble into crystalline structures (a triangular lattice of clusters of quasiparticles).

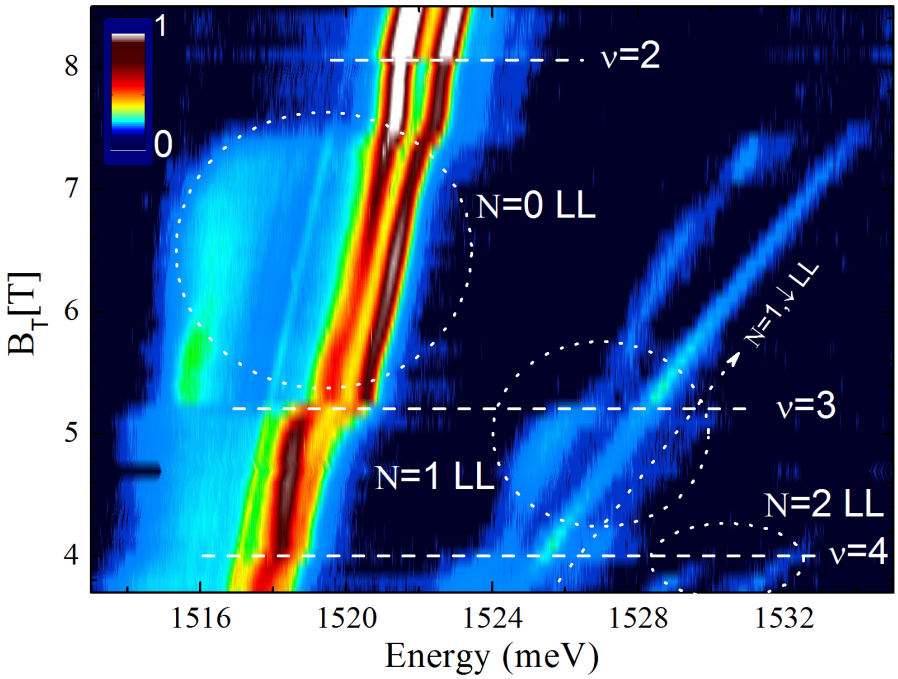

Figure 5.4: Color plot of optical emission spectra. Changes in peak intensity are represented by variations in color. The color plot describes how the intensities and scattered photon energy of optical emission spectra change with total magnetic field. The splitting of the peaks, to zeroth order, is determined by the eigenenergies of the harmonic oscillator, $E_N = \hbar\omega_c(N + 1/2)$, where N is the *Landau* level index. Dotted lines delimit sets of peaks due to a particular *Landau* level index. Dashed lines delimit integer filling factors identified by certain features of the *Landau* fan diagram.

5.3 Results and Discussion

5.3.1 Overview

Determining precisely the magnetic field for $\nu = 3$ (and other filling factors) is important for the interpretation of our results. One method is to vary the magnetic field until the maximum spin wave intensity is observed. Alternatively, a simpler measurement of the optical emission can be made. Figure 5.4 shows how the luminescence peaks fan out with changes in magnetic field. After matching peaks to emission from occupied Landau levels, one monitors when a certain Landau level (or its spin branch) becomes unoccupied, with increasing magnetic field, by deter-

mining at which field its spectral weight vanishes. This vanishing spectral weight indicates the traversing of an integer filling factor. Optical emission is useful for determining some features of the 2DES, even though interpretation of luminescence spectra can be quite challenging. While a detailed analysis of luminescence is beyond the scope of this discussion, some studies claim that optical emission reveals spin properties of FQHE systems [106, 125]. Ref. [125] claims that optical emission describes the state at $\nu = 5/2$ as being spin unpolarized. It is unclear however how formation of domains in the quantum fluid would influence luminescence spectra and the interpretation of the results in Ref. [125].

The optical emission spectra in Fig. 5.4 show the depopulation of *Landau* levels with increasing magnetic field. In addition to nicely illustrating the existence of *Landau* levels discussed in Chapter 2, analyzing the *Landau* Fan Diagram (collection of optical emission spectrum with energy spacing that changes with magnetic field), allows us to determine the spin orientation of spin split *Landau* levels by analyzing left circularly polarized (LCP) and right circularly polarized (RCP) spectra [139]. For instance, Fig. 5.4 shows three peaks that are linked to emission from the N=1 LL. Circular polarization measurements reveal that the two lower energy peaks originate from energy levels which have the same spin orientation. The highest energy peak originates from an energy level with reversed spin orientation. The highest energy peak is linked to the upper spin branch. The two lower energy emission lines are linked to the lower spin branch. Furthermore, we expect that the optical emission from the $N = 1, \downarrow$ LL (upper spin branch) to be quenched before the emission of the lower spin branch, as magnetic field is increased. This is just what we see in Fig. 5.4 as the magnetic field approaches 5.3 T. It is noteworthy that traversing an IQHE state via sweeping the magnetic field results in a kink in the N=0 LL emission. This effect is a consequences of many-body effects linked to charge degrees of freedom [139].

Optical emission studies help to determine the location of a filling factor with respect to B[T] and the location of optical gaps used for resonance enhancement of light scattering. Further to this, the spin degrees of freedom of the N=1 LL can be addressed by resonance inelastic light scattering (RILS) and resonance Rayleigh scattering (RRS). RILS data focus on spectral weight with non-zero energy shifts from the incident laser wavelength, while RRS data comprise only the spectral weight of elastically scattered light. The optical transitions for RRS are similar to those of RILS save for the fact that $\omega_L = \omega_S$. Electrons are excited from some initial state $|1\rangle$, to some intermediate state $|2\rangle$. Subsequently, a scattered photon is emitted by the reverse process - from $|2\rangle$ to $|1\rangle$. There is no energy transfer to the system[140]. Both RILS and RRS provide unique probes into condensed matter systems. For instance, the spin degrees of freedom in the N=1 LL are monitored by changes in the RILS intensity of the long wavelength spin wave (SW) at the Zeeman energy, E_Z [95]. Unexpectedly, the spin wave intensity, an indicator of spin polarization, collapses rapidly for $\nu < 3$. The RRS effect that, like the collapse of the mode at E_Z, appears below $\nu = 3$, reveals that the quantum fluids in the partially populated N=1 LL are highly inhomogeneous, breaking up into "puddles" that have characteristic sub-micron dimensions. Details will be discussed below.

Figure 5.5 shows the collapse of the SW mode at E_Z for $\nu < 3$. As we will see in Fig. 5.6, this is accompanied by the emergence of continua of excitations (below and above E_Z) that can be regarded as low-lying excitations of new quantum phases in the N=1 LL. As will be discussed below, the similar resonance enhancements of the low-lying continua and of RRS is evidence that the possible lost spin polarization, seen as the replacement of the peak at E_Z by a low-lying continuum of excitations, arises from the domains ("puddles") of quantum fluids that emerge for $\nu < 3$.

Most likely, the emergence of "puddles" are linked to competition between quantum phases reported in other experiments [17, 130, 38, 141, 142]. The present results

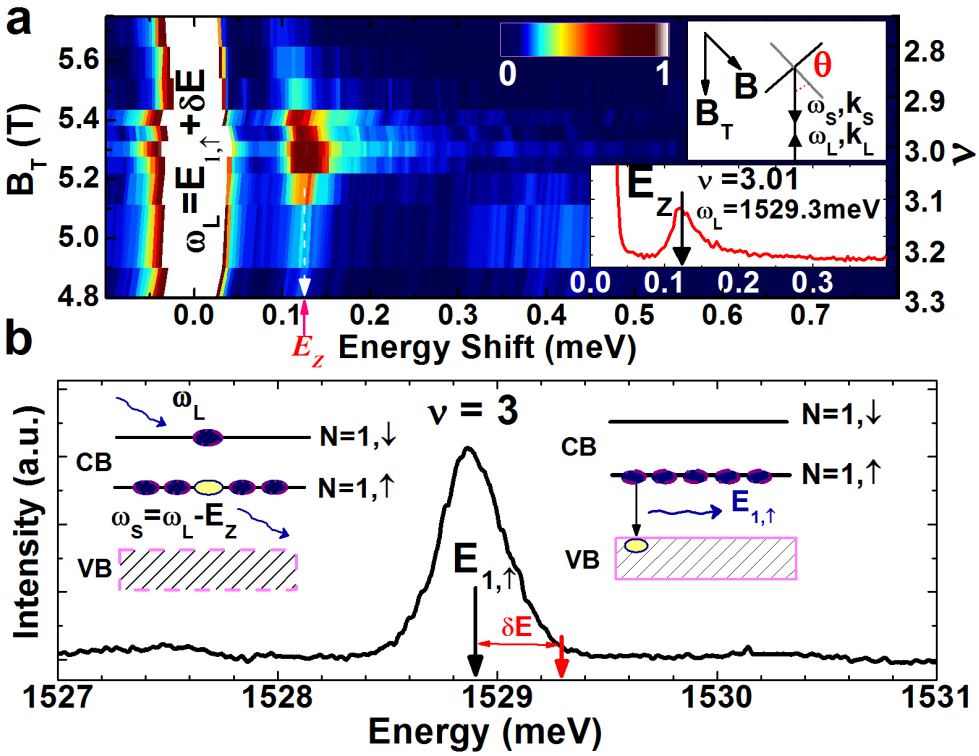

Figure 5.5: Evidence of loss of spin polarization away from $\nu = 3$. (a) Color plot of resonant inelastic light scattering spectra with varying magnetic field shows the spin wave (SW) at the Zeeman energy, E_Z. The intensity of the SW attenuates away from $\nu = 3$ (B_T=5.32T). The top inset shows the light scattering geometry. The bottom inset exhibits a spectrum at $\nu = 3.01$. (b) N=1 optical emission involved in resonance enhancement of light scattering (B_T=5.3T,θ=20^o, T=40 mK). The left inset shows the two step inelastic light scattering process for the SW. The right inset is the energy level diagram for optical emission from the $N = 1, \uparrow$ LL.

differ from prior work in revealing a potential loss of full spin polarization and that this remarkable character persists to temperatures as high as 1K and above. Domains which might be lacking full spin polarization are here a key feature of the quantum phases of the N=1 LL. We note that further studies of condensation into the quantum Hall state at $\nu = 5/2$ may still result in an incompressible fluid that has spin polarization and exhibits a well defined SW excitation.

5.3.2 Collapse of Spin Wave at E_Z for $\nu < 3$

The striking collapse of the scattering intensity of the SW at E_Z for $\nu \lesssim 3$ is shown in Fig. 5.5(a). The color plot shows RILS spectra, taken at different magnetic fields at the resonance value of ω_L (the value for ω_L that induces resonance enhancement, ω_R, varies with the cyclotron energy and $E_{1,\uparrow}$). All the features appear predominantly in the depolarized configuration (VH) which, according to light scattering selection rules, indicates their spin origin [143]. While Larmor's theorem requires that the SW's energy remains at the bare Zeeman energy, its overall spectral weight is expected to depend sensitively on the degree of spin polarization [12, 95]. The collapse of the SW intensity could be interpreted as revealing the reduction of spin polarization in the N=1 LL from its maximum value at $\nu = 3$. While, a reduced SW intensity is expected for $\nu > 3$ (both $N = 1, \uparrow$ and $N = 1, \downarrow$ are populated reducing the overall spin polarization), the "sudden" attenuation of the SW intensity for $\nu < 3$ is surprising ($N = 1, \uparrow$ depopulates as B increases) and suggests a rapid loss of spin polarization below $\nu = 3$. This is remarkable because simple mindedly we expect that the 2DES remains fully spin polarized after $N = 1, \downarrow$ is emptied. The lower spin branch contains electrons of the same spin orientation and consequently, in a single particle picture, the spin polarization should be constant for $3 > \nu > 2$.

5.3.3 Coexisting phases

As discussed in Chapter 2, magnetotransport and microwave resonance measurements of the second LL reveal evidence for competing electron solid and fluid phases via the presence of RIQHE phases and conventional FQHE phases. Light scattering is an alternative, unique means to probe the competition between FQHE liquid phases and electron solid phases. The coexistence should appear as the presence of two modes at the same filling factor. Strikingly, inelastic light scattering spectra

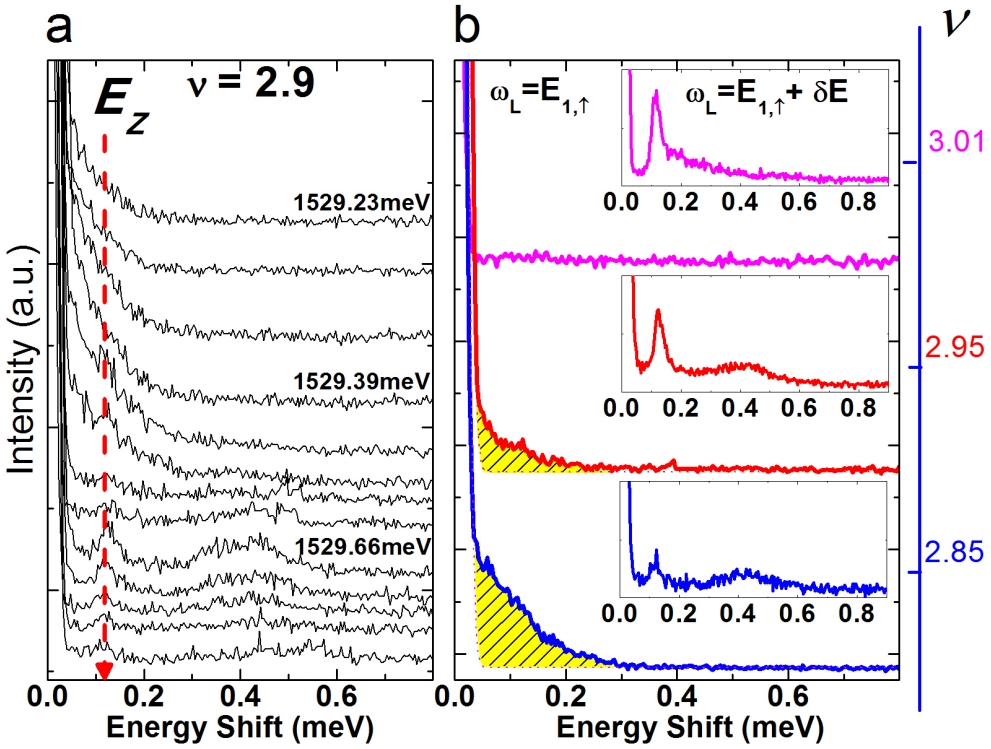

Figure 5.6: Coexistence of novel quantum phases with the ferromagnetic SW. (a) Tuning the incident photon energy for excitations at filling factor slightly away from ν=3 (ν=2.9, B_T=5.5 T, T=40mK) induces the collapse of the SW and the emergence of a continuum of low lying energy excitations. The SW resonance is at higher photon energy than that of the continuum. (b) We monitor the behavior of the low-lying excitations while tuning the filling factor [19]. We track two distinct modes below $\nu = 3$ - the SW and continuum of low-lying excitations. The insets show the SW collapse while the main panel shows the emergence of the continuum of low-lying excitations. The continuum is resonant at slightly lower incident photon energy, $\omega_L(B_T)$ (ω_L is a function of B_T) than the SW.

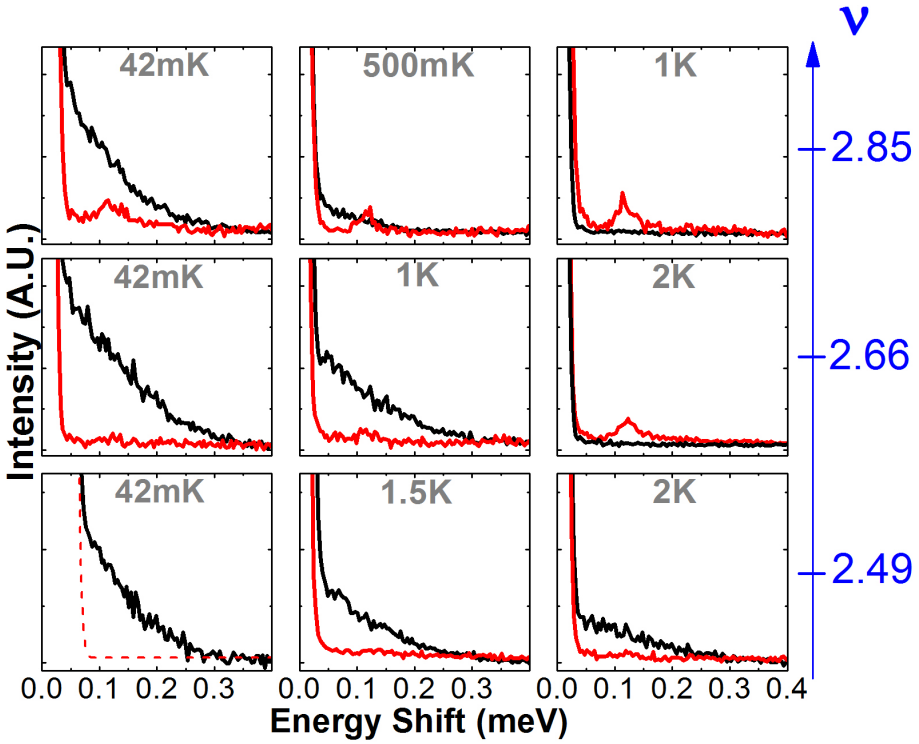

Figure 5.7: Temperature dependence measurements at various filling factors of low-lying modes. The continuum (black lines) melts at elevated temperature. The SW (red lines) reemerges at elevated temperature for $\nu \simeq 8/3$ (B_T=6.0 T) and 5/2 (B_T=6.42 T, in the red spectrum at 2K there is a glitch at E_Z not visible on the scale shown). The dashed line in the lower left panel is a guide to the eye.

could be interpreted as revealing coexistence of phases which could manifest evidence for the existence of competing RIQHE and FQHE states. For $\nu \lesssim 3$, tuning the incident photon energy results in striking spectral changes that are due to differences in resonance enhancements. This is illustrated in Fig. 5.6(a) which shows the metamorphosis of the sharp SW at E_Z to a broad continuum of lower energy excitations at ν=2.9 when tuning ω_L. The continuum extends from well below E_Z to about 0.3 meV. In Fig. 5.6(b) the evolution of the continuum (main panel) and SW (inset) intensities is shown as a function of filling factor. Since the intensity of the SW and continuum resonate at different values of ω_L, RILS spectra are shown for values of ω_L corresponding to their maximum resonant enhancement: $E_{1,\uparrow}$ for the continuum and $E_{1,\uparrow}+\delta E$ for the SW (where δE can vary but is roughly 0.4 meV). While the SW intensity is clearly reduced for $\nu \lesssim 3$, the continuum intensity, absent at $\nu = 3$, gains in strength away from $\nu = 3$ indicating its link with the loss of spin polarization. Moreover, in contrast to the N=0 LL, where Skyrmions proliferate at $\nu \sim 1$ [95], we surmise that the continuum of low-lying excitations at $\nu \lesssim 3$ have a different origin. We speculate that the continuum could be a novel type of spin excitation associated with reduced SW intensity.

This interpretation is further bolstered by the absence of continua for $\nu \lesssim 3$ in polarized configuration (HH) while still being present in depolarized configuration (VH). This contrast is lost when $\nu \lesssim 8/3$. Figure 5.7 shows the temperature dependence of the RILS spectra at three filling factors reaching to 5/2. At ν=2.85, the broad continuum seen at 40 mK melts entirely at 1 K, while the SW intensity at E_Z remains or even gains in strength. At $\nu \simeq 8/3$, the continuum dominates at low temperature, begins to melt at 1 K and is destroyed by 2 K. The sharp SW at E_Z reemerges at 1 K and is fully recovered by 2 K. While the spectral weight of the continua at $\nu \sim 8/3$ are greater in VH than in HH, they are the same in both VH and HH at $\nu \sim 5/2$ indicating a more complex excitation spectrum at ν=5/2,

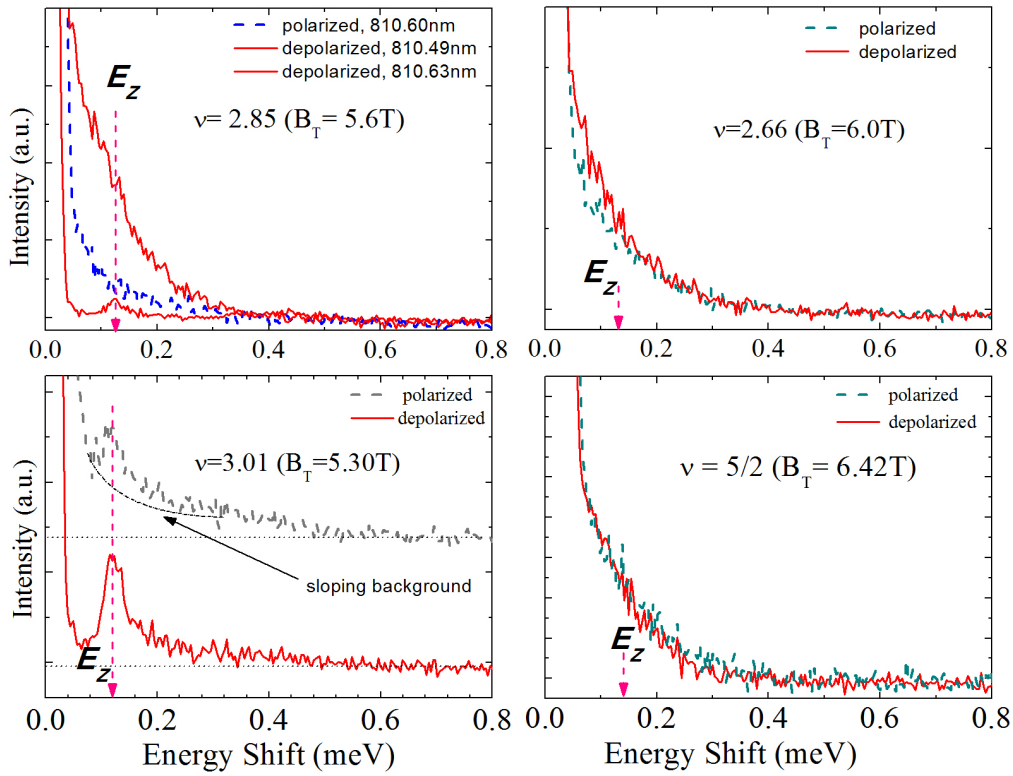

Figure 5.8: Dependence of spectral weight at different filling factors with polarization selection rules. At $\nu = 3$, the SW is seen at the Zeeman energy. Depolarized spectra are stronger than polarized spectra, showing the spin polarized nature of the state at this filling factor. For filling factors less than three, polarized spectral weight grows stronger relative to depolarized spectral weight. At $\nu = 5/2$, depolarized and polarized spectral weight are equal suggesting the presence of complex roles for both spin and charge density excitations for the state at $\nu = 5/2$.

possibly involving both charge and spin degrees of freedom (data shown in Fig. 5.8).

The temperature dependence for excitations at $\nu \simeq 5/2$ is remarkable. As the temperature is raised to 1.5K, the continuum begins to melt, and is still present, albeit greatly reduced, at 2K. In addition, a small bump is seen at E_Z - hinting at a reemerging long wavelength SW. We note that the observed continuum does not seem to be an unique feature of the magic filling factors or gapped quantum Hall states. However it is a feature of the quantum fluids of the 2nd LL and appears to grow more robust as ν is tuned below three.

5.3.4 Emergence of Domains: Inhomogeneity in the 2nd LL

The spectra in Figs. 5.6 and 5.7 suggest competing quantum phases. One phase is associated with a sharp SW at E_Z and the other with the continua of low-lying excitations. To further explore these behaviors we measured RRS spectra. Figure 5.9 reports the results at several filling factors: RRS spectra at $\nu \sim 5/2$ and 8/3 show marked resonance enhancements at energies that coincide with the maximum resonance enhancement of the continuum, and contrasts with the unremarkable RRS profile of the ferromagnetic state at $\nu \sim 3$.

RRS is linked to spatial inhomogeneities or domains of competing phases, which are on the order of the photon wavelength ($\sim 240nm$ in GaAs) [20]. The RRS results clearly demonstrate formation of domains in the quantum fluid at $\nu \lesssim 3$, that are consistent with transport measurements showing the competition between nearly degenerate quantum phases in the second LL which include spatially inhomogeneous ones associated with the RIQHE [141, 17]. In addition, domain formation at $\nu = 5/2$ could manifest from relatively large quasiparticles, as suggested in Ref. [144] which reports quasiparticles of diameter $12l_o$ (or 120 nm at 6.4 T). Though the ferromagnetic state at $\nu = 3$ is not spatially homogenous, there exists only one

phase. Furthermore, at $\nu = 3$, electrons localize in space on length scales $\lesssim 1\mu m$, greater than the photon wavelength [96]). As a result, RRS is suppressed.

5.3.4.1 Melting of "Quantum Puddles"

The temperature dependence of RRS shown in Fig. 5.10 shows a gradual weakening of the RRS upon increasing temperature and supports the picture that at low temperatures an inhomogeneous electron condensate forms at 5/2 and 8/3. We interpret the attenuation of RRS at higher temperatures as the melting of puddles of quantum phases. The inset to Fig. 5.10 shows that a Langmuir adsorption isotherm (Eqn. 5.1), that interprets the formation of inhomogeneous integer quantum Hall fluids [20], also describes results at 5/2 and 8/3. In this framework, we describe nucleation of "quantum puddles" to binding sites - forming domains in the quantum fluid. The areal intensity of the RRS, I_{RRS} is given by,

$$I_{RRS}(T) = \frac{I^0_{RRS}}{1 + CTexp(-E_b/kT)} \tag{5.1}$$

E_b is the binding energy of particles to binding sites and $C = 2\pi M k_b/N_p h^2$, where N_p can be viewed as the density of binding sites and M as the mass of the bound particle. A fit to data shown in the Fig. 5.10 inset yields an estimate of the density of binding sites, $N_P \sim 5 \times 10^9 cm^{-2}$, with M as the composite fermion (CF) mass of about 10 times the effective electron mass [145]. Using N_P, we can estimate an upper limit for the size of the domains $\sim 142nm$. The binding energy is $E_b \sim 0.06$ meV (600 mK). The presence of domains in the quantum fluid of the N=1 LL has implications for the spin properties of the system. The formation of domains has the potential to destroy the long range magnetic order and its associated long wavelength excitations. Consequently, the sharp SW at E_Z might not effectively monitor local polarization. Thus, within the domains, determining the exact nature

of the spin polarization remains challenging.

It is interesting to compare the RILS results at 8/3 and 5/2 with those for the states of their analogs in the N=0 LL - ν=2/3 and ν=1/2. At similar magnetic fields, the states at ν=2/3 and ν=1/2 are characterized by a well-defined SW at E_Z [146, 95]. This indicates spin polarized states at 2/3 and 1/2.

The temperature dependence of the continuum close to 5/2 is reminiscent of work reported by Willett et al. [147], showing that a CF Fermi sea at ν=5/2 exists within the temperature range 300mK<T<1100mK. The signature of the CF Fermi sea becomes weaker with elevated temperatures. It is possible that the continuum of low-lying excitations at 5/2 might be a signature of a CF Fermi sea.

The above results seem to indicate that the observed collapse of the SW intensity found in the N=1 LL occurs in domains of characteristic sub-micron length - a length scale so small the long wavelength SW may not be well defined. It is thus conceivable that there may be no contradiction among works reporting spin polarized states at 8/3 [38] and at 5/2 [132, 131, 135, 128, 93, 36, 148]. In this scenario, spin polarized domains could coexist with quantum Hall fluids that have lost spin polarization. The presence of residual disorder suggests that at 5/2, a new type of Skyrmion structure may proliferate in the ground state that may be the origin of the spin un-polarized domains at this filling factor[134]. Furthermore, Wojs et al. predict that long-range disorder could nucleate puddles of quasiparticles, which could be composed of Skyrmions or Anti-Skyrmions. At 5/2 the dimension of the spin polarized domains might be sufficiently small to disrupt completely the long wavelength SW. Therefore at this filling factor we cannot dismiss the possibility of polarized domains at low temperature.

Further research is required to determine if un-polarized, together with polarized domains may be a general feature of the quantum fluids in the 2nd LL (including at $\nu = 5/2$) - continua being linked to partially polarized or un-polarized domains.

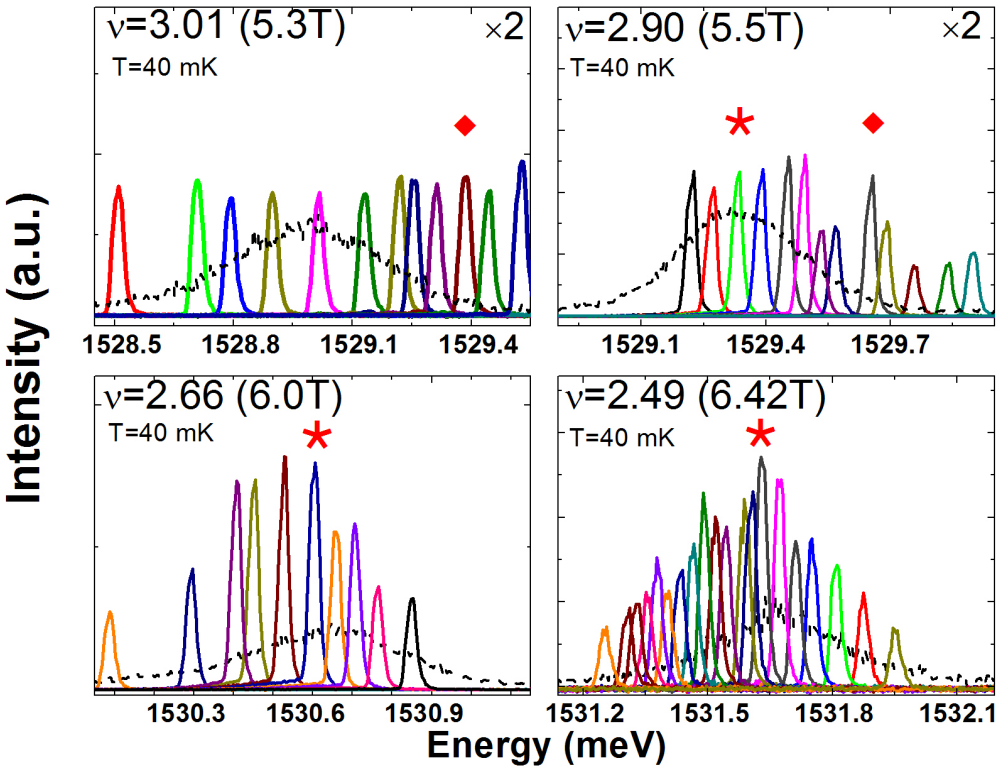

Figure 5.9: RRS resonance profiles for ν=3.01, 2.9, 2.66 and 2.49. No resonance enhancement is seen for the ferromagnetic state at $\nu = 3$. At $\nu = 2.9$ some structure in the resonance profile develops. At $\nu = 2.66$ and $\nu = 2.49$, a resonance is seen at $E_{1,\uparrow}$. Black dashed lines represent optical emission while colored peaks represent elastically scattered light intensity. Diamonds (Stars) represent the spectra in which the SW (continuum) has a maximum resonance.

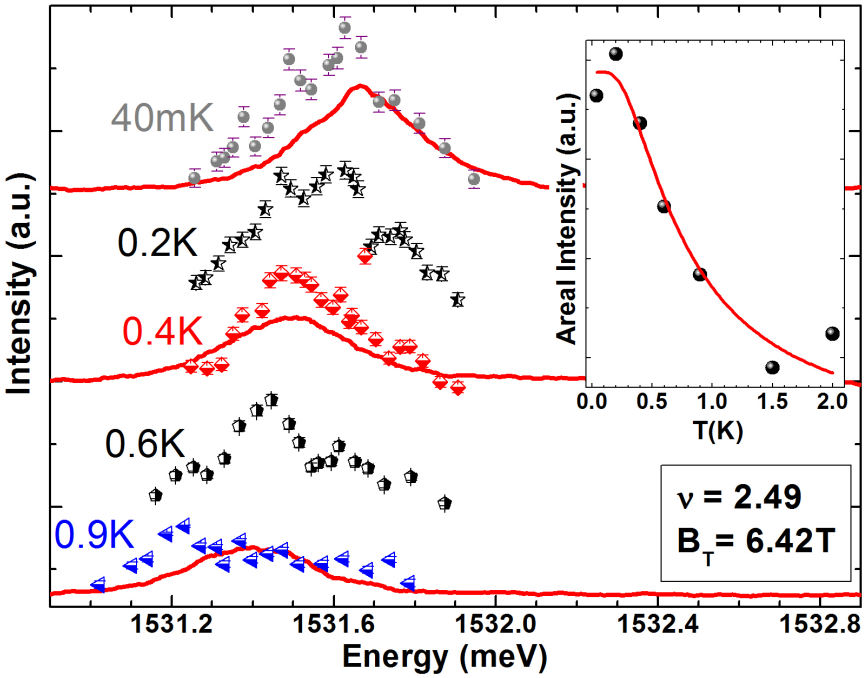

Figure 5.10: Temperature dependence of RRS for $\nu \sim 5/2$. Optical emission spectra (continuous lines) along with the laser peak heights (scatter plots) of RRS intensity are displayed. A peak in the resonance enhancement of the elastically scattered light coincides with the maximum intensity of the continuum. This enhancement is attenuated at elevated temperatures. The inset shows the relationship between the area under the RRS profile and temperature. The solid line represents a fit to the data using the Langmuir isotherm[20].

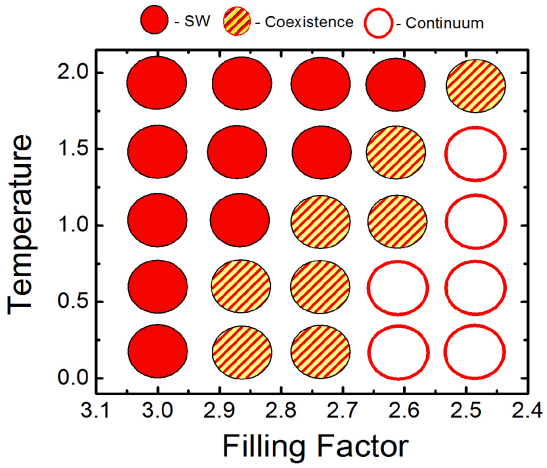

Figure 5.11: Cartoon showing the presence of sharp SW modes and broad continuum modes with changes in both temperature and filling factor.

A cartoon illustrating the interplay between the SW and the continuum is given in Fig. 5.11. A possible mechanism for the formation of continua of spin excitations as reported here could be similar to that of spin-flip excitations in the N=0 LL [146], whose spectral weight below E_Z emerges if the CF Fermi energy is greater than the CF spin reversal gap energy. In addition, the evidence from light scattering for coexisting phases near 5/2 could be linked to characteristics associated with the Moore-Read state. As discussed early in the Chapter, Parameswaran et al. [26] explain how the Moore-Read state, as a type-I superconductor with $\xi \gg \lambda$ will give rise to frustrated phase separation of phases in the presence of Coulombic interaction, when ν is tuned slightly away from half filling. The work predicts domain formation of quantum phases close to 5/2, in agreement with my finding.

5.4 Summary

I have presented the first light scattering studies of quantum Hall states of the N=1 LL, with a focus of better understanding the spin degrees of freedom of the state at $\nu = 5/2$. A collapse of the long wavelength SW at E_Z for $\nu \lesssim 3$ may not indicate in a conclusive fashion the loss of full spin polarization in the N=1 LL from its maximum at $\nu = 3$. The absence of a mode at E_Z for $\nu \simeq 8/3$ and $\nu \simeq 5/2$, and the emergence of quantum phases composed of sub-micron domains seen in RRS pose striking new challenges for the interpretation of roles of spin degrees of freedom in the second LL. Novel domain structures could disrupt the long wavelength SW and be composed of both spin polarized and spin unpolarized regions. This is especially the case for the quantum fluids around $\nu = 5/2$.

Chapter 6

Third *Landau* level and electron crystallization

6.1 Overview

The spin degrees of freedom of phases in the third Landau level are probed by resonant inelastic light scattering. The long wavelength spin wave mode, which monitors the degree of spin polarization, is at the Zeeman energy in the ferromagnetic state at ν=5. For $\nu < 5$ the spin wave intensity remains robust. This is contrary to the rapid collapse of the SW in the 2nd Landau level (as discussed in the previous chapter), suggesting different roles for spin degrees of freedom in the second and third Landau levels. The caveat being that the spin wave may not be a good indicator of spin polarization under certain conditions, such as under the formation of domains of sufficiently small size. Recall that these considerations were discussed at the end of Chapter 3 and in Chapter 5. A continuum of low-lying excitations emerges for $\nu \lesssim 4 + 4/5$, and coincides with the emergence of competing electron solid and fluid phases at that filling factor [7, 23]. Signatures of competing spin wave and continuum modes persist to half-filling ($\nu = 4 + 1/2$). These results could be evidence for

competing conventional quantum Hall states and charge density waves in the 3rd Landau level, and manifest intriguing roles of spin degrees of freedom in the N=1 LL and N=2 LL.

6.2 Background

As discussed in the previous chapter, the second LL contains the state at $\nu = 5/2$ [126, 127], a topic of great current interest. For this reason, other phases of the second Landau level along with those of the third Landau level have attracted interest. Efforts are being made to better understand how the physics of the states in the lowest Landau level are different from those of higher Landau levels ($N \geq 1$). Several studies have examined these higher LLs [7, 40, 149] and describe the unusual features of the states therein. In this chapter I will focus on the $N = 2$ LL. In this third LL there exists insulating phases that have the R_{xy} values of neighboring integer filling factors but have non-integer filling [150]. The filling factors that define these insulating phases typically occur at $\nu = [\nu] + 1/4$ and $\nu = [\nu] + 3/4$, where $[\nu]$ is an integer of four or greater (we define $\nu = [\nu] + \bar{\nu}$). These phases, known as re-entrant integer quantum Hall states (RIQHE) or "bubble" phases, also occur in the $N = 1$ LL as seen in the previous Chapter. There is also evidence for anisotropic transport seen at half filling of the $N \geq 2$ LL. These anisotropic phases are known as "stripe" phases. "Bubble" and "stripe" phases, delimited in Fig. 6.1, are interpreted as charge density waves. "Bubbles" are theorized to consist of a pinned triangular lattice of clusters of electrons (which explains their insulating behavior). Each cluster contains M electrons (when M equals one, we recover the familiar Wigner crystal [56]). Figure 6.2 shows the structure of the triangular lattice comprising the bubble phase. "Stripe" phases are understood to be unidirectional charge density waves [22, 67], which are like "lines of charge" running parallel to

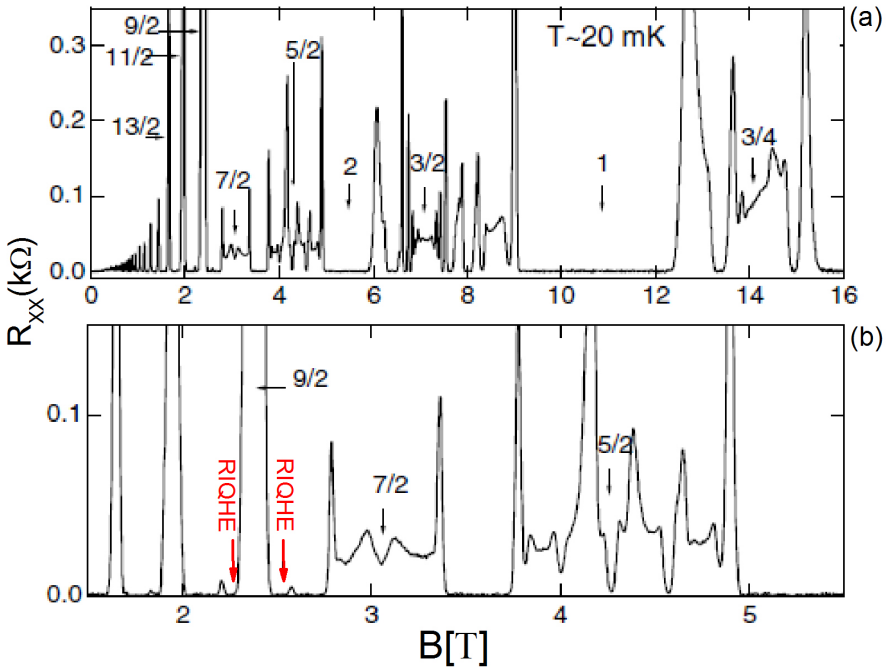

Figure 6.1: (a) Magnetoresistance trace extracted from Ref.[7] shows the longitudinal resistance with respect to magnetic field for filling factors in the N=1 LL and N=2 LL. (b) Shows a portion of panel a in greater detail. In the N=2 LL, an anisotropic or "stripe" phase is at $\nu = 9/2$. "Bubble" phases, indicated by 'RIQHE', lie at $\bar{\nu} = 1/4$ and $\bar{\nu} = 3/4$.

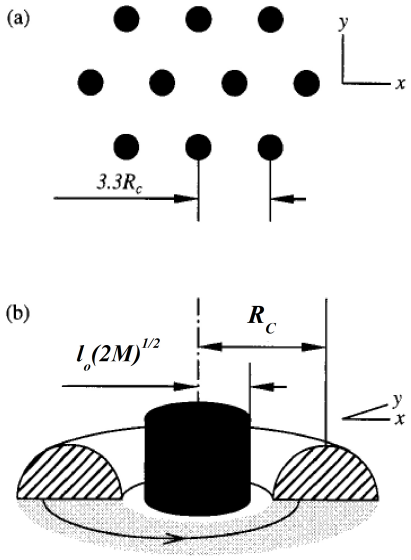

Figure 6.2: Schematic of the bubble phase. (a) Shows the triangular lattice of clusters of M electrons spaced by 3.3 R_c, where R_c=$\sqrt{(2N+1)}l_o$. (b) The enlarged view of a single cluster. The dark region shows the guiding center of the circulating charge with width depending on l_o and M as indicated. The toroidal section delimits the charge density distribution around the bubble (half of the charge density is removed). This charge density is created by electrons moving in the cyclotron orbits centered inside the bubble. The arc highlights a single electron orbit. Extracted from Ref. [21].

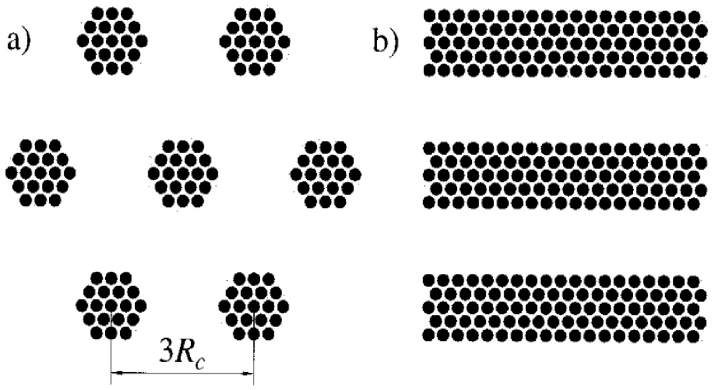

Figure 6.3: Schematic of the bubble phase and stripe phase. (a) Shows the bubble phase with M clusters explicitly shown. Each black dot represents the guiding center of a cyclotron orbit. (c) Clusters of M electrons merge to form the stripe phase. Extracted from Ref. [22].

each other. The unidirectional nature explains the anisotropy of the phase - the phase is conducting parallel to the lines of charge and insulating orthogonal to the lines of charge. Figure 6.3 shows how electron clusters in a bubble phase could merge to form a stripe phase. Quantum fluctuations of the stripe phase may give rise to a quantum nematic phase [63], which is analogous to a liquid crystal phase. A liquid crystal is a state of matter that has both liquid and crystal properties - for instance a liquid crystal can flow like a liquid but has constituent molecules which are crystalline. That is, in a nematic phase, quantum fluctuations of the stripe order are strong enough to restore full translational symmetry on large length scales (melting of the CDW or electron lattice), but still small enough to retain the local orientational order of the stripes. Though quantum fluctuations could play a very important role in the third LL, we will consider here only the "simplified" (without quantum fluctuations) version of charge density waves for the sake of simplifying the discussion.

Evidence for the structural nature of the bubble and stripe phases can be found in microwave resonance measurements. Figure 6.4 shows that resonances in the conductivity of microwave resonance measurements suggests the presence of an electron lattice or crystalline structure in the 2DES[23]. Recent work by Kukushkin et al.[151] uses surface acoustic waves (SAW) to measure the dispersion of the Hall stripe phases at $\nu = 9/2$. This work confirms that a 2DES can form unidirectional charge density waves (or nematic phases) at $\nu = 9/2$ and highlights the collective behavior of these neutral modes. The work also agrees with theoretical predictions [24, 152]. Figure 6.5 shows the dispersion of the neutral mode at $\nu = 9/2$.

Comparing and contrasting the behavior of different values of $\bar{\nu}$ with changes in $[\nu]$ or *Landau* level index may provide some clues to understanding the behavior of 5/2 as well as other FQHE states. For instance, we can compare 5/2 $(2 + 1/2)$ to half filling factors in other LLs such as $\nu = 1/2$ $(0 + 1/2)$ or 9/2 $(4 + 1/2)$, in the

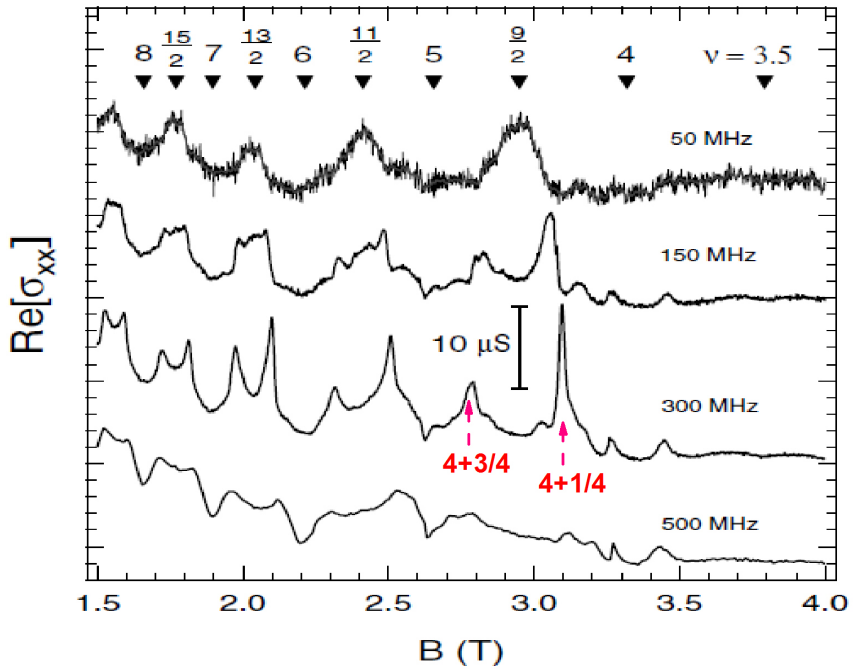

Figure 6.4: The real part of the diagonal conductivity, $Re[\sigma_{xx}]$, versus magnetic field, B[T] for several frequencies (50, 150, 300, and 500 MHz). Select filling factors are shown. The microwave electric field, E_m, was polarized along the $\langle 110 \rangle$ easy direction. The temperature is 50mK. Extracted from Ref. [23]

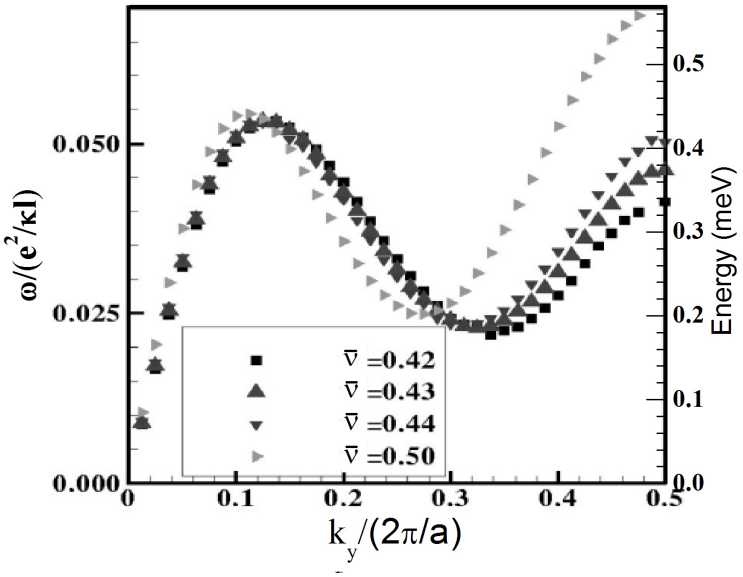

Figure 6.5: Dispersion relation of vibrational modes of the modulated stripe phase in the $N = 2$ LL for wave vector k along the direction of the stripes. "a" is the period of the modulations along the stripes. The energy units are $e^2/\varepsilon l_o$ and are converted to meV for $B_T = 3.69T$ [$\nu = 9/2$] using a multiplicative factor of $\sim 8.1meV/(e^2/\varepsilon l_o)$ as shown on the right scale. Extracted from Ref. [24]

N=0 LL and N=2 LL respectively. The second LL lies at the crossroads between the N=0 LL and the N=2 LL, regimes dominated by conventional quantum Hall states and charge density wave states respectively. Light scattering studies of the N=2 LL states should complement existing work on electron solid bubbles phases and stripe phases. In the previous chapter, motivated by the enigmatic behavior of states in the N=1 LL, we compared and contrasted the states of the N=1 LL with those of the N=0 LL. In this chapter, we instead make comparisons among states in the second and third LL.

The states of the lowest *Landau* level are dominated by the conventional fractional quantum Hall states as described by the Jain-Laughlin series[52]. To the contrary, in higher *Landau* levels (N$\geq$ 2), quantum Hall states become unstable[153]. This regime is instead dominated by charge density wave phases [67, 63, 23, 7]. I present here for the first time, light scattering studies of phases in this regime.

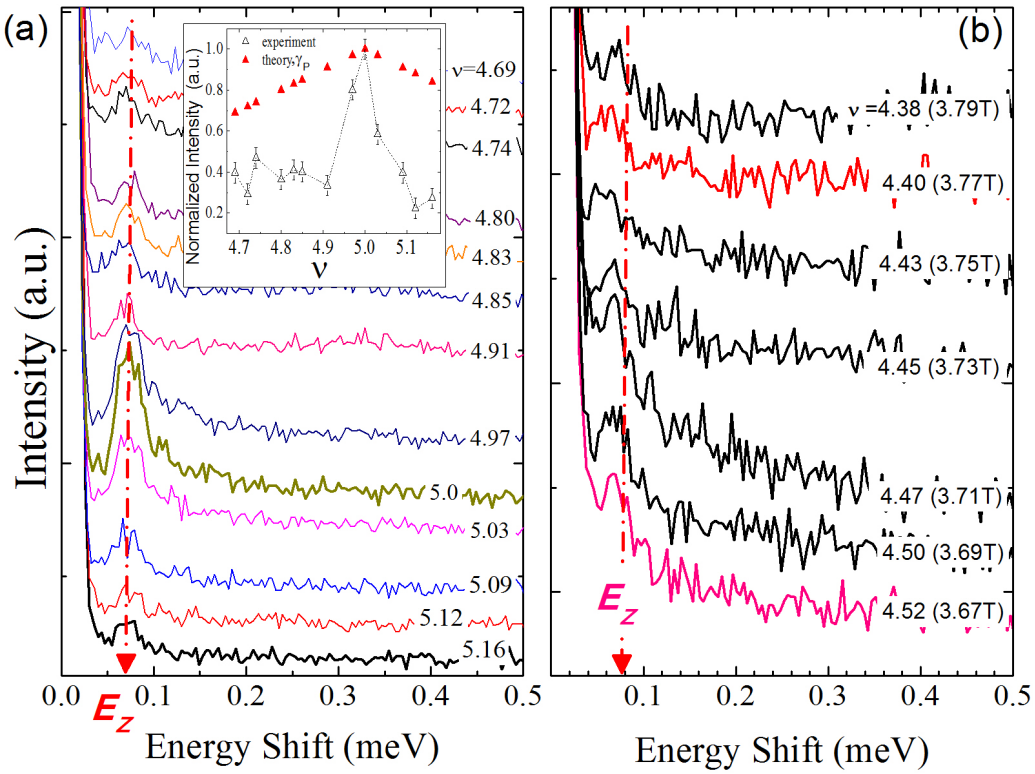

Figure 6.6: Evidence of reduced spin polarization for filling factors away from the ferromagnetic state at $\nu = 5$. (a) Spin wave at filling factors close to $\nu = 5$. The inset shows the intensities of SW's from the main panel compared with estimates of the SW intensity based on γ_I, as discussed in Chapter 3. (b) Light scattering for a different range of filling factors starting further from $\nu = 5$, at half filling (B_T=3.32T at $\nu = 5$, θ=20^o, T=40 mK).

Light scattering probes the bulk states of electron phases in this regime - complementing magnetotransport measurements (which have impact of edge states). In addition, light scattering selection rules allows us to distinguish between spin and charge degrees of freedom.

6.3 Results and Discussion

The physics of the spin degrees of freedom of the electron phases in the N=2 LL is addressed for the first time by resonance inelastic light scattering (RILS). We compare filling factors $\nu = [\nu]+\bar{\nu}$, where $[\nu]$ corresponds to integer filling ($[\nu]$=4 here)

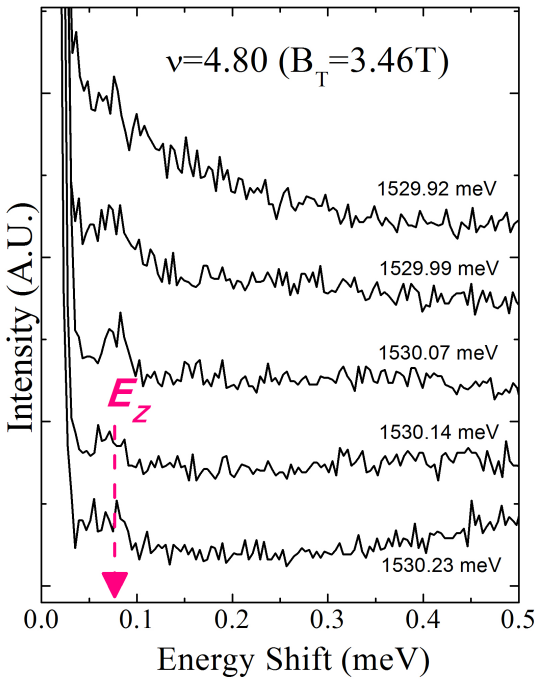

Figure 6.7: At $\nu = 4 + 4/5$ tuning incident photon energy, ω_L induces changes in the light scattering spectra from sharp spin wave (higher ω_L) at E_Z to a broad continuum of low-lying excitations (lower ω_L).

and $\bar{\nu}$ is analogous to the lowest LL filling. For instance, we will compare several values of $\bar{\nu}$ (in particular, $\bar{\nu}$= 1/2, 3/4 and 4/5) for $[\nu]$=2 and 4. The spin degrees of freedom are monitored by changes in the RILS intensity of the long wavelength spin wave (SW) at E_Z [95]. At precisely odd integer filling ($\nu = [\nu] = 1, 3, 5, ...$) this SW intensity is maximized. As we discussed in Chapter 5, the SW intensity collapses rapidly for $\nu < 3$. Recall from Chapter 3 that the SW may be used as an indicator of spin polarization, with the caveat that there may be conditions, such as domain formation, that could alter this property. Nevertheless, a rapid collapse of the SW is not seen for $\nu < 5$. The SW at the ferromagnetic state at $\nu = 5$ has a maximum intensity as shown in Fig. 6.6. For $\nu < 5$, the SW intensity decreases slightly but persists to ν=4+1/2. However, the reduction is faster than the reduction of phase space from depopulation of the N=2 LL with lowering $\bar{\nu}$. In the N=2 LL, the continuum of excitations emerges well below $\nu = 5$, at $\nu \sim 4+4/5$,

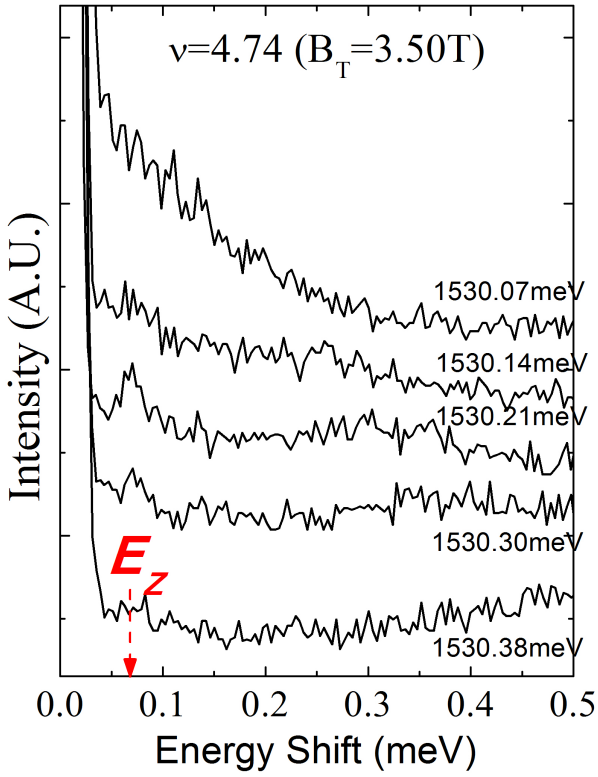

Figure 6.8: Light scattering for the states at $\nu \sim 4 + 3/4$. Tuning the incident photon energy, ω_L causes changes in the spectral weight of the light scattering from a sharp spin wave at E_Z to a broad continuum of low energy excitations.

as shown in Fig. 6.7. Dissimilarly, in the N=1 LL, the rapid collapse of the SW mode for $\nu \lesssim 3$ is accompanied by the emergence of continua of excitations for $\nu \lesssim 2.94$. The spectra for $\nu \lesssim 5$ as shown in Fig. 6.6 and Fig. 6.7 have features which appear predominantly in the depolarized configuration (VH). According to light scattering selection rules, this indicates their spin origin[143]. While Larmor's theorem requires that the SW's energy remains at the bare Zeeman energy, its overall spectral weight is expected to depend sensitively on the degree of spin polarization [12, 95]. The collapse of the SW intensity is thus interpreted as revealing a reduction in the number of spin polarized electrons in the N=2 LL from its maximum value at $\nu = 5$. Nevertheless, there could exist alternative explanations for the reduced SW intensity for $\nu < 5$, as discussed at the end of Chapter 3 and in Chapter

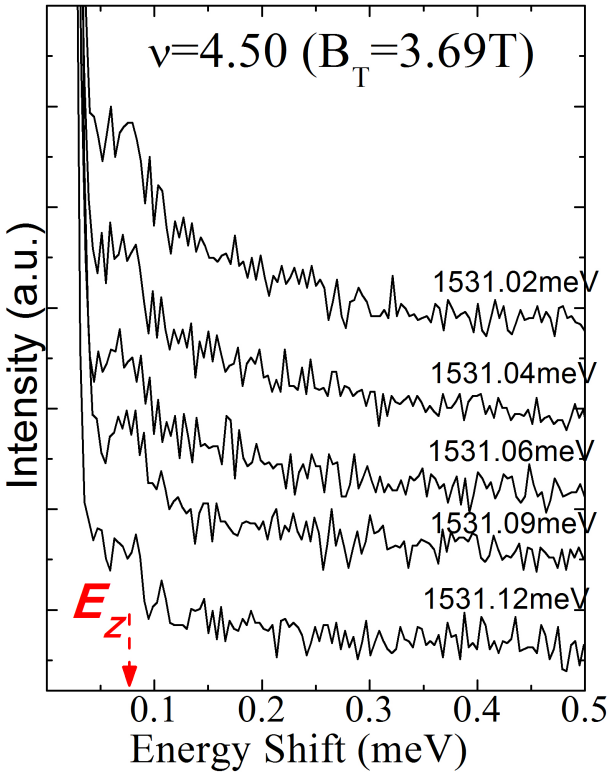

Figure 6.9: Light scattering for the states at $\nu \sim 4 + 1/2$. Tuning the incident photon energy, ω_L causes changes in the spectral weight of the light scattering from a sharp spin wave at E_Z (higher ω_L) to a broad continuum of low energy excitations (lower ω_L).

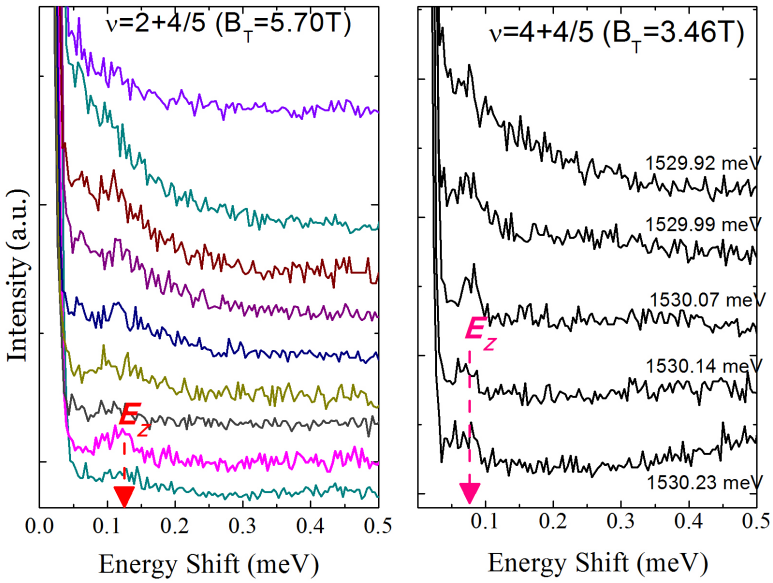

Figure 6.10: Comparison of low-energy modes at filling factors ν=2+4/5 and 4+4/5. Sharp SW modes and broad continuum modes are present in both sets of spectra.

5. A reduced SW intensity is expected for $\nu > 5$ (both $N = 2, \uparrow$ and $N = 2, \downarrow$ are populated reducing the overall spin polarization). The attenuation of the SW intensity for $\nu < 5$ is expected to scale with the number of electrons available for light scattering (that is, $N = 2, \uparrow$, which depopulates as B increases and $\nu \longrightarrow 2$). That is, even though the 2DES has a net spin polarization, the intensity of the SW will be reduced as the number of spin polarized electrons is reduced. The phase space available for electrons to participate in light scattering is reduced.

Tuning the incident photon energy results in striking spectral changes that are due to differences in resonance enhancements. For $\nu \lesssim 4+4/5$, the sharp SW mode at E_Z and broad continuum mode of low energy excitations coexist and resonate at different incident photon energies (the SW resonates at higher incident photon energy than that of the continuum). Similar behavior is seen down to half filling. Figure 6.7, Fig. 6.8 and Fig. 6.9 illustrate the coexistence of sharp SW and broad continuum modes for $\nu < 5$. The coexistence of modes implies the coexistence of phases which involve varying spin degrees of freedom.

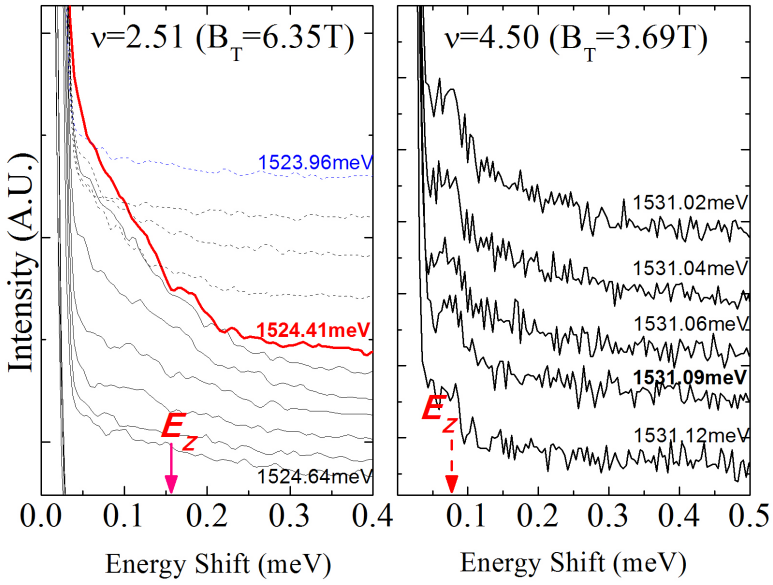

Figure 6.11: Comparison of low-energy modes at filling factors ν=2+1/2 and 4+1/2

Whereas a continuum of low-lying excitations emerges for $\nu \lesssim 3$ (that is, just below $\nu = 3$) [66], we find different behavior for just below $\nu = 5$. For $[\nu]$=4, a continuum of low energy excitations arises for $\bar{\nu} < 4/5$, significantly below integer filling. Figure 6.10 compares light scattering spectra at $\bar{\nu}$ =4/5 for $[\nu]$=2 and 4 and shows that both sets of spectra are qualitatively similar. However, as shown in Fig. 6.11, when $\bar{\nu} = 1/2$, spectra are markedly different. That is, the SW is absent for $[\nu]$=2 [66] but reemerges in the third LL, when $[\nu]$=4. The difference in spectral weight at half filling in the N=1 and N=2 LL suggests different roles of spin degrees of freedom in the N=1 and N=2 LL. The coexistence of the low-energy continuum and SW is also present at ν = 4+1/2, as well as ν =4+3/4. Remarkably, the continuum appears to be a general feature of light scattering excitations for the range $4 + 4/5 \geq \nu \geq 4 + 1/2$.

Gervais et al. [7] show that at $\nu = 4 + 4/5$ there exists evidence for competing electron solids and fractional quantum Hall fluid phases. Ref. [7] claims that $\nu = 4 + 4/5$, at low temperature (T<80mK), is characterized by an electron solid

phase. However, at slightly higher temperature, 80 mK$< T <$ 120 mK, a fractional quantum Hall state dominates. Since the emergence of electron solid phase coincides with the appearance of the continuum of low-lying energy excitations, we speculate that the continuum might be linked to the presence of charge density wave states. The coexistence of a sharp spin wave and a broad continuum may therefore be connected to the presence of both a fractional quantum Hall fluid and charge density waves, at the same filling factor, as discussed in Ref. [7]. As seen in Chapter 4 and Chapter 5, we might expect that a FQHL, if spin polarized, to exhibit a SW. The dispersion of the stripe phase in Fig. 6.5 has energy that approaches zero as $k \to 0$. Since light scattering detects the critical points of the dispersion, we might expect to find spectral weight at zero or close to zero energy. Zero energy spectral weight may be a general feature charge density waves in the 2nd LL. The spectral weight we observe approaching zero energy shift, in Fig. 6.9, might be due to the dispersion of the stripe phase. Consequently, our results could be interpreted as revealing the competition between charge density waves and conventional fractional quantum Hall states in the third LL. Nevertheless, further work needs to be done to verify this hypothesis. For instance, temperature dependence measurements could be conducted that would probe the melting transition of these electron solid bubble phases and stripe phases [35]. In addition, as discussed in Chapter 5, resonant Rayleigh scattering measurements could probe the domain structure of the 2DES in the third LLs [20, 66].

In addition, Lewis et al. [23] show that filling factors 4+1/4 and 4+3/4 are dominated by electron solid phases with evidence for electron crystallization also at $\nu = 4+1/5$ and $\nu = 4+4/5$. Theoretical studies suggest that the state at $4+1/2$ is dominated by a stripe phase [67]. I speculate that these charge density wave phases are linked to the continuum mode seen by light scattering.

Furthermore, data in Fig. 6.12 tentatively suggest the existence of high energy

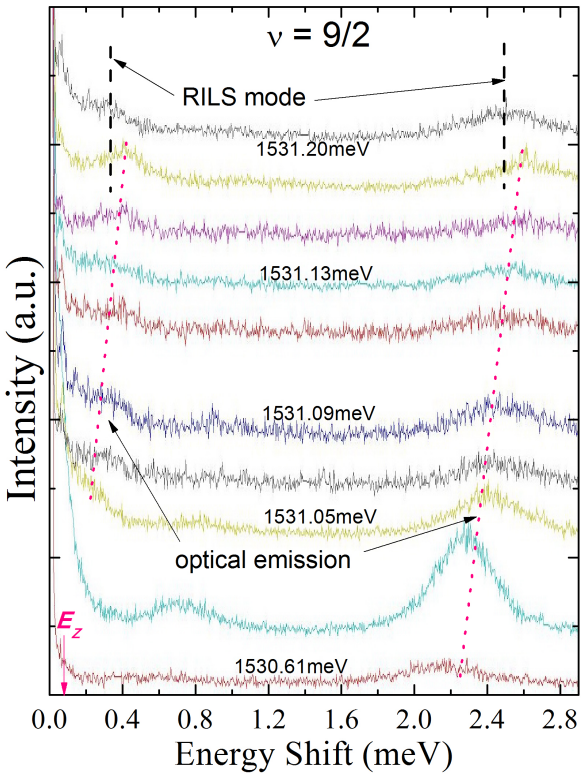

Figure 6.12: Spectra showing the possible existence of two high energy modes at filling factor ν=4+1/2. Slanted lines indicate the presence of optical emission that shifts to the right with increasing incident photon energy. Vertical lines delimit peaks that do not behave like optical emission and are likely Raman scattering modes resulting from critical points in the dispersion of neutral mode excitations of $\nu = 9/2$.

modes detected by light scattering. In particular, Fig. 6.12 shows spectra at $\nu = 9/2$ which might reveal the detection of critical points in the dispersion (at large wave vectors) of neutral modes at this filling. The ability to detect large wave vector modes was discussed in Chapter 4. Break-down of wave vector conservation allowed the detection of high energy modes via RILS. Spectra in Fig. 6.12 show a SW, luminescence which shifts with increasing ω_L (bottom spectrum to top spectrum) and spectral weight which is RILS that could be due to neutral modes of the 2DES. The high energy mode from RILS data at 0.32meV can be compared with theoretical estimates of 0.39meV [24] (Fig. 6.5) and other experimental SAW measurements of 0.016meV [151]. The mode energy from SAW measurement, albeit it much lower than that of RILS is not alarmingly so, as similar a study of FQHE high energy modes, as discussed in Chapter 4, suggests that SAW measurements [154] underestimate the energies of dispersive modes when compared with RILS measurements [5].

6.4 Summary

I probe electron phases in the third Landau level by inelastic light scattering. The low-lying excitations of bulk states are analyzed with an emphasis on spin degrees of freedom. I find RILS evidence that indicates marked differences between the second and third Landau levels, in particular their spin degrees of freedom. I speculate that light scattering spectra showing continua of low-lying excitations in this regime could constitute evidence for charge density waves. In addition, the presence of these low-lying continuum modes might manifest the possibility to detect vibrational modes (see Fig. 6.5) of a triangular lattice of electrons via light scattering. I present these preliminary results in the hope that they will encourage investigation to gain further insight into charge density wave phases and their competition with electron

fluid phases in the N=2 LL.

Chapter 7

Ferromagnetic state at $\nu = 3$: distinctive spin wave dispersion and inter-LL excitations

7.1 Overview

In Chapter 4, we studied light scattering signatures arising from features of the dispersion curve of composite fermions at finite wavevector. I highlighted that critical points and inflection points in the dispersion curve of Λ level excitons can be detected via light scattering. Moreover, I described measurements of CF excitons traversing multiple Λ levels. In this chapter, I discuss studies involving *Landau* levels at $\nu = 3$. I report, for the first time, a kink in the dispersion curve for the spin wave at finite wavevector [25]. Larmor's theorem dictates that the long wavelength SW has excitation energy fixed at the bare Zeeman energy. In the large wavevector limit, the excitation energy becomes largely equivalent to the Coulomb exchange energy. Similar modes have previously been measured by light scattering in the $N = 0$ LL for $\nu = 1$ [95] and $\nu = 1/3$ [155]. The inflection point in the dispersion of

the spin wave at $\nu = 3$ is seen at neither $\nu = 1$ nor $\nu = 1/3$. In addition, I discuss measurements of inter-*Landau* level excitations [16] at $\nu = 3$. From the measurements of spin-flip modes (inter-Landau level excitations involving changes in spin degrees of freedom) we can estimate Coulomb exchange interactions in the 2DES. The appearance of spin-flip modes is tied to the ferromagnetic state at $\nu = 3$ and might be useful as a probe of spin degrees of freedom at other filling factors.

7.2 Introduction

There is great current interest in the role of the spin degree of freedom in the remarkable quantum Hall phases in the N=1 Landau level [34, 18, 156]. Studies reported here at $\nu = 3$ might help build the foundation for future investigation of fractional quantum Hall states of the $N = 1$ LL, such as ν=7/3, 8/3 and 5/2. That is, it might serve as an alternative probe of spin degrees of freedom to that described in Chapter 5. Measurements at $\nu = 3$ discussed in this section exploit excitations between different *Landau* levels which appear to be sensitive to the ferromagnetic state at $\nu = 3$. It is this sensitivity to spin polarization which might be exploited for other quantum Hall states.

In addition, in this thesis I explore how the behavior of quantum fluids changes with *Landau* level index. A major difference between the lowest and second LL is that the latter possess nodes in their wavefunctions while the former does not [40]. The nodes reduce the short-range Coulomb repulsion between electrons and allow the 2DES to phase separate via the exchange effect. The differences in the wavefunctions are expected to engender differences in the dispersion of modes, such as the spin wave. In this Chapter, I present some light scattering studies of the integer quantum Hall state, $\nu = 3$, and examine it's intra-Landau and inter-Landau level excitations. We examine how the dispersion of the spin wave is altered with

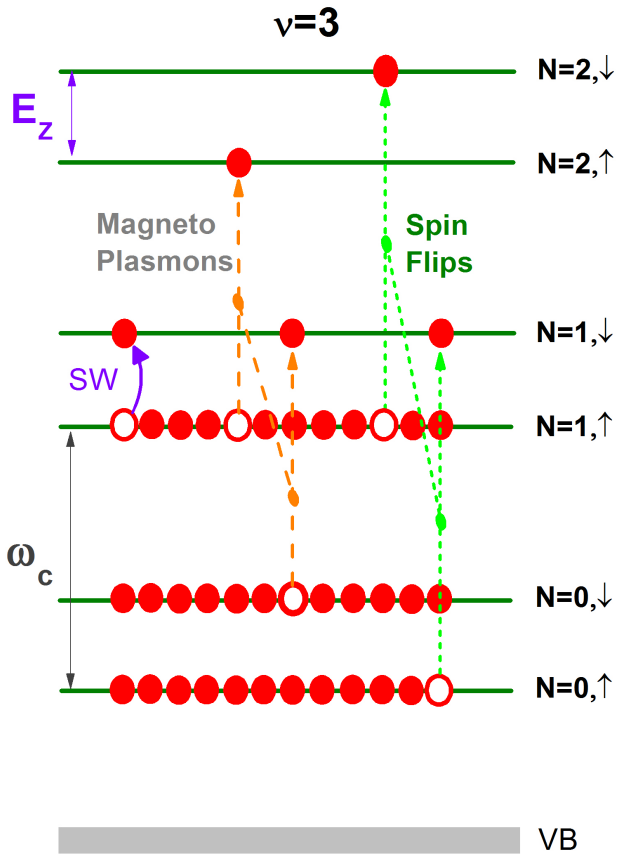

Figure 7.1: Landau level diagram at $\nu = 3$ showing transition for intra-Landau level and inter-Landau level excitations. The spin wave (SW) is the only intra-Landau level excitation. The magnetoplasmon like excitations involve transitions across the cyclotron gap that do not change spin orientation. Spin flip excitations are those that involve both a change in Landau level index and orientation of spin. The two magnetoplasmon like excitations are coupled to each other. The two spin flip excitations are also coupled to each other.

changes in Landau level index. In addition, we discuss how the energy in inter-LL excitations are modified by many body effects. Figure 7.1 shows a schematic of the intra-Landau level and inter-Landau level excitations that are present at $\nu = 3$. The dispersions of these excitations have been calculated for $\nu = 1$, in the seminal work by Kallin and Halperin [12], and more recently for $\nu = 3$ in Ref. [16].

In the case of the spin wave, a distinctive kink at finite wavevector in the dispersion is found from Hartree Fock calculations [25]. As we have seen in Chapter 4, light scattering methods can detect the critical points and inflection points in dispersion curves due to van Hove singularities in the density of states. At integer filling factors, Hartree Fock calculations serve as a powerful predictive tool to study the dispersion of intra-Landau level and inter-Landau level excitations. We compare experimental results with our theoretical framework and provide commentary and insights on the differences of the lowest LL and the second LL.

7.2.1 Collective excitations in the $\nu = 3$ quantum Hall ferromagnet

Figure 7.2a shows the schematic representation of five lowest energy collective excitations in the case of filling factor ν=3 – one intra-Landau level (LL) and four excitations across the cyclotron gap. They are shown as magnetoexcitons consisting of an electron promoted from a filled Landau level and bound to an effective hole left in the "initial" LL. This representation is exact in the limit of strong magnetic field where the parameter $r_c = E_c/\hbar\omega_c$ is small [157, 158, 12]. E_c is the Coulomb energy and $\hbar\omega_c$ is the cyclotron energy.

The set of dispersion curves of the collective modes can be described in the

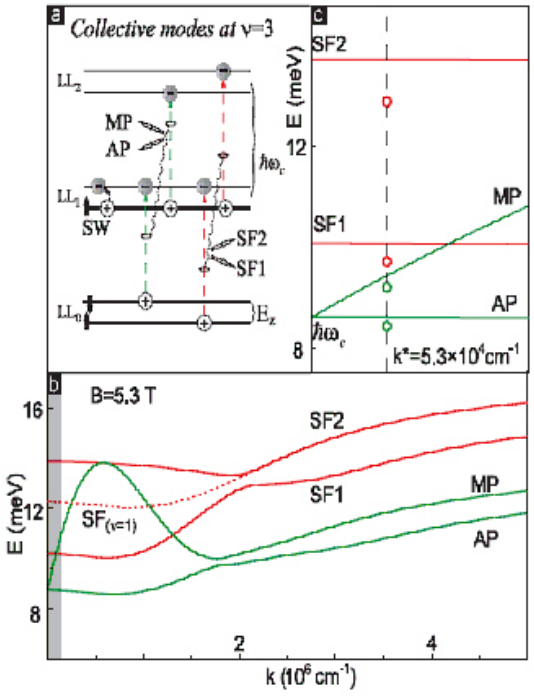

Figure 7.2: (a): Schematic representation of the formation of collective modes at $\nu = 3$ from single-electron transitions. The spin wave (SW) is described as a single spin-flip transition within half-filled $N = 1$ LL. MP and AP are formed as inphase and antiphase combinations of two inter-LL transitions with $\delta S_z = 0$ (shown in green). Cyclotron spin-flip modes SF1 and SF2 arise from analogous combinations of inter-LL transitions with $\delta S_z = -1$ (shown in red). (b): Dispersion curves of inter-LL excitations calculated for $B_T = 5.3\,\mathrm{T}$ within the first-order Hartree-Fock approximation are shown. Here the finite thickness of the 2D electron system is taken into account via the geometric form-factor. The dashed line represents the dispersion of the cyclotron spin-flip mode at $\nu = 1$ at the same magnetic field. (c): The zoomed-in image of the long-wavelength region of Fig. 7.2b shaded in light grey. The dashed vertical line indicates the experimental in-plane momentum $\mathrm{k}^* = 5.3 \times 10^4\,\mathrm{cm}^{-1}$. Open circles represent the experimental data. Extracted from Ref. [16].

following way [12]:

$$E_{m,\delta S_z}(k) = m\hbar\omega_c + g\mu_B B\delta S_z + \Delta E_{m,\delta S_z}(k), \tag{7.1}$$

where m is the change in the LL index and $g\mu_B B\delta S_z$ is the bare Zeeman energy associated with the spin-flip mode. The last term, $\Delta E_{m,\delta S_z}(k)$ is responsible for the dispersion and comprises contributions from the many-body Coulomb interaction and exchange energies in the initial and the excited states. We focus on the excitation spectra with $m = 0$ and $m = 1$.

At $\nu = 3$ the four inter-LL transitions with $m = 1$ shown in Fig. 7.2a are not independent. They couple via the Coulomb interaction to yield two pairs of excitations. The two inter-LL excitations with no change in the spin degree of freedom ($\delta S_z = 0$) are the in-phase magnetoplasmon (MP) mode and the antiphase magnetoplasmon (AP) mode [16]. The two excitations (coupled modes) with changes in the spin degree of freedom ($\delta S_z = -1$) are the cyclotron spin-flip excitations SF1 and SF2 [16].

In first-order perturbation theory, the dispersion curves of the two pairs of coupled modes (either $\delta S_z = 0$ or $\delta S_z = -1$ modes) are defined as follows [16]:

$$\begin{aligned} E_{1,2}(k) &= \frac{\mathcal{E}_1(k) + \mathcal{E}_2(k)}{2} \\ &\pm \sqrt{\left(\frac{\mathcal{E}_1(k) - \mathcal{E}_2(k)}{2}\right)^2 + \Delta_{12}(k)^2} \end{aligned} \tag{7.2}$$

where $\mathcal{E}_{1,2}(k)$ are the energies of single-particle transitions either with or without spin-flip, $\Delta_{12}(k)$ is responsible for coupling. For the $\delta S_z = 0$ modes (MP and AP excitations), this theory yields a vanishing Coulomb term $\Delta E(k)$ in the long wavelength limit [16]. The MP (AP) mode can be derived from Eqn. 7.2 using the positive (negative) sign therein.

The dispersion of SF1 and SF2 at $\nu = 3$ was calculated [16] in terms of matrix elements $\tilde{V}^{(1)}_{\alpha\beta\gamma\delta}(k)$ introduced in Ref. [12]:

$$\begin{aligned} \mathcal{E}_1(k) &= \hbar\omega_c + |g\mu_B B| + \Sigma_{0\uparrow,1\downarrow} - \tilde{V}^{(1)}_{1001}(k) \\ \mathcal{E}_2(k) &= \hbar\omega_c + |g\mu_B B| + \Sigma_{1\uparrow,2\downarrow} - \tilde{V}^{(1)}_{2112}(k) \\ \Delta_{12}(k) &= \tilde{V}^{(1)}_{1102}(k) \end{aligned} \tag{7.3}$$

where $\Sigma_{0\uparrow,1\downarrow} = \tilde{V}^{(1)}_{0000}(0)+\tilde{V}^{(1)}_{0101}(0)-\tilde{V}^{(1)}_{1010}(0)$ and $\Sigma_{1\uparrow,2\downarrow} = \tilde{V}^{(1)}_{1010}(0)+\tilde{V}^{(1)}_{1111}(0)-\tilde{V}^{(1)}_{2020}(0)$ are the differences of exchange self-energies in the excited and ground states for the two single spin-flip transitions between adjacent LLs depicted in Fig. 7.2a. The calculated dispersion curves for all four inter-Landau level excitations with $B = 5.3\,\mathrm{T}$ taken from Ref. [16] and reproduced in Fig. 7.2b. For comparison with experiment, the finite thickness of the 2D-electron system was taken into account.

7.3 Experimental Technique

The experimental methods in this Chapter vary only slightly from those presented in Chapter 3. Inelastic light scattering measurements were performed on a high quality $GaAs/Al_{0.3}Ga_{0.7}As$ heterostructure. A 24 nm-wide single quantum well (SQW) with $n = 3.85 \times 10^{11}\,\mathrm{cm}^{-2}$ and low temperature mobility $\mu \gtrsim 17 \times 10^6\,\mathrm{cm}^2/\mathrm{V}\cdot\mathrm{s}$ at T=300 mK. Recall, that the wave vector transferred from the photons to the 2D system is $q = (2\omega_L/c)\sin\theta$, much smaller than $1/l_o$, where $l_o = \sqrt{\hbar c/eB}$ is the magnetic length. Measurements for excitations across the cyclotron gap were conducted at 1.7K, compared with those on the SW at 40mK. This elevated temperature of 1.7K increased the effective electron density. The filling factor was adjusted accordingly by slightly increasing the magnetic field to $B_T = 5.6T$ to maintain $\nu = 3$. Spectral weight from inelastic light scattering and luminescence were distinguished in the

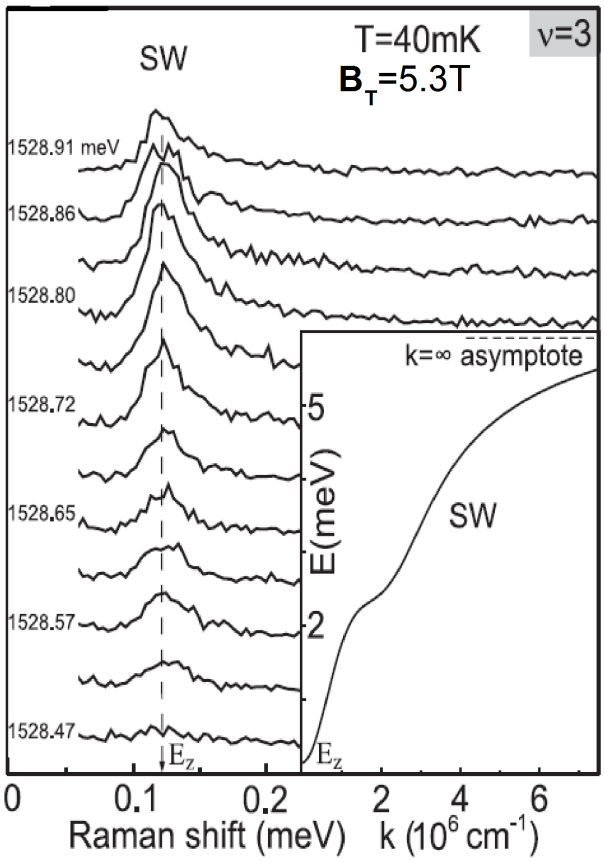

Figure 7.3: Inelastic light scattering spectra of the intra-LL SW mode at $\nu = 3$ and $B_T = 5.3$ T taken at different laser photon energies (shown on the left). The inset shows the SW dispersion curve calculated within the Hartree-Fock approximation, for a 24nm wide quantum well. At the experimental in-plane momentum, the energy of SW is indistinguishable from E_Z. Extracted from Ref. [16, 25].

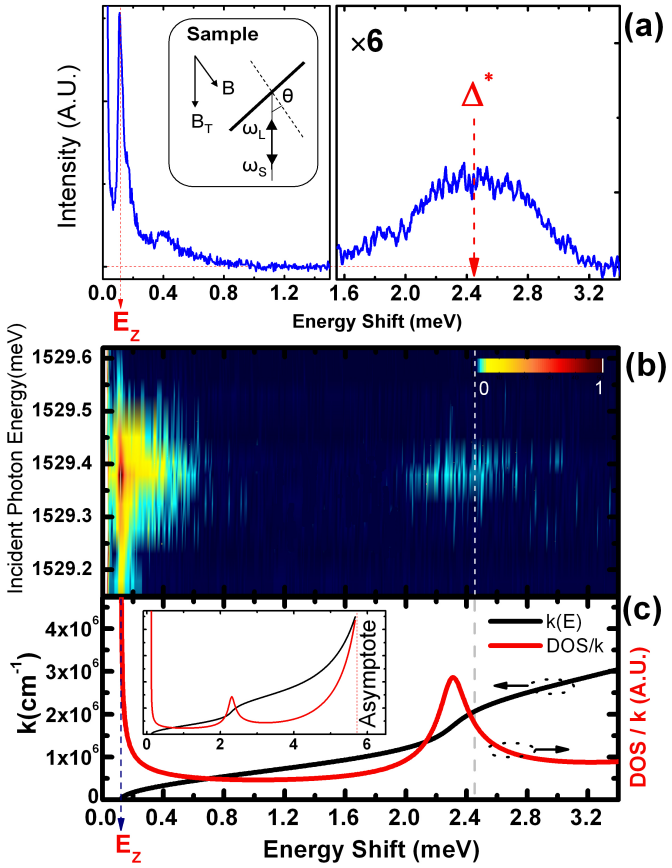

Figure 7.4: (a) Left panel shows the SW and right panel shows spectral weight due to a kink in dispersion. (b) color plot both the SW and the spectral weight due to the kink in the dispersion. (c) the dispersion of the SW is shown alongside the density of states.

manner described in Chapter 4: on an energy shift scale, inelastic light scattering peaks are fixed while luminescence peaks move with changes in incident photon energy.

7.4 Results and Discussion

7.4.1 Ferromagnetic state at $\nu = 3$ and its distinctive dispersion spin wave: intra-LL excitations

The resonant enhancement of the intensities of light scattering spectra of the spin wave at $\nu = 3$ is displayed in Fig. 7.3. This intra-Landau level excitation has m=0 (no change in LL index). The SW energy corresponds to the leftmost part of the dispersion shown in the inset in Fig. 7.3. Very small changes in the laser photon energy ($\sim 0.5\,\mathrm{meV}$) dramatically affect the line intensity, indicating the importance of resonance enhancement. The strong SW seen in Fig. 7.3 is consistent with the ferromagnetic character of the quantum Hall state at $\nu = 3$[66] as discussed in Chapter 5. The dispersion in the inset of Fig. 7.3[16] shows a marked kink at finite wavevector. Figure 7.4 depicts the spectral weight resulting from this kink (at k$\sim$1.5$\times 10^6 cm^{-1}$). Experimental evidence for the distinctive dispersion at $\nu = 3$ is reported here for the first time. Fig. 7.4a shows the SW at E_Z in the left panel. In the right panel is displayed the spectral weight due to the kink in the dispersion (shown in Fig. 7.4c). Fig. 7.4c comprises the dispersion of the SW mode and the corresponding density of states. Fig. 7.4b is a color plot showing scattered photon energy and intensity of SW spectra with varying incident photon energy. Both the SW and the spectral weight at 2 meV is seen to exhibit the effect of resonant enhancement of the light scattering cross-section. The breakdown of wavevector conservation due to the presence of residual disorder, even in the

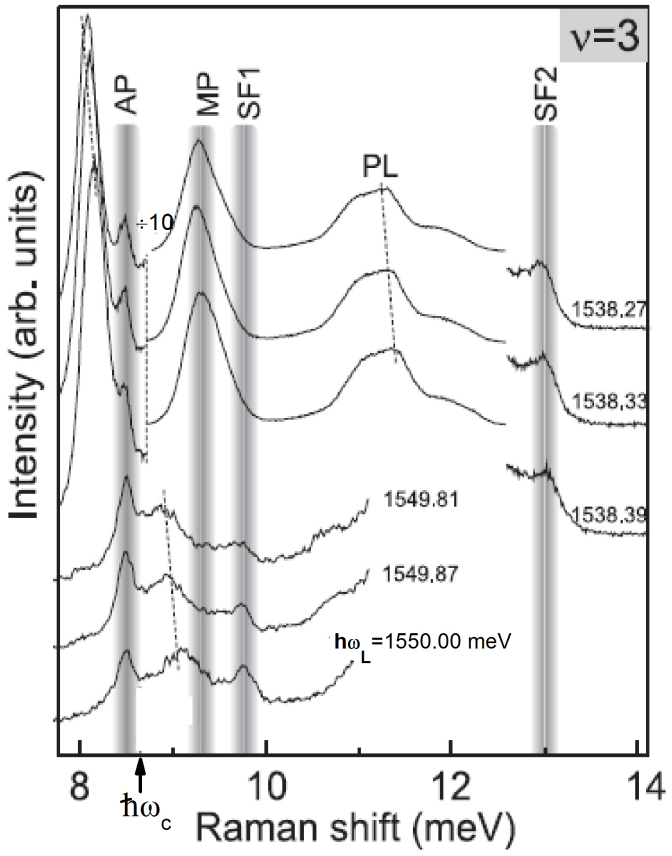

Figure 7.5: Inelastic light scattering spectra of inter-LL excitations at $\nu = 3$ and $B = 5.3$ T taken at different incident photon energies (indicated at the right side of the spectra). The three upper spectra correspond to the resonant incident photon energies when electrons are promoted from the valence band to the second Landau level. Lower spectra are taken at resonant conditions when electrons are excited to the third Landau level. Grey vertical columns mark inelastic light scattering lines. The rest of the spectrum is composed of the luminescence bands, marked by dashed slanted lines. PL labels the photoluminescence. AP and MP are the antiphase magnetoplasmon and the magnetoplasmon respectively. SF1 and SF2 are the coupled spin-flip excitations. Extracted from Ref. [16].

highest quality samples available, provides the ability to detect the finite wavevector inflection point using light scattering, as discussed in Chapter 4. The kink in the calculated dispersion of the SW at $\nu = 3$, which does not occur at $\nu = 1$, is due to the difference in the wavefunctions of states in the lowest LL and higher LL's[40].

7.4.2 Inter-*Landau* Level excitations

Ref. [16] reports resonance enhancement of inter-Landau level excitations at $\nu = 3$. Fig. 7.5 displays a sequence of typical spectra measured at several laser photon energies. Inelastic light scattering lines from all four inter-Landau level excitations are present in the spectra. The three upper spectra were taken at resonant conditions such that incident photons excite electrons from the valence band to the states in the $N = 2$ LL. At these conditions raman lines from AP, MP and SF2 were all observed. Lines corresponding to AP and SF2 were seen separately, though the MP line overlaps the luminescence band and is therefore strongly enhanced in intensity and somewhat broadened. The three lower spectra were measured at other resonant conditions - electrons were promoted from the valence band to the $N = 3$ LL. In this case, AP and SF1 Raman lines were observed.

The magnetoplasmon (MP) and antiphase plasmon (AP) are seen shifted from the cyclotron energy (depicted by an arrow in Fig. 7.5) by 0.61 meV and -0.19 meV respectively. The blue shift of the MP results from the 2D-plasma energy at the non-zero in-plane momentum used in the experiment. In fact, the MP is the only dispersive mode in the range of experimentally accessible momenta within the assumption of wavevector conservation (see Fig. 7.2). The energy of AP is below $\hbar\omega_c$ by 0.19 meV. Theory developed in Ref. [159], gives $\Delta E_{\mathrm{AP}}(0) \approx -0.25$ meV for this magnetic field and quantum well width.

In the case of the two cyclotron spin-flip modes SF1 and SF2 which are blue-

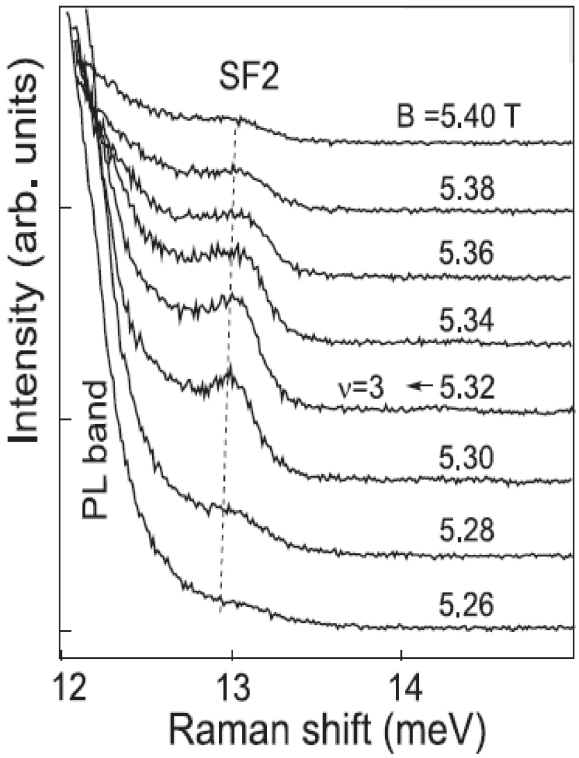

Figure 7.6: The magnetic field evolution of the inelastic light scattering spectrum of SF2 in the vicinity of $\nu = 3$, taken at the fixed incident photon energy $\hbar\omega_L$=1538.33 meV. At $|\Delta B| \sim 0.15$ T the line nearly vanishes from the spectrum. The strong peak in the left most part of the spectrum originates from photoluminescence. Extracted from Ref. [16].

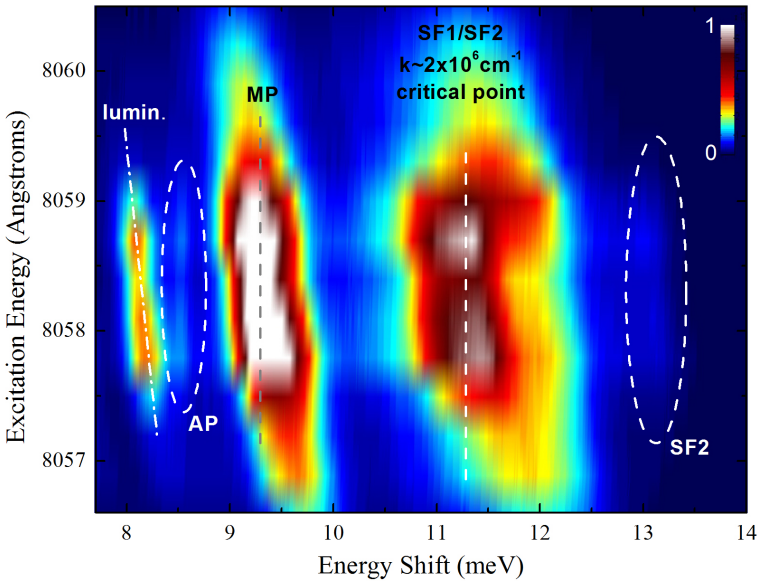

Figure 7.7: Color plot shows that the break-down of wavevector conservation accesses critical points of the dispersion curve for inter-LL excitations at $\nu = 3$. The spectral weight due to the critical points of SF1 and SF2 modes at $k \sim 2 \times 10^6 cm^{-1}$

shifted from $\hbar\omega_c$, we compare the experimental energy shifts with those calculated theoretically [16] (within the first-order Hartree-Fock approximation, taking into account the quantum well width [see Fig. 7.2c]). The shift of SF2 energy from $\hbar\omega_c$ from theory is 5.0 meV, while experiment yields 4.3 meV [16]. The experimental and theoretical values agree quite well, provided the actual width of the quantum well is taken into account.

We also find a marked dependence on magnetic field in which SF1 and SF2 modes are observed only in the narrow interval $\Delta B \simeq 0.15\,\mathrm{T}$ around $\nu = 3$ (see Fig. 7.6). Outside this field range, the lines disappear from the spectrum. We conclude that the stability of spin-flip excitations is inherent of the ferromagnetic state $\nu = 3$. The Coulomb energy of SF2 is close to the estimated full exchange energy of electrons in the $N = 1$ LL. The latter is represented by the short wavelength energy limit of the SW at $\nu = 3$. This value is about three-fourths of the analogous quantity for the fully spin polarized state at $\nu = 1$.

The results in Fig. 7.7 show resonance enhancement revealing breakdown of wave vector conservation in light scattering from inter-Landau level excitations. The color plot shows the energy shift and intensity of peaks as incident photon energy is tuned. The peaks at about 11.5meV could be due to the critical points of the dispersion of the SF1 and SF2 modes at $k \sim 2 \times 10^6 cm^{-1}$. Theoretical values of these critical points are around 12.5meV. Furthermore, it's possible that spectral weight from the long wavelength MP mode delimited in Fig. 7.7 also overlaps with critical points of the MP and AP at $k \sim 1.8 \times 10^6 cm^{-1}$.

7.5 Summary

We have studied the dispersion of the intra-*Landau* level spin wave excitation, the inter-*Landau* level spin-flip excitations and the inter-*Landau* level plasmons. We report, for the first time, spectral weight in light scattering spectra which reveals a critical point (at finite wavevectors) in the SW dispersion at $\nu = 3$. Hartree Fock calculations indicate a kink in the SW dispersion at an energy matching light scattering results. The distinctive dispersion for the SW at $\nu = 3$ is not observed at $\nu = 1$. We interpret its origin as arising from a difference in the character of the second LL. In addition, we discussed four inter-Landau level collective excitations. Among these excitations are two inter-*Landau* level spin-flip modes which interact repulsively in the long wavelength limit. As a result, the more energetic SF2 acquires an enhanced exchange contribution to the energy. The experimentally measured energies of all the critical points in the SW dispersion and inter-LL excitations and are in good agreement with the Hartree-Fock calculations in Ref. [16].

Chapter 8

Future Studies

In this chapter I outline some preliminary results that seem promising for building a deeper understanding of the physics of exotic electron phases in high magnetic fields. I will focus on the 2nd LL, especially on $\nu = 5/2$. When preliminary results are not available, I will propose some experiments that have the potential for advancing scientific pursuits in quantum Hall studies of higher Landau levels.

8.1 Coexistence and competition of phases in the 2nd *Landau* level and beyond

One interesting result in Chapter 5 deals with the emergence of phase separation in the 2nd LL. We use resonance Rayleigh scattering (RRS) to probe the formation of domains arising from this phase separation. Here I report some intriguing RRS data for filling factors around $\nu = 5/2$ and speculate on a plausible interpretation of these data. Further to this I will highlight some additional measurements that might be useful for understanding more about domains in the second LL.

I have shown that domains of distinct electron phases form in the 2nd LL, in particular at $\nu \sim 5/2$. The domain formation is manifested through a resonance in

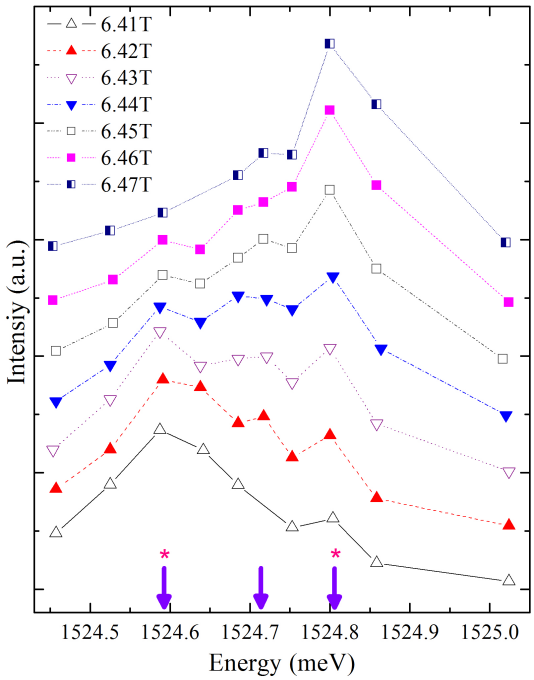

Figure 8.1: RRS profiles at several magnetic fields around $\nu = 5/2$ ($B_T \sim 6.42T$). The three arrows delimit the energies for three possible resonances. The difference in energy between the first and the last two arrows is roughly equivalent to the change in the cyclotron energy over the range of fields used (ΔB=0.06 T). The sum of the spectral weight of the three peaks is skewed towards lower energy at lower fields and skewed towards higher energy at higher fields.

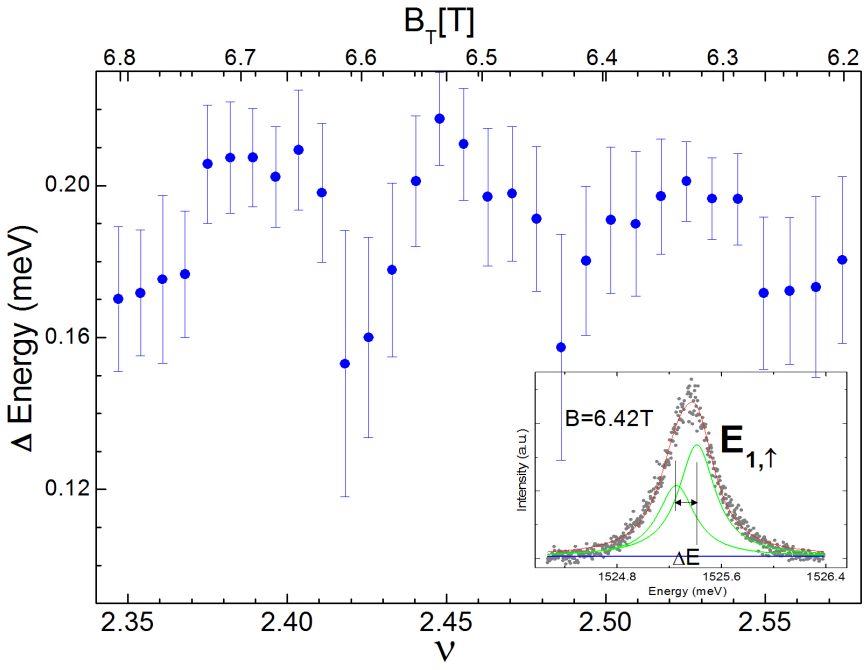

Figure 8.2: Energy splitting of the $N = 1, \uparrow$ optical emission. The optical emission is fit using two Lorentzian functions. The difference in the peak positions are plotted in the main panel. The inset shows the optical emission spectrum at $B_T = 6.42$T.

Rayleigh scattering when the incident photon energy matches some characteristic energy of the system. Figure 8.1 shows how the RRS profile close to $\nu = 5/2$ changes with small steps in magnetic field. There appears to be some resonance enhancement in Rayleigh scattering due to optical gaps at two separate energies (at least). Resonance enhancement from the higher energies increases with increasing magnetic field. An interpretation of this behavior is that "sub-levels" form within the *Landau* level which facilitate the enhancement at these energies. *Moller* et al.[39] predict the existence of two excitonic states at $\nu = 5/2$ which would manifest as two peaks in optical emission. Evidence for splitting of the $N = 1, \uparrow$ luminescence peak is shown in Fig. 8.2; the magnitude of this splitting varies with filling factor. Consequently, optical emission bolsters the evidence for more than one optical gap at $\nu \sim 5/2$.

Recall from Chapter 5 that Wojs et al.[134] describe how Skyrmions (from

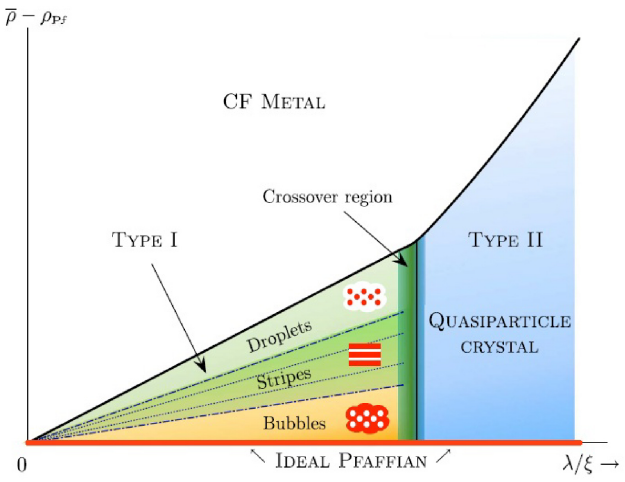

Figure 8.3: Schematic phase diagram of the Pfaffian phases with Coulomb interactions as a function of density deviation from $\nu = 5/2$ and the parameter λ/ξ. Possible configurations of the various domain structures are shown, with Pfaffian (red) and metallic (white) phases. If the quasiparticle coupling strength is increased, a type-II superconductor is recovered, that is not unstable to agglomeration. Extracted from Ref. [26].

quasielectron pairing) and Anti-Skyrmions (from quasihole pairing) have lower and higher energy, respectively, than their quasiparticle constituents. Evidence for this Skyrmion-Anti-Skyrmion asymmetry could be present in Fig. 8.1. Elements of the work by Wojs et al.[134], namely predictions for long-range disorder causing quasiparticles to nucleate into puddles, can also be seen by Parameswaran et al.[26]. Parameswaran et al. claim frustrated phase separation emerges close to $\nu = 5/2$. I speculate that the formation of domains of these phases causes an effective splitting in the $N = 1, \uparrow$ *Landau* level. Fig. 8.3 illustrates the formation of domains, comprised of Pfaffian (red) and metallic (white) phases. The domains can form bubbles, stripes or droplets (anti-bubbles) as shown in the figure. Figure 8.4 emphasizes some important features in Fig. 8.3: exactly at $\nu = 5/2$, the Pfaffian phase (shown in magenta) is expected to dominate while the metallic phase (shown in white) is absent. As the filling factor is tuned away from 5/2, the density of the Pfaffian phase decreases [26]. We can define $\delta n = \bar{n} - n_{Pf}$, the difference between the density of

the positive background and the Pfaffian phase, which increases as ν is tuned away from 5/2. The transition from panel (a) to (c) illustrates the effects of increasing δn. The Pfaffian phase density decreases while the density of metallic phase increases. The left panel describes the case of short-range interaction (no Coulomb interaction) while the right panel includes long-range interactions. In the latter case, the phases agglomerate in order to lower their energy cost. Fig. 8.4a shows the case where δn is small and bubbles of metallic phase form a triangular lattice. As the density of the Pfaffian phase is lowered, a stripe phase is formed, shown in Fig. 8.4(b). As the density of the Pfaffian phase is lowered even further, "droplets" of Pfaffian phase form in a percolating metallic phase. That is, the morphology of the 2DES changes as ν is tuned slightly away from 5/2 [26]. I expect that it is possible to monitor these changes using RRS, since RRS can be used to measure inhomogeneity. I speculate that Fig. 8.1 is indicative of how inhomogeneity changes with filling factor. That is, the change in the shape of the resonance profile might be linked to the changing morphology of the mixed phases close to 5/2. Nevertheless, further work must be done to verify this hypothesis.

RRS should not be limited to monitoring changes in δn, it should also be able to track changes in the coupling parameter, λ/ξ. Recall from Chapter 5 that λ/ξ represents the strength of the quasiparticle coupling, analogous to the coupling of cooper pairs (where ξ is the coherence length and λ is the penetration depth). In the strong (weak) coupling regime, we expect to see the behavior of a type-II (type-I) superconductor. Tuning the coupling strength might be achieved by varying the width of the quantum well. This hypothesis is supported by the work by Peterson et al. [31] which predicts that the Pfaffian state is strengthened by finite layer thickness. I assume that our experimental realization of the phases around 5/2 exists in the weak coupling limit.

It would be useful to perform RRS measurements at other filling factors in the

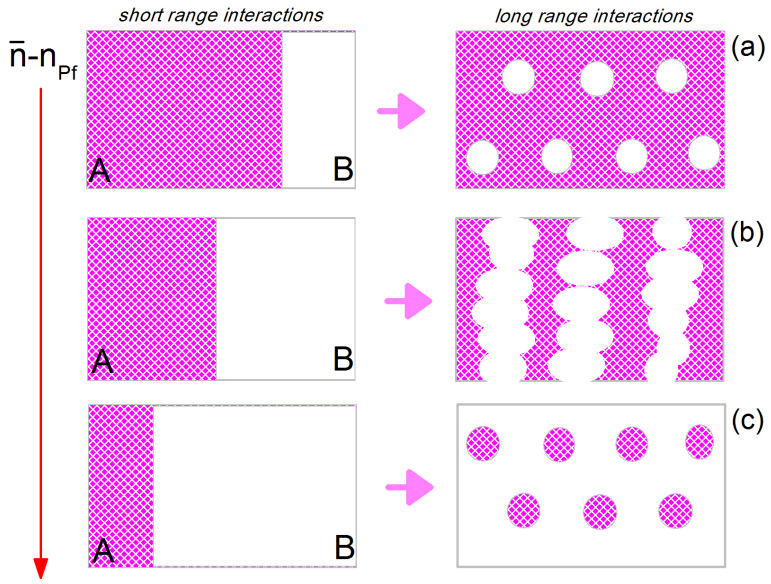

Figure 8.4: Two phases - type A and type B (Pfaffian and metallic phases respectively) - that comprise the 2DES around $\nu = 5/2$, based on the discussion in Ref.[26]. As the filling factor is tuned away from $\nu = 5/2$, the density of the Pfaffian phase decreases. (a), (b) and (c) show the relative amounts of type A to type B as $\delta n = \bar{n} - n_{Pf}$ increases. The left panel shows the case where only short-range interactions are considered (no Coulomb interactions) while the right panel incorporates the effects of long-range (Coulomb) interactions - frustrated phase separation emerges [26].

second and third LL's. These measurements would include temperature dependence studies. Lewis [35] studies the temperature dependence of charge density wave phases using microwave resonance measurements and reports a depinning of the bubbles phase at elevated temperature. A comparison of temperature dependent RRS measurements with the work by Lewis, would not only bolster our work but also provide a more complete picture of charge density wave behavior in the 2nd and 3rd LL's. Furthermore, Langmuir isotherm analyses, as discussed in Chapter 5, would allow us to compare the sizes and binding energies of domains of phases at different filling factors.

In addition, a tilt-dependence study of RRS measurements in the 2nd LL, and especially at 5/2, would explore how the formation of domains might be linked to the destruction of the quantum Hall state at 5/2 [33]. Tilt-dependence measurements are a useful probe of the spin degrees of freedom [146], examining in particular how the ratio of the Zeeman energy to the Coulomb energy affects electron phases. The measurements described in this thesis are limited to a fixed tilt angle.

8.2 Further exploration of the N=0,1 and 2 LL phases

In addition to RRS measurements, a study of RILS could be elucidating: one could monitor how low-lying excitations at $\nu = 5/2$ change with small changes in filling factor. Furthermore, as discussed in the previous section, tilt-dependence measurements provide another means of exploring exotic phases in the 2nd and 3rd LL's. These measurements could also be applied to studying low-lying modes using RILS. That is, one could monitor how low-lying excitations change with tilt. One hypothesis is that the state of 5/2 might recover a spin wave at slightly larger tilt, in analogy

to the work by Dujovne et al. at $\nu = 1/2$ [146], where a well defined SW in induced by increasing the tilt of the sample (increasing the ratio of the Zeeman energy to the Coulomb energy). The states at $\nu = 8/3$ and $7/3$ could also be included in this kind of measurement, for similar reasons.

Additionally, a comparison between $5/2$ and $7/2$ should be made - the behavior of these states is expected to be the same in the absence of *Landau* level mixing [160]. It could be enlightening to discover how the low-lying excitations of the states at $\nu = 7/2$ and $5/2$ differ. A comparison between these states could provide a means of determining the effect of *Landau* level mixing at $5/2$ and $7/2$. Moreover, tuning electron density, thereby tuning the magnetic field at which $5/2$ or $7/2$ is accessed, could provide a means to systematically probe the impact of *Landau* level mixing on these states.

8.3 Exploration of high energy excitations at other filling factors

Chapter 4 discussed high energy CF excitations at $\nu = 1/3$. I find that there is evidence for high energy modes at filling factors beyond the lowest LL ($N = 0, \uparrow$). Preliminary results from RILS data reveal high energy modes, at energies significantly greater than E_Z, at filling factors in the upper spin branch of the $N = 0$ LL ($N = 0, \downarrow$) and also in the $N = 1$ LL. The interpretation of these high energy modes is unclear. Work by Scarola et al. describes the collapse of CF excitons in the higher LLs ($N > 1$ LL) [153]. Thus, the high energy modes we find using RILS may be linked to Λ level structure, or could perhaps find an interpretation in other venues. Figure 8.5 and 8.6 show RILS data delimiting "high energy" excitations at $\nu = 4/3$ and $\nu = 5/3$ respectively. Similar data are shown in Fig. 8.7 for $\nu = 3/2$. It is likely that the former could be readily explained in the

context of excitations across multiple Λ levels. Contrastingly, we expect a CF Fermi sea at $\nu = 3/2$, with infinitely closely spaced energy levels. Presently, details of the mechanism of these excitations are unknown. I speculate that they are linked to excitations of the CF sea, analogous to the SDE and CDE modes at zero field from Chapter 3. Figure 8.8 shows spectral weight, albeit weak, delimiting a high energy mode at $\nu = 8/3$; the origin of which could stem from excitations across several Λ levels. Figure 8.9 shows intriguing RILS spectra in the polarized configuration of a charge density mode with energy less than E_Z at $\nu = 4/3$. Though the origin of this mode is uncertain, the inset in Fig. 8.9 describes a plausible mechanism for the excitation. Further measurements involving tuning magnetic field, sample tilt, polarization selection rules and temperature dependence need to be performed in order to better characterize the nature of these modes.

Remarkably, preliminary data displayed in Fig. 8.10 highlight a "high" energy excitation at $\nu \sim 5/2$. *Moller* et al. [39] predict a dispersive mode of unpaired CFs at $\nu = 5/2$. It is conceivable that the critical points in the dispersion have been detected by light scattering. Further work needs to be done to confirm the origin of this excitation.

Other exciting venues for research involve revisiting the work done in Chapter 7 on cyclotron spin flip modes at temperatures low enough to probe additional many body effects, if any. An interesting comparison could be made between low temperature data ($\sim 40mK$) and the work presented in Chapter 7, measured at $T > 1K$.

Another research path uses light scattering to monitor the effect quantum well structure has on quantum Hall states. Peterson et al. [31] predict that wide quantum wells ($\sim 400\mathring{A}$) stabilize the 5/2 state. It is therefore conceivable, that with 5/2 stabilized by a wide quantum well, a spin wave excitation could be detected by light scattering. Of course, other tunable parameters exist such as density[37] and

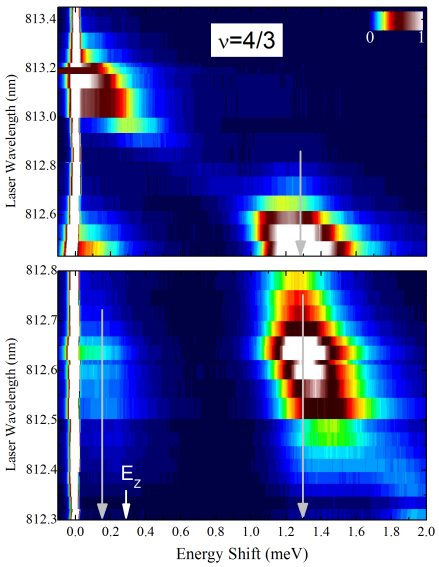

Figure 8.5: Colorplot of excitations in the quantum fluid at $\nu = 4/3$ (B_T=11.9T). Excitations up to 1.3meV are detected. All excitations are delimited by dotted lines shown in the figure. The upper and lower panel differ in the range of incident photon energies used in the RILS measurement.

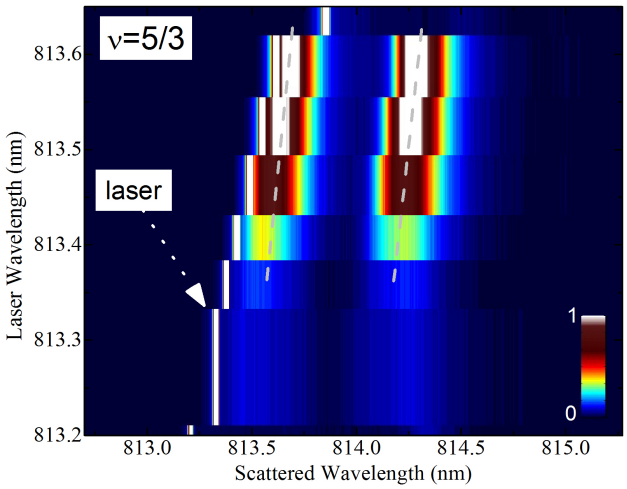

Figure 8.6: Colorplot showing some evidence for inelastic light scattering at $\nu = 5/3$. The plot is on an absolute energy scale; inelastic light scattering spectra shift with increasing incident photon energy. The highest excitation shown has energy shift $\sim 1.4meV$.

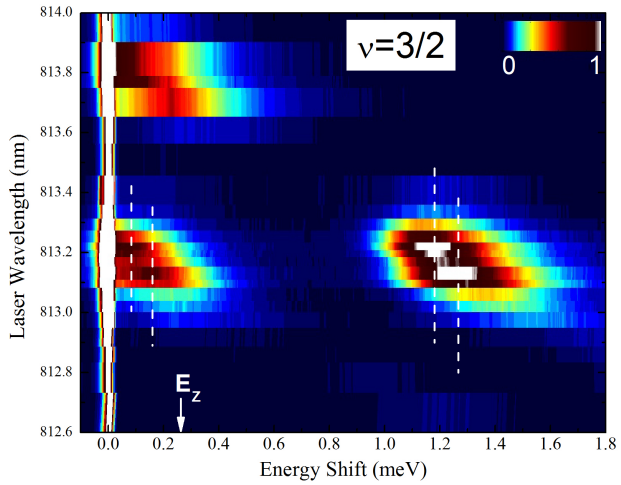

Figure 8.7: Colorplot of excitations in the quantum fluid at $\nu = 3/2$ (B_T=10.5T). Excitations up to 1.3meV are detected. Well defined excitations are delimited by dotted lines shown in the figure.

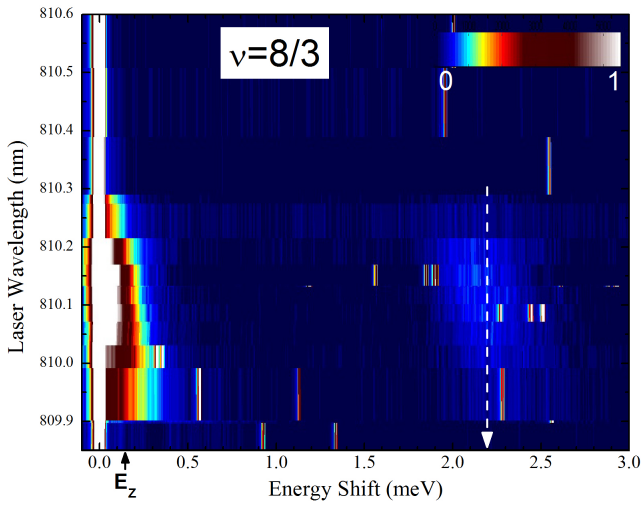

Figure 8.8: Colorplot showing some evidence for inelastic light scattering at $\nu = 8/3$ (B_T=6.0T). The highest excitation shown has energy shift $\sim 2.2meV$.

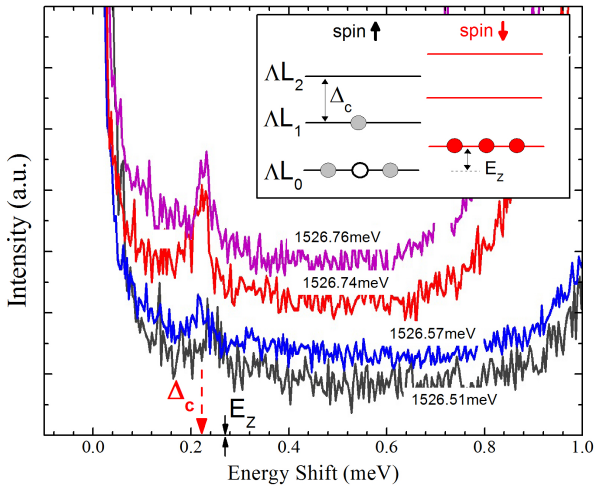

Figure 8.9: Spectra of charge density excitations in the quantum fluid at $\nu = 4/3$ (B_T=11.9T). The charge density excitation from polarized spectra is seen at 0.22meV. The excitation is delimited by a dotted line and labeled Δ_c. The SW is absent in both polarized and depolarized spectra. The inset shows the energy level diagram for a spin unpolarized 4/3 state[27]. The diagram delimits a possible origin for the excitation shown in the main panel. Notice that Δ_c is larger than E_Z in the diagram but smaller than E_Z in the spectra. Presumably, the lower value for Δ_c is due to the Coulomb exchange energy (like an exciton binding energy).

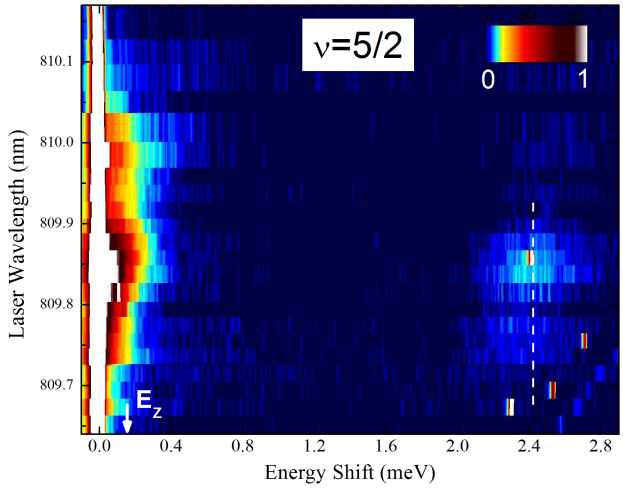

Figure 8.10: Colorplot of excitations in the quantum fluid at $\nu \sim 5/2$ (B_T=6.35T). Excitations up to 2.4meV are detected. Well defined excitations are delimited by dotted lines shown in the figure.

Al concentration [161], both of which have some effect on the activation gap of the state at 5/2. A higher density sample allows the state at 5/2 to be accessed at a higher magnetic field ($\nu \propto n/B$) and consequently with a higher Zeeman energy. It is conceivable that the value of E_Z could affect the spin properties of the state at 5/2. The *Al* concentration in the AlGaAs/GaAs heterostructure affects the remote impurity (RI) donors in the quantum well (that is, the impurities outside the quantum well)[161]. Varying the *Al* concentration varies the amount of disorder due to RI donors, which has been shown to affect the quality of the state at $\nu = 5/2$ [161].

Chapter 9

Concluding Remarks

I present this work at a time of great interest in the state at $\nu = 5/2$ and other states in the higher *Landau* levels. The promise of advances in topological quantum computing fans the flame of scientific curiosity and brings us closer to understanding all the complex phases emerging from electron-electron interactions in high magnetic fields. The work presented in this dissertation represents some of the advances made in characterizing electron phases, especially at $\nu \sim 5/2$, and suggests the next steps in deepening the understanding of 5/2 physics and of quantum Hall physics in general.

Chapters 2 and 3 provide an overview of the physics of electrons in high magnetic field and of optical spectroscopy, the method by which we study these electron systems. In particular, we use resonance light scattering to probe low energy modes of quantum phases with sensitivity to spin and charge degrees of freedom, as well as spatial inhomogeneity. This multifaceted tool provides a new perspective in a field with a great deal many studies using magnetotransport. In Chapter 4, I show that composite fermions at $\nu = 1/3$ are robust topological quasiparticles which have well defined energy level structure up to "high" energies. This study introduces the possibility of doing similar work at $\nu = 5/2$ as a means of exploring the topological

robustness of the state at 5/2.

The low energy modes of states at $3 \geq \nu \geq 5/2$ are examined in Chapter 5. The collapse of the SW suggests the loss of spin polarization for $3 \gtrsim \nu \gtrsim 5/2$; while the emergence of a continuum of low energy excitations alongside the SW implies phase coexistence, in the form of novel domain structures, arises in the 2nd LL. One interpretation of these results contradicts the widely held belief of a spin polarized state at 5/2. Another highlights that sub-micron sized "puddles" of spin polarized 5/2 fluid could exist that destroy the long range order of SW excitations.

To learn more about how the behavior of half-filling fractions varies with *Landau* level, I compare and contrast the low energy excitations of states in the second and third LL. I find remarkable behavior in the spin degrees of freedom - the SW persists to half-filling in the third LL whereas it collapses in the second LL; this suggests intriguing roles of spin degrees of freedom in the 2nd and 3rd LL. In addition, the conventional wisdom of the physics of the third LL, leads us to believe that it comprises mostly charge density waves. I propose some experiments to corroborate this interpretation and to complement existing studies.

Chapter 7 reports new features in the dispersion of the SW at large wavevector, which is seen at $\nu = 3$, but not reported at the analogous $N = 0$ LL state of $\nu = 1$. I speculate that could arise from a difference between wavefunctions of the first and second LL; which results in disparate behavior of the respective SW dispersions. In addition, I present measurements of inter-LL excitations and propose that these measurement could serve as another means of monitoring spin degrees of freedom.

This foray into the electron systems of the first, second and third LL ends with suggestions of venues for future research. This stitch in the vast quantum Hall research effort has the promise of weaving a great fabric of understanding - elucidating both the nature of and the transition from conventional quantum Hall states, to even-denominator quantum Hall states with exotic non-abelian braiding statis-

tics, to the charge density wave phases of higher LLs. The knowledge to be gained may not only gratify a great many academic pursuits, but could also usher in a new era of technological innovation.

Bibliography

[1] Evan O. Kane. Band structure of indium antimonide. *Journal of Physics and Chemistry of Solids*, 1(4):249, 1957.

[2] K. von Klitzing, G. Dorda, and M. Pepper. New method for high-accuracy determination of the fine-structure constant based on quantied Hall resistance. *Phys. Rev. Lett.*, 45(494), 1980.

[3] D.C. Tsui, H.L. Störmer, and A.C. Gossard. Two-dimensional magnetotransport in the extreme quantum limit. *Phys. Rev. Lett.*, 48(1559), 1982.

[4] J.K. Jain. *Composite Fermions*. Cambridge University Press, first edition, 2007.

[5] Trevor D. Rhone, Dwipesh Majumder, Brian S. Dennis, Cyrus Hirjibehedin, Irene Dujovne, Javier G. Groshaus, Yann Gallais, Jainendra K. Jain, Sudhansu S. Mandal, Aron Pinczuk, Loren Pfeiffer, and Ken West. Higher-energy composite fermion levels in the fractional quantum Hall effect. *Phys. Rev. Lett.*, 106(9):096803, Mar 2011.

[6] W. Pan, J.S. Xia, E.D. Adams, R.R. Du, H.L. Störmer, D.C. Tsui, L.N. Pfeiffer, and K.W. Baldwin aand K.W. West. New results at half-fillings in the second and third Landau level. *Physica B*, 298:113–120, 2001.

[7] G. Gervais, L. W. Engel, H. L. Störmer, D. C. Tsui, K. W. Baldwin, K. W. West, and L. N. Pfeiffer. Competition between a fractional quantum Hall liquid and bubble and Wigner crystal phases in the third Landau level. *Phys. Rev. Lett.*, 93(26):266804, Dec 2004.

[8] C. F. Hirjibehedin, Irene Dujovne, I. Bar-Joseph, A. Pinczuk, B. S. Dennis, L. N. Pfeiffer, and K. W. West. Resonant enhancement of inelastic light scattering in the fractional quantum Hall regime at $\nu = 1/3$. *Solid State Communications*, 127(12):799 – 803, 2003.

[9] A. Pinczuk, B. S. Dennis, L. N. Pfeiffer, and K. W. West. Inelastic light scattering in the regimes of the integer and fractional quantum Hall effects. *Semicond. Sci. Technol.*, 9(1865), 1994.

[10] Nicolas Cavassilas, Frédéric Aniel, Kais Boujdaria, and Guy Fishman. Energy-band structure of GaAs and Si: A sps^* $k \cdot p$ method. *Phys. Rev. B*, 64(11):115207, Aug 2001.

[11] GaAs: band structure and carrier concentration, http://www.ioffe.ru/SVA/NSM/Semicond/GaAs/bandstr.html.

[12] C. Kallin and B. I. Halperin. Excitations from a filled Landau level in the two-dimensional electron gas. *Phys. Rev. B*, 30(10):5655–5668, Nov 1984.

[13] A. Pinczuk, Jagdeep Shah, R.C. Miller, A.C. Gossard, and W. Wiegmann. Optical processes of 2D electron plasma in GaAs-(AlGa)As heterostructures. *Solid State Communications*, 50(8):735 – 739, 1984.

[14] P. M. Platzman and Song He. Resonant Raman scattering from mobile electrons in the fractional quantum Hall regime. *Phys. Rev. B*, 49(19):13674–13679, May 1994.

[15] J.K. Jain, private communication.

[16] A. B. Van'kov, T. D. Rhone, A. Pinczuk, I. V. Kukushkin, Loren N. Pfeiffer, Ken W. West, and V. Umansky. Observation of exchange coulomb interactions in the quantum Hall state at $\nu = 3$. *Phys. Rev. B*, 83(24):245325, Jun 2011.

[17] J. S. Xia, W. Pan, C. L. Vicente, E. D. Adams, N. S. Sullivan, H. L. Störmer, D. C. Tsui, L. N. Pfeiffer, K. W. Baldwin, and K. W. West. Electron correlation in the second Landau level: A competition between many nearly degenerate quantum phases. *Phys. Rev. Lett.*, 93(17):176809, Oct 2004.

[18] C. R. Dean, B. A. Piot, P. Hayden, S. Das Sarma, G. Gervais, L. N. Pfeiffer, and K. W. West. Contrasting behavior of the 5/2 and 7/3 fractional quantum Hall effect in a tilted field. *Phys. Rev. Lett.*, 101(18):186806, Oct 2008.

[19] The mode at 0.4meV is strongest at $\nu = 2.9$. While the origin of this mode is unclear at present, we note that it resonates with the SW. Drozdov et al. have recently also reported an extra SW mode around odd-integer quantum Hall states at much lower density [162].

[20] Stefano Luin, Vittorio Pellegrini, Aron Pinczuk, Brian S. Dennis, Loren N. Pfeiffer, and Ken W. West. Resonant Rayleigh scattering from bilayer quantum Hall phases. *Phys. Rev. Lett.*, 97(21):216802, Nov 2006.

[21] M. M. Fogler and A. A. Koulakov. Laughlin liquid to charge-density-wave transition at high Landau levels. *Phys. Rev. B*, 55:9326–9329, Apr 1997.

[22] M. M. Fogler, A. A. Koulakov, and B. I. Shklovskii. Ground state of a two-dimensional electron liquid in a weak magnetic field. *Phys. Rev. B*, 54:1853–1871, Jul 1996.

[23] R. M. Lewis, P. D. Ye, L. W. Engel, D. C. Tsui, L. N. Pfeiffer, and K. W. West. Microwave resonance of the bubble phases in 1/4 and 3/4 filled high Landau levels. *Phys. Rev. Lett.*, 89(13):136804, Sep 2002.

[24] R. Côté, C. B. Doiron, J. Bourassa, and H. A. Fertig. Dynamics of electrons in quantum Hall bubble phases. *Phys. Rev. B*, 68(15):155327, Oct 2003.

[25] A.B. Van'kov, private communication.

[26] S. A. Parameswaran, S. A. Kivelson, S. L. Sondhi, and B. Z. Spivak. Weakly coupled Pfaffian as a type I quantum Hall liquid. *Phys. Rev. Lett.*, 106:236801, Jun 2011.

[27] R. R. Du, A. S. Yeh, H. L. Störmer, D. C. Tsui, L. N. Pfeiffer, and K. W. West. Fractional quantum Hall effect around $\nu = \frac{3}{2}$: Composite fermions with a spin. *Phys. Rev. Lett.*, 75:3926–3929, Nov 1995.

[28] A. Pinczuk, B. S. Dennis, L. N. Pfeiffer, and K. West. Observation of collective excitations in the fractional quantum Hall effect. *Phys. Rev. Lett.*, 70(25):3983–3986, Jun 1993.

[29] N. Read. Paired fractional quantum Hall states and the ν=5/2 puzzle. *Physica B: Condensed Matter*, 298(1-4):121 – 128, 2001.

[30] R. H. Morf. Transition from quantum Hall to compressible states in the second Landau level: New light on the $\nu = 5/2$ enigma. *Phys. Rev. Lett.*, 80(7):1505–1508, Feb 1998.

[31] Michael. R. Peterson, Th. Jolicoeur, and S. Das Sarma. Finite-layer thickness stabilizes the Pfaffian state for the 5/2 fractional quantum Hall effect: Wave function overlap and topological degeneracy. *Phys. Rev. Lett.*, 101(1):016807, Jul 2008.

[32] Chetan Nayak, Steven H. Simon, Ady Stern, Michael Freedman, and Sankar Das Sarma. Non-abelian anyons and topological quantum computation. *Rev. Mod. Phys.*, 80(3):1083–1159, Sep 2008.

[33] J.P. Eisenstein, R.L. Willett, H.L. Stormer, L.N. Pfeiffer, and K.W. West. Activation energies for the even-denominator fractional quantum Hall effect. *Surface Science*, 229(1-3):31 – 33, 1990.

[34] G. A. Csáthy, J. S. Xia, C. L. Vicente, E. D. Adams, N. S. Sullivan, H. L. Störmer, D. C. Tsui, L. N. Pfeiffer, and K. W. West. Tilt-induced localization and delocalization in the second Landau level. *Phys. Rev. Lett.*, 94(14):146801, Apr 2005.

[35] R. M. Lewis, Yong Chen, L. W. Engel, P. D. Ye, D. C. Tsui, L. N. Pfeiffer, and K. W. West. Measurements of the temperature dependence of the bubble phase. *Physica E: Low-dimensional Systems and Nanostructures*, 22(1-3):119 – 121, 2004. 15th International Conference on Electronic Propreties of Two-Dimensional Systems (EP2DS-15).

[36] L. Tiemann, G. Gamez, N. Kumada, and K. Muraki. *Proceedings of the 19th International Conference on the Application of High Magnetic Fields in Semiconductor Physics and Nanotechnology (HMF-19), Fukuoka, Japan, unpublished*, 2010.

[37] S. Das Sarma, G. Gervais, and Xiaoqing Zhou. Energy gap and spin polarization in the 5/2 fractional quantum Hall effect. *Phys. Rev. B*, 82(11):115330, Sep 2010.

[38] C. R. Dean, B. A. Piot, P. Hayden, S. Das Sarma, G. Gervais, L. N. Pfeiffer, and K. W. West. Contrasting behavior of the 5/2 and 7/3 fractional quantum Hall effect in a tilted field. *Phys. Rev. Lett.*, 101(18):186806, Oct 2008.

[39] Gunnar Möller, Arkadiusz Wójs, and Nigel R. Cooper. Neutral fermion excitations in the Moore-Read state at filling factor $\nu = 5/2$. *Phys. Rev. Lett.*, 107:036803, Jul 2011.

[40] J.P. Eisenstein. Two-dimensional electrons in excited Landau levels: evidence for new collective states. *Solid State Comm.*, 117:123, 2001.

[41] R. Dingle, H. L. Störmer, A. C. Gossard, and W. Wiegmann. Electron mobilities in modulation-doped semiconductor heterojunction superlattices. *Appl. Phys. Lett.*, 33(665), 1978;. H.L. Stormer, A. Pinczuk, A.C. Gossard and W. Wiegmann, Influence of an undoped (AlGa)As spacer on mobility enhancement in GaAs-(AlGa)As superlattices, *ibid*, 38(691), 1981.

[42] Gerald Bastard. *Wave mechanics applied to semiconductor heterostructures*. Halsted Press, first edition, 1988.

[43] N.W. Ashcroft and N.D. Mermin. *Solid State Physics*. Brooks/Cole, 1976.

[44] E. H. Hall. On a new action of the magnet on electric currents. *Am. J. Math*, 2(287), 1879.

[45] K. von Klitzing. The quantized Hall effect. *Rev. Mod. Phys.*, 58(519), 1986.

[46] Horst L. Störmer, Daniel C. Tsui, and Arthur C. Gossard. The fractional quantum Hall effect. *Rev. Mod. Phys.*, 71(2):S298–S305, Mar 1999.

[47] D.C. Tsui. Nobel lecture: Interplay of disorder and interaction in two-dimensional electron gas in intense magnetic fields. *Rev. Mod. Phys.*, 71(891), 1999.

[48] R. Shankar. *Principles of Quantum Mechanics*. World Scientific, 2nd edition, 1994.

[49] R. B. Laughlin. Anomalous quantum Hall effect: An incompressible quantum fluid with fractionally charged excitations. *Phys. Rev. Lett.*, 50(18):1395–1398, May 1983.

[50] F. D. M. Haldane. Fractional quantization of the Hall effect: A hierarchy of incompressible quantum fluid states. *Phys. Rev. Lett.*, 51:605–608, Aug 1983.

[51] P.W. Anderson. More is different. *Science*, 177(393), 1972.

[52] J. K. Jain. Composite-fermion approach for the fractional quantum Hall effect. *Phys. Rev. Lett.*, 63(2):199–202, Jul 1989.

[53] J.K. Jain. *Phys. Today*, page 53:39, 2000.

[54] O. Heinonen (Editor). *Composite Fermions: a unified view of the quantum Hall regime*. World Scientific, 1998.

[55] L.D. Landau and E.M. Lifshitz. *Statistical Physics, Course of Theoretical Physics, Volume 5*. Elsevier, 3rd edition, 1980.

[56] E. Wigner. On the interaction of electrons in metals. *Phys. Rev.*, 46(11):1002–1011, Dec 1934.

[57] H. Fukuyama, P. M. Platzman, and P. W. Anderson. Two-dimensional electron gas in a strong magnetic field. *Phys. Rev. B*, 19:5211–5217, May 1979.

[58] Kun Yang, F. D. M. Haldane, and E. H. Rezayi. Wigner crystals in the lowest Landau level at low-filling factors. *Phys. Rev. B*, 64(8):081301, Aug 2001.

[59] Daijiro Yoshioka and Hidetoshi Fukuyama. Charge density wave state of two-dimensional electrons in strong magnetic fields. *Journal of the Physical Society of Japan*, 47(2):394–402, 1979.

[60] E. H. Rezayi, F. D. M. Haldane, and Kun Yang. Charge-density-wave ordering in half-filled high Landau levels. *Phys. Rev. Lett.*, 83:1219–1222, Aug 1999.

[61] F. D. M. Haldane, E. H. Rezayi, and Kun Yang. Spontaneous breakdown of translational symmetry in quantum Hall systems: Crystalline order in high Landau levels. *Phys. Rev. Lett.*, 85:5396–5399, Dec 2000.

[62] Michael M. and Fogler. Dynamics of disordered quantum Hall crystals. *Physica E: Low-dimensional Systems and Nanostructures*, 22(1-3):98 – 103, 2004. 15th International Conference on Electronic Propreties of Two-Dimensional Systems (EP2DS-15).

[63] Eduardo Fradkin and Steven A. Kivelson. Liquid-crystal phases of quantum Hall systems. *Phys. Rev. B*, 59(12):8065–8072, Mar 1999.

[64] M. P. Lilly, K. B. Cooper, J. P. Eisenstein, L. N. Pfeiffer, and K. W. West. Anisotropic states of two-dimensional electron systems in high Landau levels: Effect of an in-plane magnetic field. *Phys. Rev. Lett.*, 83:824–827, Jul 1999.

[65] R. M. Lewis, Yong P. Chen, L. W. Engel, D. C. Tsui, L. N. Pfeiffer, and K. W. West. Microwave resonance of the reentrant insulating quantum Hall phases in the first excited Landau level. *Phys. Rev. B*, 71:081301, Feb 2005.

[66] Trevor D. Rhone, Jun Yan, Yann Gallais, Aron Pinczuk, Loren Pfeiffer, and Ken West. Rapid collapse of spin waves in nonuniform phases of the second Landau level. *Phys. Rev. Lett.*, 106(19):196805, May 2011.

[67] M. O. Goerbig, P. Lederer, and C. Morais Smith. Competition between quantum-liquid and electron-solid phases in intermediate Landau levels. *Phys. Rev. B*, 69(11):115327, Mar 2004.

[68] C. V. Raman and K. S. Krishnan. A new type of secondary radiation. *Nature*, 121(3048):501, March 1928.

[69] W. Hayes and R. Loudon. *Scattering of Light by Crystals*. John Wiley & Sons, 1978.

[70] W.H. Weber and R. Merlin (Eds.). *Raman Scattering in Materials Science*. Springer, first edition, 2000.

[71] M.H. Brodsky, E. Burstein, M. Cardona, L.M. Falicov, M.V. Klein, R.M. Martin, A. Pinczuk, A.S. Pine, and Y.R. Shen. *Light Scattering in Solids, volume 8 of Topics Appl. Phys.* Springer-Verlag, 1975.

[72] G. Baym. *Lectures on Quantum Mechanics*. Addison-Wesley, Reading, Massachusetts, 1990.

[73] D.C. Hamilton and A.L. McWhorter. *Light Scattering Spectra of Solids*. Springer, Berlin, Heidelberg, New York, 1969.

[74] F. A. Blum. Inelastic light scattering from semiconductor plasmas in a magnetic field. *Phys. Rev. B*, 1(3):1125–1135, Feb 1970.

[75] G. Abstreiter, M. Cardona, and A. Pinczuk. *Light Scattering in Solids IV, volume 54 of Topics Appl. Phys.* Springer-Verlag, 1984.

[76] P. A. Wolff. Thomson and Raman scattering by mobile electrons in crystals. *Phys. Rev. Lett.*, 16(6):225–228, Feb 1966.

[77] E. Burstein, A. Pinczuk, and D.L. Mills. Inelastic light scattering by charge carrier excitations in two-dimensional plasmas: Theoretical considerations. *Surface Scien*, 98:451–468, August 1980.

[78] Javier G. Groshaus, Irene Dujovne, Yann Gallais, Cyrus F. Hirjibehedin, Aron Pinczuk, Yan-Wen Tan, Horst Störmer, Brian S. Dennis, Loren N. Pfeiffer, and Ken W. West. Spin texture and magnetoroton excitations at $\nu = 1/3$. *Phys. Rev. Lett.*, 100(4):046804, Jan 2008.

[79] H. D. M. Davies, J. C. Harris, J. F. Ryan, and A. J. Turberfield. Spin and charge density excitations and the collapse of the fractional quantum Hall state at $\nu = 1/3$. *Phys. Rev. Lett.*, 78(21):4095–4098, May 1997.

[80] I. K. Marmorkos and S. Das Sarma. Magnetoplasmon excitation spectrum for integral filling factors in a two-dimensional electron system. *Phys. Rev. B*, 45(23):13396–13399, Jun 1992.

[81] Our analysis assumes, as appropriate for weak disorder, that the mode wave vector remains a good quantum number and the net effect of disorder is to allow coupling to large wave vector excitation modes [80, 78].

[82] Marie S-C. Luo, Shun Lien Chuang, Stefan Schmitt-Rink, and Aron Pinczuk. Many-body effects on intersubband spin-density and charge-density excitations. *Phys. Rev. B*, 48(15):11086–11094, Oct 1993.

[83] A. Pinczuk, J. M. Worlock, H. L. Strmer, R. Dingle, W. Wiegmann, and A. C. Gossard. Intersubband spectroscopy of two dimensional electron gases: Coulomb interactions. *Solid State Communications*, 36(1):43 – 46, 1980.

[84] A. Pinczuk, S. Schmitt-Rink, G. Danan, J. P. Valladares, L. N. Pfeiffer, and K. W. West. Large exchange interactions in the electron gas of GaAs quantum wells. *Phys. Rev. Lett.*, 63(15):1633–1636, Oct 1989.

[85] R. Loudon. *The Quantum Theory of Light*. Clarendon Press, London, 1973.

[86] Walter Kohn. Cyclotron resonance and de Haas-van Alphen oscillations of an interacting electron gas. *Phys. Rev.*, 123(4):1242–1244, Aug 1961.

[87] A. Pinczuk, B. S. Dennis, D. Heiman, C. Kallin, L. Brey, C. Tejedor, S. Schmitt-Rink, L. N. Pfeiffer, and K. W. West. Spectroscopic measurement of large exchange enhancement of a spin-polarized 2D electron gas. *Phys. Rev. Lett.*, 68(24):3623–3626, Jun 1992.

[88] M. A. Eriksson, A. Pinczuk, B. S. Dennis, C. F. Hirjibehedin, S. H. Simon, L. N. Pfeiffer, and K. W. West. Collective excitations in low-density 2D electron systems. *Physica E: Low-dimensional Systems and Nanostructures*, 6(1-4):165 – 168, 2000.

[89] A. Pinczuk, J. P. Valladares, D. Heiman, A. C. Gossard, J. H. English, C. W. Tu, L. Pfeiffer, and K. West. Observation of roton density of states in two-dimensional Landau-level excitations. *Phys. Rev. Lett.*, 61(23):2701–2704, Dec 1988.

[90] A. Pinczuk, J.P. Valladares, D. Heiman, L.N. Pfeiffer, and K.W. West. Light scattering determination of roton densities of states in two-dimensional Landau level excitations. *Surface Science*, 229(1-3):384 – 387, 1990.

[91] I. K. Marmorkos and S. Das Sarma. Magnetoplasmon excitation spectrum for integral filling factors in a two-dimensional electron system. *Phys. Rev. B*, 45(23):13396–13399, Jun 1992.

[92] D. Mujumder, S.S. Mandal, and J.K. Jain. Collective excitations of composite fermions across multiple λ levels. *Nature Physics*, 5(6):403–406, 2009.

[93] Gregory Moore and Nicholas Read. Nonabelions in the fractional quantum Hall effect. *Nuclear Physics B*, 360(2-3):362 – 396, 1991.

[94] Y. Gallais, T.H. Kirschenmann, C.F. Hirjibehedin, I. Dujovne, A. Pinczuk, L.N. Pfeiffer, and K.W. West. Spin excitations in the fractional quantum Hall regime at $\nu \leq 1/3$. *Physica E*, 34(1-2):144–147, 2006.

[95] Yann Gallais, Jun Yan, Aron Pinczuk, Loren N. Pfeiffer, and Ken W. West. Soft spin wave near $\nu = 1$: Evidence for a magnetic instability in skyrmion systems. *Phys. Rev. Lett.*, 100(8):086806, Feb 2008.

[96] Jens Martin, Shahal Ilani, Basile Verdene, Jurgen Smet, Vladimir Umansky, Diana Mahalu, Dieter Schuh, Gerhard Abstreiter, and Amir Yacoby. Localization of fractionally charged quasi-particles. *Science*, 305(5686):980–983, 2004.

[97] C.F. Hirjibehedin, I. Dujovne, I. Bar-Joseph, A. Pinczuk, B.S. Dennis, L.N. Pfeiffer, and K.W. West. Resonanct enhancement of inelastic light scattering in the fractional quantum Hall regime at ν=1/3. *Solid State Commun.*, 127(12):799–803, 2003.

[98] Irene Dujovne, A. Pinczuk, Moonsoo Kang, B. S. Dennis, L. N. Pfeiffer, and K. W. West. Evidence of Landau levels and interactions in low-lying excitations of composite fermions at $1/3 \leq \nu \leq 2/5$. *Phys. Rev. Lett.*, 90(3):036803, Jan 2003.

[99] Massimo Gurioli, Juan Martinez-Pastor, Marcello Colocci, Christiane Deparis, Bruno Chastaingt, and Jean Massies. Thermal escape of carriers out of GaAs/Al_xGa_{1-x}As quantum-well structures. *Phys. Rev. B*, 46(11):6922–6927, Sep 1992.

[100] Pawel Hawrylak, Nicolas Pulsford, and Klaus Ploog. Magneto-optics of acceptor-doped GaAs/$Ga_{1-x}Al_xAs$ heterostructures in the quantum Hall

regime: Resonant magnetoexcitons and many-electron effects. *Phys. Rev. B*, 46(23):15193–15199, Dec 1992.

[101] J.L. Osbourne, A.J. Shields, M.Y. Simmons, N.R. Cooper, D.A. Ritchie, and M. Pepper. Magneto-optical study of excitonic states in 2DEGs near filling factor $\nu = 1$. *Physica B*, (249-251):538–543, 1998.

[102] Gleb Finkelstein, Hadas Shtrikman, and Israel Bar-Joseph. Shake-up processes of a two-dimensional electron gas in GaAs/AlGaAs quantum wells at high magnetic fields. *Physica B: Condensed Matter*, 249-251:575 – 579, 1998.

[103] V. E. Zhitomirskii, V. E. Kirpichev, A. I. Filin, V. B. Timofeev, B. N. Shepel', and K. von Klitzing. Optical detection of spin relaxation of 2D electrons during photoexcitation. *Journal of Experimental and Theoretical Physics Letters*, 58:439, September 1993.

[104] Flavio Plentz, Don Heiman, Aron Pinczuk, Loren N. Pfeiffer, and Ken W. West. Spin-dependent photoluminescence at ν =1 filling factor. *Physica B*, (249-251):558–561, 1998.

[105] P.O. Holtz, Q.X. Zhao, and B. Monemar. Shake-up intersubband transitions observed in $GaAs$/AlGaAs quantum wells. *Superlattices and Microstructures*, 17(1):23–26, 1995.

[106] I. V. Kukushkin, K. v. Klitzing, and K. Eberl. Spin polarization of two-dimensional electrons in different fractional states and around filling factor $\nu = 1$. *Phys. Rev. B*, 55(16):10607–10612, Apr 1997.

[107] B.B. Goldberg, D. Heiman, A. Pinczuk, L.Pfeiffer, and K.W. West. Magneto-optics in the integer and fractional quantum Hall and electron solid regimes. *Surface Science*, 263(1-3):9 – 17, 1992.

[108] Michael Levin and Ady Stern. Fractional topological insulators. *Phys. Rev. Lett.*, 103(19):196803, Nov 2009.

[109] Xu Du, Ivan Skachko, Fabian Duerr, Adina Luican, and Eva Y. Andrei. Fractional quantum Hall effect and insulating phase of Dirac electrons in graphene. *Nature*, 462(7270):192–195, 2009.

[110] K.I. Bolotin, F. Ghahari, M.D. Shulman, H.L. Störmer, and P. Kim. Observation of the fractional quantum Hall effect in graphene. *Nature*, 462(7270):196–199, 2009.

[111] C.G. Callan, I.R. Klebanov, J.M. Maldacena, and A. Yegulalp. Magnetic fields and fractional statistics in boundary conformal field theory. *Nuclear Physics B*, 443(3):444–464, 1995.

[112] Y.J. Lin, R.L. Compton, K. Jimenez-Garcia, J.V. Porto, and I.B Spielman. Synthetic magnetic fields for ultracold neutral atoms. *Nature*, 462(7273):628–32, 2009.

[113] Wen X. Topological orders in rigid states. *International journal of modern physics. B, Condensed matter physics, statistical physics, applied physics.*, 4:239–71, 1990.

[114] S. M. Girvin, A. H. MacDonald, and P. M. Platzman. Collective-excitation gap in the fractional quantum Hall effect. *Phys. Rev. Lett.*, 54(6):581–583, Feb 1985.

[115] F. D. M. Haldane and E. H. Rezayi. Finite-size studies of the incompressible state of the fractionally quantized Hall effect and its excitations. *Phys. Rev. Lett.*, 54(3):237–240, Jan 1985.

[116] Gautam Dev and J. K. Jain. Band structure of the fractional quantum Hall effect. *Phys. Rev. Lett.*, 69(19):2843–2846, Nov 1992.

[117] Song He, S. H. Simon, and B. I. Halperin. Response function of the fractional quantized Hall state on a sphere. II. exact diagonalization. *Phys. Rev. B*, 50(3):1823–1831, Jul 1994.

[118] Vito W. Scarola, Kwon Park, and Jainendra K. Jain. Rotons of composite fermions: Comparison between theory and experiment. *Phys. Rev. B*, 61(19):13064–13072, May 2000.

[119] M. Byszewski, B. Chwaliszi, D. K. Maude, M. L. Sadowski, M. Potemski, T. Saku, Y. Hikayama, S. Studenikin, D. G. Austing, A. S. Sachrajda, and P. Hawrylak. Optical probing of composite fermions in a two-dimensional electron gas. *Nature Physics*, 2, April 2006.

[120] Ganpathy Murthy. Hamiltonian theory of disorder at $\nu = 1/3$. *Phys. Rev. Lett.*, 103(20):206802, Nov 2009.

[121] Ady Stern. Non-abelian states of matter. *Nature*, 464:187–193, Mar 2010.

[122] C. F. Hirjibehedin, Irene Dujovne, A. Pinczuk, B. S. Dennis, L. N. Pfeiffer, and K. W. West. Splitting of long-wavelength modes of the fractional quantum Hall liquid at $\nu = 1/3$. *Phys. Rev. Lett.*, 95(6):066803, Aug 2005.

[123] Sudhansu S. Mandal and J. K. Jain. Activation energies for spin-reversed excitations in the fractional quantum Hall effect. *Phys. Rev. B*, 64(12):125310, Sep 2001.

[124] K. Park and J. K. Jain. Two-roton bound state in the fractional quantum Hall effect. *Phys. Rev. Lett.*, 84(24):5576–5579, Jun 2000.

[125] M. Stern, P. Plochocka, V. Umansky, D.K. Maude, M. Potemski, and I. Bar-Joseph. Optical probing of the spin polarization of the $\nu = 5/2$ quantum Hall state. *Phys. Rev. Lett.*, 105(9):096801, 2010.

[126] R. Willett, J. P. Eisenstein, H. L. Störmer, D. C. Tsui, A. C. Gossard, and J. H. English. Observation of an even-denominator quantum number in the fractional quantum Hall effect. *Phys. Rev. Lett.*, 59(15):1776–1779, Oct 1987.

[127] J. P. Eisenstein, R. Willett, H. L. Störmer, D. C. Tsui, A. C. Gossard, and J. H. English. Collapse of the even-denominator fractional quantum Hall effect in tilted fields. *Phys. Rev. Lett.*, 61(8):997, Aug 1988.

[128] W. Pan, H. L. Störmer, D. C. Tsui, L. N. Pfeiffer, K. W. Baldwin, and K. W. West. Experimental evidence for a spin-polarized ground state in the ν=5/2 fractional quantum Hall effect. *Solid State Communications*, 119(12):641 – 645, 2001.

[129] Ady Stern. Anyons and the quantum Hall effect a pedagogical review. *Annals of Physics*, 323(1):204 – 249, 2008. January Special Issue 2008.

[130] G. A. Csáthy, J. S. Xia, C. L. Vicente, E. D. Adams, N. S. Sullivan, H. L. Störmer, D. C. Tsui, L. N. Pfeiffer, and K. W. West. Tilt-induced localization and delocalization in the second Landau level. *Phys. Rev. Lett.*, 94(14):146801, Apr 2005.

[131] A. E. Feiguin, E. Rezayi, Kun Yang, C. Nayak, and S. Das Sarma. Spin polarization of the $\nu = 5/2$ quantum Hall state. *Phys. Rev. B*, 79(11):115322, Mar 2009.

[132] M. Storni, R. H. Morf, and S. Das Sarma. Fractional quantum Hall state at $\nu = 5/2$ and the moore-read Pfaffian. *Phys. Rev. Lett.*, 104(7):076803, Feb 2010.

[133] Trevor D. Rhone, Jun Yan, Yann Gallais, Aron Pinczuk, Loren Pfeiffer, and Ken West. Traversing the states of the second Landau level - loss of spin polarization away from ν=3. Number BAPS.2010.MAR.Y2.3, APS Meeting, Portland OR, March 2010.

[134] Arkadiusz Wójs, Gunnar Möller, Steven H. Simon, and Nigel R. Cooper. Skyrmions in the Moore-Read state at $\nu = 5/2$. *Phys. Rev. Lett.*, 104(8):086801, Feb 2010.

[135] Chi Zhang, T. Knuuttila, Yanhua Dai, R. R. Du, L. N. Pfeiffer, and K. W. West. $\nu = 5/2$ fractional quantum Hall effect at 10 T: Implications for the Pfaffian state. *Phys. Rev. Lett.*, 104(16):166801, Apr 2010.

[136] Arkadiusz Wójs, Csaba Tőke, and Jainendra K. Jain. Landau-level mixing and the emergence of Pfaffian excitations for the 5/2 fractional quantum Hall effect. *Phys. Rev. Lett.*, 105(9):096802, Aug 2010.

[137] Boris Spivak and Steven A. Kivelson. Transport in two dimensional electronic micro-emulsions. *Annals of Physics*, 321(9):2071 – 2115, 2006.

[138] C. Ortix, J. Lorenzana, and C. Di Castro. Frustrated phase separation in two-dimensional charged systems. *Phys. Rev. B*, 73:245117, Jun 2006.

[139] B. B. Goldberg, D. Heiman, M. Dahl, A. Pinczuk, L. Pfeiffer, and K. West. Localization and many-body interactions in the quantum Hall effect determined by polarized optical emission. *Phys. Rev. B*, 44(8):4006–4009, Aug 1991.

[140] William W. Parson. *Modern Optical Spectroscopy.* Springer, 2007.

[141] J. P. Eisenstein, K. B. Cooper, L. N. Pfeiffer, and K. W. West. Insulating and fractional quantum Hall states in the first excited Landau level. *Phys. Rev. Lett.*, 88(7):076801, Jan 2002.

[142] R. M. Lewis, Yong P. Chen, L. W. Engel, D. C. Tsui, L. N. Pfeiffer, and K. W. West. Microwave resonance of the reentrant insulating quantum Hall phases in the first excited Landau level. *Phys. Rev. B*, 71(8):081301(R), Feb 2005.

[143] Y. Yafet. Raman scattering by carriers in Landau levels. *Phys. Rev.*, 152(2):858–862, Dec 1966.

[144] J. Nuebler, V. Umansky, R. Morf, M. Heiblum, K. von Klitzing, and J. Smet. Density dependence of the $\nu=\frac{5}{2}$ energy gap: Experiment and theory. *Phys. Rev. B*, 81:035316, Jan 2010.

[145] I. V. Kukushkin, J. H. Smet, D. Schuh, W. Wegscheider, and K. von Klitzing. Dispersion of the composite-fermion cyclotron-resonance mode. *Phys. Rev. Lett.*, 98(6):066403, Feb 2007.

[146] Irene Dujovne, A. Pinczuk, Moonsoo Kang, B. S. Dennis, L. N. Pfeiffer, and K. W. West. Composite-fermion spin excitations as ν approaches 1/2: Interactions in the Fermi sea. *Phys. Rev. Lett.*, 95(5):056808, Jul 2005.

[147] R. L. Willett, K. W. West, and L. N. Pfeiffer. Experimental demonstration of Fermi surface effects at filling factor 5/2. *Phys. Rev. Lett.*, 88(6):066801, Jan 2002.

[148] W. Pan, N. Masuhara, N. S. Sullivan, K. W. Baldwin, K. W. West, L. N. Pfeiffer, and D. C. Tsui. Impact of disorder on the 5/2 fractional quantum hall state. *Phys. Rev. Lett.*, 106:206806, May 2011.

[149] J. P. Eisenstein, K. B. Cooper, L. N. Pfeiffer, and K. W. West. Insulating and fractional quantum Hall states in the first excited Landau level. *Phys. Rev. Lett.*, 88(7):076801, Jan 2002.

[150] J. P. Eisenstein, M. P. Lilly, K. B. Cooper, L. N. Pfeiffer, and K. W. West. New collective states of 2D electrons in high Landau levels. *Physica E: Low-dimensional Systems and Nanostructures*, 9(1):1 – 8, 2001.

[151] I. V. Kukushkin, V. Umansky, K. von Klitzing, and J. H. Smet. Collective modes and the periodicity of quantum Hall stripes. *Phys. Rev. Lett.*, 106(20):206804, May 2011.

[152] R. Côté and H. A. Fertig. Collective modes of quantum Hall stripes. *Phys. Rev. B*, 62(3):1993–2007, Jul 2000.

[153] V. W. Scarola, Kwon Park, and J. K. Jain. Excitonic collapse of higher Landau level fractional quantum Hall effect. *Phys. Rev. B*, 62(24):R16259–R16262, Dec 2000.

[154] I. K. Kukushkin, J. H. Smet, V. W. Scarola, V. Umansky, and K. von Klitzing. Dispersions of the excitations of fractional quantum Hall states. *Science*, 324(5930):1044–1047, 2009.

[155] I.1 Dujovne, C.F. Hirjibehedin, A. Pinczuk, Moonsoo Kang, B.S. Dennis, L.N. Pfeiffer, and K.W. West. Light scattering observations of spin reversal excitations in the fractional quantum Hall regime. *Solid State Commun.*, 127(2):109–115, 2003.

[156] T. D. Rhone, J. Yan, Y. Gallais, A. Pinczuk, L. Pfeiffer, and K. West. Coexistence of quantum phases in the quantum Hall regime of the 2^{nd} Landau

level. Number BAPS.2009.MAR.J23.1, Pittsburgh, Pennsylvania, March 2009. APS, March Meeting Talk.

[157] Yu.A. Bychkov, S.V. Iordanskii, and G.M. Eliashberg. Two-dimensional electrons in a strong magnetic field. *JETP Lett.*, 33(143), 1981.

[158] Yu.A. Bychkov and E.I. Rashba. Two-dimensional electron-hole system in a strong magnetic field: biexcitons and charge-density waves. *Sov. Phys. JETP*, 58(1062), 1983.

[159] L. V. Kulik, S. Dickmann, I. K. Drozdov, A. S. Zhuravlev, V. E. Kirpichev, I. V. Kukushkin, S. Schmult, and W. Dietsche. Antiphased cyclotron-magnetoplasma mode in a quantum Hall system. *Phys. Rev. B*, 79(12):121310, Mar 2009.

[160] R. Morf and N. d'Ambrumenil. Disorder in fractional quantum Hall states and the gap at $\nu = 5/2$. *Phys. Rev. B*, 68:113309, Sep 2003.

[161] Koji Muraki, Gerardo Gamez, $\nu = 5/2$ Fractional Quantum Hall State in Low-Mobility Electron Systems: Different Roles of Disorder, arXiv:1101.5856v1 [cond-mat.mes-hall].

[162] I. K. Drozdov, L. V. Kulik, A. S. Zhuravlev, V. E. Kirpichev, I. V. Kukushkin, S. Schmult, and W. Dietsche. Extra spin-wave mode in quantum Hall systems: Beyond the skyrmion limit. *Phys. Rev. Lett.*, 104(13):136804, Apr 2010.

Appendix A

Definitions

variable	value	definition
e	4×10^{10} esu	magnitude of electron charge
$\hbar$	1.055×10^{-27}erg s	Planck's constant
c	$2.99 \times 10^{10} cm/s$	speed of light
$\hbar c$	$1973.26960 eV\mathring{A}$	
m_e	$9.1 \times 10^{-28} g$	free electron mass
μ_B	$e\hbar/2m_e = 0.05788 meV/T$	Bohr magneton
k_B	$0.08617 meV/K$	Boltzmanns constant
T		temperature
q		excitation wavevector
k		light scattering wavevector
n		2D areal density
ω_L		incoming photon frequency
λ_L		incoming photon wavelength
ω_S		outgoing (scattered) photon frequency
B		perpendicular magnetic field
B_T		total magnetic field
ϕ		even number of vortices
p, ν^*		composite fermion filling factor
l_o	$\sqrt{\hbar c/eB}$	magnetic length
E_F	$\hbar^2 \pi n/m^*$	Fermi energy of 2D electron system
E_c	$e^2\sqrt{\pi n}\epsilon$	Coulomb energy
ν	hcn/eB	electron Landau level filling factor
m^*	$0.063 m_e$	electron conduction band mass in GaAs
ϵ	13	dielectric constant in GaAs
g	-0.44	Lande factor in GaAs

Table A.1: Summary of variables and constants along with their values.

variable	definition
$2D$	two dimensional
AP	antiphase magnetoplasmon
CB	conduction band
CDE	charge density excitation
CDW	charge density wave
CF	composite fermion
FQH	fractional quantum Hall
FWHM	full width at half maximum
IQH	integer quantum Hall
LL	Landau level
ΛL	composite fermion energy level
MBE	molecular beam epitaxy
MP	magnetoplasmon
PL	photoluminescence
QW	quantum well
SDE	spin density excitation
SF	spin flip
SW	spin wave
VB	valence band
WC	Wigner Crystal

Table A.2: Summary of abbreviations and their definitions